EDJROSSÈ EDMOND TOSSOU

EXTENSION OF THE 2DH SAINT-VENANT HYDRODYNAMIC MODEL FOR FLOWS WITH VERTICAL ACCELERATION

Thèse présentée
à la Faculté des études supérieures de l'Université Laval
dans le cadre du programme de doctorat en génie civil
pour l'obtention du grade de Philosophiae Doctor (Ph.D.)

DÉPARTEMENT DE GÉNIE CIVIL
FACULTÉ DES SCIENCES ET DE GÉNIE
UNIVERSITÉ LAVAL
QUÉBEC

2009

Résumé

Cette étude présente le modèle bidimensionnel horizontal (2DH) de Serre qui constitue une extension de celui de Saint-Venant (SV) auquel des termes supplémentaires d'accélération verticale sont ajoutés pour tenir compte de la présence de pression dynamique dans l'écoulement. Ses hypothèses sont exposées puis ses équations constitutives sont clairement développées en vue de faciliter sa compréhension. Afin d'éliminer la principale source de difficulté justifiant son manque de popularité et le rendre compatible avec la plupart des schémas numériques, un nouveau format est ensuite établi en séparant les dérivées spatiales de celles temporelles. Partant d'une expansion en séries de Taylor de deuxième ordre, des termes de diffusion artificielle sont ajoutés aux équations dynamiques puis à celle de continuité. Le système résultant est alors résolu à l'aide de la méthode standard des éléments finis utilisant des éléments triangulaires dits non-conformes en raison de leurs intéressantes propriétés d'orthogonalité. La simulation d'un bassin en eau calme puis d'un écoulement permanent uniforme à l'aide du code Matlab® correspondant aboutit exactement aux résultats analytiques escomptés. Le test de propagation d'onde solitaire est également satisfaisant (phase et amplitude). De plus, le modèle simule également bien l'écoulement de rupture de barrage. Cependant, les ondes prédites par le modèle de SV avancent plus vite que celles de Serre. La pression dynamique retarde donc la propagation de ces ondes. L'augmentation de la pente du fond accélère les ondes aussi bien pour Serre que pour SV mais réduit l'écart entre les fronts correspondant aux deux modèles. Un comportement inverse est observé lorsque le fond devient davantage rugueux ainsi que quand le ratio des niveaux d'eau aux deux extrémités du domaine s'accroît. La méthode de diffusion ajoutée s'est également révélée efficace pour la capture des ondes de rupture de barrage sans détérioration de la qualité des resultats numériques. Enfin, après avoir éliminé l'hypothèse de fluide non visqueux selon la verticale posée par Serre, le modèle 'Saint-Venant Plus' (SVP) est développé pour pouvoir tenir compte des contraintes visqueuses verticales significatives dans certains écoulements naturels. Cependant, la resolution numérique de SVP ne fait pas partie des objectifs de cette thèse qui présente seulement une comparaison théorique de la formulation mathématique de SVP avec celles des deux autres modèles (Serre et SV).

Abstract

This study presents the horizontal two-dimensional (2DH) Serre equations, which include supplementary vertical acceleration terms in the Saint-Venant (SV) model to take into account the presence of dynamic pressure within the flow. For a better understanding of this model, its theory has been explained and its constitutive equations have been clearly developed. In order to eliminate the principal reason for its lack of popularity and to make it compatible with the usual numerical schemes, a new mathematical formulation has been established by separating the spatial derivatives from the temporal ones. Based on a second-order Taylor series expansion, artificial diffusion terms were added to the dynamic and continuity equations to upwind the model. The resulting system is solved by the standard finite element method (FEM) using triangular nonconforming elements because of their interesting orthogonality properties. The corresponding Matlab® computer program simulates well calm water basin and permanent uniform flow, leading exactly to their respective, expected analytical solutions. A good agreement is obtained for the simulation of the solitary wave propagation (phase and amplitude). The dambreak flows are also well simulated with the Serre numerical model. However, the SV waves outrun the Serre's. As such, dynamic pressure is truly present in a dambreak flow and it delays the propagation of the dambreak waves. On one hand, it was noted that as the bed slope increases, the celerity for the Serre wave (bore) traveling downstream increases more rapidly than the SV one. Consequently, the amount of the outdistancing of the SV bore decreases with increasing the bed slope. On the other hand, as bed roughness and water depths ratio increase, outdistancing increases. Moreover, by adding artificial diffusion terms, the shocks are captured more efficiently. Finally, by eliminating the Serre assumption of inviscid flow over the vertical, the 'Saint-Venant Plus' (SVP) model was developed to take into account the significant vertical viscous frictions encountered in some natural flows. However, its numerical solution is not presented here because it is not the focus. Thus, a theoretical comparison of the SVP mathematical formulation with the Serre and SV equations is simply proposed.

Avant-propos

Qu'il me soit permis d'adresser ici mes vifs remerciements à tous ceux qui ont contribué d'une manière ou d'une autre à l'heureux aboutissement de cette œuvre en l'occurrence:

Mon Directeur de recherches, le Professeur Jean-Loup ROBERT pour son encadrement parfait, pour les transferts de connaissances et enfin pour ses multiples gestes de générosité.

Mon Co-directeur de recherches, le Professeur Brian MORSE pour son adhésion spontanée au développement de ce modèle, pour son support financier, pour ses apports techniques significatifs au projet et enfin pour sa contribution déterminante à ma formation en recherche opérationnelle.

Mes parents et alliés qui m'ont toujours soutenu et encouragé.

Ma conjointe Lucie ST-GELAIS pour son attachement, pour les sacrifices consentis et pour sa conviction ainsi que ses parents Normand ST-GELAIS et Réjeanne DESBIENS.

Les généreux donateurs des différentes bourses de doctorat dont j'ai bénéficié durant cette formation, notamment, le Canadien National (CN), le Fonds Marthe-et-Robert-Ménard, la Fondation de l'Université Laval, Hydro-Québec et le Conseil National de Recherches en Sciences Naturelles et en Génie du Canada (CRSNG) via la subvention du projet stratégique (SPS) de modélisation de bris de barrage en situations hivernales.

Le Professeur Daniel Le ROUX de l'Université de Lyon (Université Lyon 1, CNRS), qui a accompagné techniquement le développement du présent modèle puis le Professeur Abdelatif OUAHSINE de l'Université Technologique de Compiègne pour ses précieux conseils.

Les Professeurs de l'Université Laval qui ont contribué à ma formation avec une pensée spéciale pour Feu Yvon OUELLET.

Les Techniciens du Laboratoire d'Hydraulique de l'Université Laval pour leur amitié.

Mes ami(e)s du Canada et du Bénin.

Par ailleurs, il convient de mentionner que cette thèse est rédigée en anglais car son contenu est directement extrait de trois articles (en anglais) soumis dans des revues scientifiques internationales pour publications et les commentaires sont toujours attendus. Il s'agit de:

1) '*Dambreak Flow Simulation using a Finite Element Solution of the 2DH Serre model*' soumis à la revue («Journal of Advances in Water Resources»). Par ordre de contribution à sa préparation et à sa rédaction, j'en suis le premier auteur alors que le Professeur Jean-Loup ROBERT en est le deuxième; le Professeur Brian MORSE, le troisième puis le Professeur Daniel Le ROUX, le quatrième.

2) '*2D Vertically-Averaged Serre Hydrodynamic Model*' soumis à la revue («Journal of Advances in Water Resources»). Par ordre de contribution à sa préparation et à sa rédaction, j'en suis le premier auteur alors que le Professeur Jean-Loup ROBERT en est le deuxième; le Professeur Brian MORSE, le troisième puis le Professeur Daniel Le ROUX, le quatrième

3) '*Extented Saint-Venant Model for Fully Non-Hydrostatic Pressure Flows*' soumis à la revue («Journal of Water Research»). Par ordre de contribution à sa préparation et à sa rédaction, j'en suis le premier auteur alors que le Professeur Jean-Loup ROBERT en est le deuxième; le Professeur Brian MORSE, le troisième puis le Professeur Daniel Le ROUX, le quatrième.

À mes parents défunts,
Antoine Sossou TOSSOU et Ahohounmè MADOU TCHOBO
Hommages respectueux.

«Le travail, mon enfant...et après le travail,
l'indépendance. Telle doit être la devise de votre génération»

Bernard B. DADIÉ, ***Climbié***

Table of contents

List of figures

List of symbols

Symbols	Definitions
$\overrightarrow{F_{ext}}$	Exterior forces to a given control volume within the flow
$\overrightarrow{F_p}$	Pressure forces
$\vec{a}$	Total acceleration
$\overrightarrow{F_{vis}}$	Viscosity forces
ρ	Fluid density
$\left(\vec{i} \quad \vec{j} \quad \vec{k}\right)$	The orthonormal point with the vertical axis positively upwards
$\left(x, \quad y, \quad z\right)$	The Cartesian coordinates with z upwards
$\left(u, \quad v, \quad w\right)$	The three velocity components
p	Pressure
t	Time
τ_{ij}	The viscous stresses with $i = 1,..,3$ and $j = 1,..,3$
μ	The dynamic viscosity of the fluid
$\nu = \mu/\rho$	The cinematic viscosity of the fluid
ν_t	Eddy viscosity
U and V	The vertically-averaged values of u and v respectively
τ_x^s and τ_y^s	The friction stresses at the free surface of the flow in the x and y directions respectively
τ_x^f and τ_y^f	The friction stresses on the bottom boundary in the x and y directions respectively
$\nu_{xx}, \nu_{xy}, \nu_{yx}, \nu_{yy}$	The total diffusion coefficients

η	The position of the free surface of the flow
H	Total water depth
z_f	The bed elevation
$\overrightarrow{a_t}$	The tangential acceleration
$\overrightarrow{a_n}$	The normal acceleration
w_f	The vertical velocity at the bottom of the flow
w_{fs}	The vertical velocity at the solid bottom of the flow
w_η	The vertical velocity calculated at the free surface of the flow
w_H	The vertical velocity of the water column
p_η	The pressure at the free surface
D/Dt	The material derivative
g	The gravitational acceleration
α	The Serre total water depth increase acceleration
β	The Serre vertical acceleration at the bottom of the flow
U_z and V_z	The supplementary mean velocity components in the x and y directions respectively due to the Serre vertical acceleration
a_{zx} and a_{zy}	The supplementary convection and diffusion terms in the x and y directions respectively due to the Serre vertical acceleration
C_{up}	The upwinding factor between 0 and 1
Δt	The time step
C_c	The Chézy's coefficient
K_s	The Strickler's roughness coefficient
R_H	The hydraulic radius

D	The global domain of study
D^e	The element domain
R_1, R_2 and R_3	The integral formulation of the weighted-residuals of the two dynamic equations and of the continuity one respectively
φ_U and φ_V	The weight functions for the first and for the second dynamic equations
φ_H	The weight function for the continuity equation
$\vec{n}$	The unit normal vector
n_x and n_y	The two components of the unit normal vector in the x and y directions respectively
Γ	The boundary of the domain
q_n	The unit discharge of the flow through the boundary
N_H	The basis functions associated respectively to each of the three vertex nodes of the reference element
N	The basis functions associated to the mid-side nodes of the reference element
ψ	The natural abscissa on a reference element
ξ	The natural ordinate on a reference element
$\tilde{\eta}$	The discrete expression of η
$\widetilde{H}$	The discrete expression of H
$\widetilde{z_f}$	The discrete expression of z_f
$\widetilde{U}$	The discrete expression of U
$\widetilde{V}$	The discrete expression of V
$\left[M^e\right]$	The element mass matrix
$\left[K^e\right]$	The element stiffness matrix

$\{F^e\}$	The element force vector
$\{F_s^e\}$	The element force vector due to the Serre supplementary terms
$[M]$	The assembled mass matrix
$[K]$	The assembled stiffness matrix
$\{F\}$	The assembled force vector
$\{F_s\}$	The assembled force vector due to the Serre supplementary terms
θ	The coefficient that defines the temporal approximation scheme
R_1^e, R_2^e and R_3^e	The discrete expressions of R_1, R_2 and R_3 respectively
$\{U^e\}$	The element nodal values of U
$\{V^e\}$	The element nodal values of V
$\{H^e\}$	The element nodal values of H
N_{CFL}	Number of Courant-Friedrichs-Lewy for the stability condition
S_x and S_y	The bottom slopes in the x and y directions respectively
λ	The wavelength
δ	The wave amplitude
H_0	The undisturbed water depth for $T = 0$ for solitary wave
x_0	The initial position of the solitary wave crest or the position of the dam
c	The theoretical celerity of the solitary wave
T	The total duration of the simulation (the time length)
H_u	The water depth at the upstream in a dambreak flow

H_d	The water depth at the downstream in a dambreak flow
H_m	The water depth at the middle of the domain in a dambreak flow
U_m	The velocity at the middle of the domain in a dambreak flow
s_b	The celerity of the shock wave (bore) in a dambreak flow
A	The increase of the acceleration α per unit of flow depth due to the vertical viscous frictions
B	The increase of the acceleration β due to the vertical viscous frictions
RRMSE	Relative Root Mean Square Error

CHAPTER 1

Introduction

1.1.- Context and literature review

The horizontal two-dimensional (2DH) shallow water (SW) equations are several decades old and are used to describe fluid hydrodynamics (water velocity and water level) for free surface flows. Those equations are also conventionally called 2DH Saint-Venant (SV) equations in order to pay homage to Jean-Claude Barré de Saint-Venant who is the first to write a one-dimensional version (Barré de Saint-Venant 1871; Viollet et al. 1998). The SV equations result from the vertical integration of the three-dimensional (3D) Partial Differential Equations (PDE) of incompressible and Newtonian fluid motion in a gravity field. When integrating over the depth, the SV core assumption is that the vertical acceleration of the motion of the fluid in the flow is negligible. For the flows that are inviscid over the vertical, ignoring the vertical acceleration is equivalent to stating that the pressure is hydrostatically distributed (zero at the free surface and increasing in a linear fashion down to the bed). Physically speaking, this implies that there is no sudden variation in the flow over the vertical and that the vertical curvature of the streamlines is small (i.e., negligible convective and normal components of the vertical acceleration).

For many applications, the SV assumptions do not lead to significant errors. However, in other cases, many natural flows do have non-linear pressure distributions as, for example, when waves meet obstacles; at free overfalls; in sharp meanders; in curved open channels; at sudden changes in slope; after abrupt channel closure near a gate; at a depression or rise in the river bed; etc. Sometimes, the dynamic nature of the pressure is

small but at other times, it may be surprisingly large. For example, Zarrati et al. (2004) claim to have observed experimentally shock pressures reaching 25 times their hydrostatic value near the location of the sudden change in slope. Also, a significant characteristic of the free overfalls is that there is a strong departure from hydrostatic distribution of pressure in the vicinity of the drop because of the strong accelerated down flow (Hager 1983; Montes 1992; Marchi 1993; Khan and Steffler 1996; Rubin 1997). In the same light, Basco (1989) demonstrated the weakness of SV for modeling dambreak flows since he showed that the vertical acceleration could be quite significant. In effect, for this type of flow, movement varies rapidly in time and the vertical curvature of the streamlines is significant. Based on a Lagrangian resolution of the vertical two-dimensional version (2DV) of the Navier-Stokes (NS) equations for dambreak simulations, Pohle (1952) and Strelkoff (1986) established that pressure distribution is significantly non-hydrostatic immediately after rupture. Dressler (1954) observed experimentally that the flow depth and the breach discharge do not instantaneously reach constant values at the dam location but, because the pressure is non-hydrostatic, they gradually establish themselves over time. In addition, Kosorin (1983) demonstrated that non-hydrostatic pressure reduced the celerity of the dambreak wave by as much as 30 % when compared to Ritter's analytic solution based on the hydrostatic pressure hypothesis. In all of these conditions, the hydrostatic pressure hypothesis severely limits the use of the SV model.

To model dynamic pressure situations, many authors have resorted to using the NS equations (Stansby and Zhou 1998; Jankowski 1999; Casulli and Zanolli 2002; Namin et al. 2001; Stelling and Zijlema 2003). Their direct resolution can fully account for vertical accelerations in the flow but the complexity of the equations and the associated computing cost lessen the models' feasibility (Xia and Jin 2006). Subsequent to SV, the Boussinesq model was established. However, the main limitation of the most common Boussinesq equations is that they are only valid for shallow water (Meftah et al. 2004). For example, in order to get a phase velocity difference smaller than 5 %, water depth must be less than $1/5^{th}$ of the equivalent wavelength in deep water (McCowan 1987). Thus, some extended and higher order versions were developed to extend the validity domain to deep water or more commonly, to improve the wave dispersion property of the

model (Madsen and Sorensen 1992; Nwogu 1993). Some comparisons with a number of practical problems (e.g., weirs, contractions, flumes and overfalls) were made in the literature. In many applications, good agreement between the numerical results from those Boussinesq-type models and experiments was noted (Law 1997; Zerihum 2004; Zerihum and Fenton 2006; Zerihum and Fenton 2007; Fenton and Zerihum 2007).

There have also been some attempts to modify the SV equations directly by adding a dynamic pressure correction. Ghamry and Steffler (2002) chose to impose different vertical profiles for both pressure and horizontal velocity components onto the SV model. Even if this approach has been successful for some applications, it remains that the precision of this type of model depends largely on the complexity of the assumed pressure profile. When resolving the equations, many coefficients must be evaluated and often become so numerous that the added effort significantly increases computing time. Moreover, the different imposed profiles are arbitrary and do not necessarily have any physical significance. In one application (free overfall simulations), the assumed quadratic pressure distribution is limited in predicting the measured pressure profile accurately at the brink section (Khan and Steffler 1996). Another attempt to overcome the hydrostatic pressure hypothesis has been to introduce layered 2DH models. An initial application of this type assumed a linear distribution of pressure in each layer while a more recent application assumes a quadratic profile (Xia and Jin 2006). This approach offers no more physical justification pertinent to the different supposed profiles and the precision of these models require many layers of small depths. As a result, computing time becomes very significant.

The need to account for the dynamic pressure effects also led to the proposal of the Serre model (Serre 1953). Its principal assumption is that there is a linear variation in the vertical velocity component from the bottom through to the free surface. This vertical acceleration can result from rapid changes in flow depths or from highly-curved flow paths (local and convective vertical acceleration). Assuming this gradient in vertical velocity necessarily implies that the pressure deviates from its linear (hydrostatic) distribution. In its mathematical formulation, the Serre model resembles that of SV with the principal difference being that the two dynamic (momentum) equations carry

additional terms to account for the effects of the resulting dynamic pressure. The presence of higher derivatives in those additional terms is also a mathematical difference that will require additional computational effort.

The Serre equations are little known in the literature and have very rarely been exploited. The reason is that they are very difficult to resolve numerically since the PDE contain (1) higher order terms and (2) mixed (spatial-temporal) derivative terms. For example, at present, despite the very many SV FEM versions available, to our knowledge, there is not a single Serre FEM available (Hervouet 2003) although there is (i) a finite difference version using a MacCormack type scheme (Antunes Do Carmo et al. 1993); (ii) a finite volume version (Cienfuegos et al. 2005); and (iii) there is a Serre-Boussinesq version solved by FEM using a Lax-Wendroff non-diffusive scheme (Dufresne 1997). It may also be possible that the Serre equations have not been widely applied because they are so poorly documented and/or so poorly understood.

1.2.- Objectives of the thesis

The principal objectives of this thesis are:

- ✓ To present a detailed step-by-step mathematical development of the Serre model so as to eliminate some of the confusion about it.
- ✓ To propose a new formulation of the Serre PDE in which, the spatial-temporal derivatives are separated for solid bed applications so that it can be compatible with the usual numerical schemes.
- ✓ To solve that new formulation by using the FEM and to validate the resulting numerical model by simulating some chosen hydrodynamic flow types.
- ✓ To propose an extended version (the SVP equations) by omitting the assumption of inviscid flow over the vertical as done in the Serre model (i.e., by including the

friction forces over the vertical). However, only the mathematical development of the SVP is presented and its resolution and its validation are not included in the scoops of this thesis.

1.3.- Plan of the thesis

The next chapter presents the step-by-step mathematical development of the Serre equations and the separation of the time derivatives from the spatial ones. Before their presentation, the Serre assumptions are quantified; the physical significance of the SV hypotheses are explained and the governing equations are recalled. Subsequently, the new formulation of the Serre model is solved in the third chapter by using the FEM based on the second-order Taylor-Galerkin approach. In the fourth chapter, some preliminary validation tests are proposed, which consists of simulating a calm water basin, a permanent uniform flow and a solitary wave propagation. The fifth chapter analyzes some dambreak flows. Finally, the mathematical development of the SVP is presented in the last chapter.

CHAPTER 2

Mathematical Development of the 2D Vertically-Averaged Serre Hydrodynamic Model

Introduction

The Serre model was first proposed by François Serre as an alternative to the SV since the dynamic pressure within the flow had to be taken into account (Serre 1953). The mathematical development of the Serre PDE follows the same procedure as the SV, thus leading to a very similar formulation. The main difference is that the two dynamic equations contain some additional terms due to the vertical acceleration, which is still the principal cause of the dynamic pressure, according to Serre. However, that model is little known in the literature and has very rarely been exploited. Consequently, the corresponding PDE are very poorly documented and/or very poorly understood.

This chapter presents the first objective of the thesis through a detailed step-by-step mathematical development of the Serre PDE for the purpose of eliminating some of the confusion surrounding the model. Additionally, the spatial-temporal derivatives of the Serre PDE are separated for solid bed applications and are therefore now available for FEM efforts.

In the rest of this chapter, the physical significance of the SV basic assumptions is explained. Then, the Serre main hypothesis is presented as well as the general equation for pressure and for its gradients within flow. Subsequently, the step-by-step development of the two Serre dynamic equations follows. After which, the mathematical

formulation of the resulting equations is compared to those of SV. Finally, the separation of the mixed spatial-temporal derivative terms is demonstrated.

2.1.- Recalling the basic equations

The 3D PDE of fluid motion in a gravity field, the so-called NS equations and the 3D continuity equation serve as the basis for the development of the Serre model. The NS equations are applied to real fluids (non-null viscosity) and translate, by the momentum conservation principle, the equilibrium of forces brought to bear on an elementary portion of fluid, called the control volume (Shames 1962; Van Rijn 1994). To establish this equilibrium, it is sufficient to consider a control volume in parallelepipedic form, being dx, dy and dz as dimensions of the sides, and to create an inventory of forces present, which results in this vector equation:

$$\overrightarrow{F_{ext}} + \overrightarrow{F_p} + \overrightarrow{F_{vis}} = \rho dx dy dz \vec{a} \tag{1}$$

In (1), $\overrightarrow{F_{ext}}$ represents external forces; $\overrightarrow{F_p}$ designates pressure forces while $\overrightarrow{F_{vis}}$ symbolizes forces of viscosity or friction; $\vec{a}$ designates the total acceleration while ρ is the fluid density. The product $\rho dx dy dz \vec{a}$ represents the inertial forces.

Generally, the different forces in (1) are expressed in a unitary form, giving:

$$\frac{\overrightarrow{F_{ext}}}{dxdydz} + \frac{\overrightarrow{F_p}}{dxdydz} + \frac{\overrightarrow{F_{vis}}}{dxdydz} = \rho \vec{a} \tag{2}$$

Coriolis' acceleration caused by the rotation of the earth on itself has little effect on rivers (Hervouet 2003) and is ignored in this study. Additionally, the fluid is assumed incompressible and Newtonian.

The two members of equation (2) are divided by the fluid density ρ and the resulting expression is then projected in an orthonormal point $\left(\vec{i} \quad \vec{j} \quad \vec{k}\right)$ in which, the vertical axis positively upwards, giving the Cartesian formulation of the NS equations with the continuity one as follows (Shames 1962; Van Rijn 1994):

$$\frac{\partial u}{\partial x}+\frac{\partial v}{\partial y}+\frac{\partial w}{\partial z}=0 \tag{3a}$$

$$-\frac{1}{\rho}\frac{\partial p}{\partial x}+\frac{1}{\rho}\left(\frac{\partial \tau_{xx}}{\partial x}+\frac{\partial \tau_{xy}}{\partial y}+\frac{\partial \tau_{xz}}{\partial z}\right)=\frac{\partial u}{\partial t}+u\frac{\partial u}{\partial x}+v\frac{\partial u}{\partial y}+w\frac{\partial u}{\partial z} \tag{3b}$$

$$-\frac{1}{\rho}\frac{\partial p}{\partial y}+\frac{1}{\rho}\left(\frac{\partial \tau_{yx}}{\partial x}+\frac{\partial \tau_{yy}}{\partial y}+\frac{\partial \tau_{yz}}{\partial z}\right)=\frac{\partial v}{\partial t}+u\frac{\partial v}{\partial x}+v\frac{\partial v}{\partial y}+w\frac{\partial v}{\partial z} \tag{3c}$$

$$-g-\frac{1}{\rho}\frac{\partial p}{\partial z}+\frac{1}{\rho}\left(\frac{\partial \tau_{zx}}{\partial x}+\frac{\partial \tau_{zy}}{\partial y}+\frac{\partial \tau_{zz}}{\partial z}\right)=\frac{\partial w}{\partial t}+u\frac{\partial w}{\partial x}+v\frac{\partial w}{\partial y}+w\frac{\partial w}{\partial z} \tag{3d}$$

In this system, $(x, \ y, \ z)$ represent Cartesian coordinates with z upwards; the triplet $(u, \ v, \ w)$ designates the three velocity components; p designates the pressure whereas t designates time and τ_{ij} represents the viscous stresses with $i=1,..,3$ and $j=1,..,3$.

Equation (3a) is an expression of the 3D continuity equation (conservation of mass) while the last equations (i.e., 3b, 3c and 3d) represent the 3D dynamic equations (conservation of momentum).

The Stokes' law models the viscous stresses yielding (Shames 1962):

$$\tau_{ij} = \mu\left(\frac{\partial u_i}{\partial x_j} + \frac{\partial u_j}{\partial x_i}\right) \tag{4}$$

where the fluid dynamic viscosity coefficient is μ; the velocity components are $u_1 = u$, $u_2 = v$ and $u_3 = w$; and the Cartesian coordinates are represented by ($x_1 = x$, $x_2 = y$, $x_3 = z$).

However, an eddy viscosity concept is usually applied to account for the turbulent shear stresses leading to the Boussinesq approximation (see, Boussinesq 1877; Van Rijn 1994):

$$\tau_{ij} = \rho\left(\nu + \nu_t\right)\left(\frac{\partial u_i}{\partial x_j} + \frac{\partial u_j}{\partial x_i}\right) \tag{5}$$

where $\nu = \mu/\rho$ represents the cinematic viscosity of the fluid and ν_t is the turbulent or eddy viscosity. For a more complex form of the shear stresses τ_{ij}, the reader can refer to (Levermore and Sammartino 2001).

Before starting the development of the Serre model, it is also necessary to recall the 2DH SV equations in their generalized form (Van Rijn 1994):

$$\frac{\partial H}{\partial t} + \frac{\partial\left(HU\right)}{\partial x} + \frac{\partial\left(HV\right)}{\partial y} = 0 \tag{6a}$$

$$\begin{aligned} &\frac{\partial U}{\partial t} + U\frac{\partial U}{\partial x} + V\frac{\partial U}{\partial y} + \frac{1}{\rho H}\left(\tau_x^f - \tau_x^s\right) - \frac{\partial}{\partial x}\left(\nu_{xx}\frac{\partial U}{\partial x}\right) - \frac{\partial}{\partial x}\left(\nu_{xy}\frac{\partial U}{\partial y}\right) \\ &- \frac{\partial}{\partial y}\left(\nu_{yx}\frac{\partial U}{\partial x}\right) - \frac{\partial}{\partial y}\left(\nu_{yy}\frac{\partial U}{\partial y}\right) = -g\frac{\partial \eta}{\partial x} \end{aligned} \tag{6b}$$

$$\frac{\partial V}{\partial t}+U\frac{\partial V}{\partial x}+V\frac{\partial V}{\partial y}+\frac{1}{\rho H}\left(\tau_y^f-\tau_y^s\right)-\frac{\partial}{\partial x}\left(\nu_{xx}\frac{\partial V}{\partial x}\right)-\frac{\partial}{\partial x}\left(\nu_{xy}\frac{\partial V}{\partial y}\right)$$
$$-\frac{\partial}{\partial y}\left(\nu_{yx}\frac{\partial V}{\partial x}\right)-\frac{\partial}{\partial y}\left(\nu_{yy}\frac{\partial V}{\partial y}\right)=-g\frac{\partial \eta}{\partial y} \qquad (6c)$$

In this system, g is the gravitational acceleration; U and V represent the vertically-averaged values of u and v respectively; τ_x^s and τ_y^s designate the friction stresses at the free surface of the flow (due, for example, to wind or ice), in the x and y directions respectively, while τ_x^f and τ_y^f are the friction stresses on the bottom boundary. The diffusion coefficients, denoted ν_{xx}, ν_{xy}, ν_{yx} and ν_{yy}, are used to take into account overall diffusion phenomena (molecular viscous diffusion and that due to the flow turbulence) in the flow (Van Rijn 1994). All the other variables have been defined previously.

Remember that the SV equations result from the vertical integration of the NS, simplified by neglecting the vertical acceleration of the fluid motion and by assuming that the flow is inviscid over the vertical. For the sake of conciseness, the significance of each term in equations (6) is not presented here; however, the reader can refer to the previous references where they are fully explained.

The first equation of (6) represents the 2DH continuity equation (i.e., conservation of mass) while the two following equations represent the 2DH SV dynamic equations (i.e., conservation of momentum). The principal unknown variables are the mean velocities (U and V), the position of the free surface of the flow (η) and/or the water depth (H).

2.2.- Physical significance of the SV assumptions

According to SV, pressure distribution over the vertical is hydrostatic. Noting that the tangential acceleration $\overrightarrow{a_t}$ and the normal one $\overrightarrow{a_n}$ do constitute the two components of the total vector acceleration, whereupon the vector form of NS becomes:

$$\frac{1}{\rho}\frac{\overrightarrow{F_{ext}}}{dxdydz}+\frac{1}{\rho}\frac{\overrightarrow{F_p}}{dxdydz}+\frac{1}{\rho}\frac{\overrightarrow{F_{vis}}}{dxdydz}=\overrightarrow{a_t}+\overrightarrow{a_n} \tag{7}$$

The normal acceleration $\overrightarrow{a_n}$ that appears in equation (7) does exist if only the flow path is curved. To obtain the hydrostatic pressure distribution, it is first necessary to simplify the third NS equation (3d) and then to integrate it vertically. The three requisite simplifications correspond to the true SV hypotheses, which are the following: negligible vertical component of (1) local acceleration, (2) convective acceleration, and (3) negligible vertical viscous frictions. Physically speaking, the first and the second assumptions are due to vertical flow varying gradually (i.e., no rapid change in the flow depth) and to the vertical curvature of streamlines of the current that is negligible. Sudden variations over the vertical (e.g., just after a dambreak event) are not addressed by SV. Moreover, free overfalls, non-uniform flow resulting from a dambreak, flow at a sudden change in slope, and flow at the point of flooding or at an obstruction in the river bed cannot be represented with SV since, in these cases, the vertical curvature of the flowlines cannot be ignored. Finally, the third hypothesis implies that the viscous friction effects in the vertical can be ignored (inviscid flow over the vertical). The viscous shear stresses terms in the third NS momentum equation are then neglected.

2.3.- Serre assumptions

The Serre equations rest fundamentally upon the hypothesis that the horizontal velocities are assumed constant over the vertical (i.e., $u = U$ and $v = V$). Consequently, the vertical velocity component varies linearly from the bottom through to the free surface (Serre 1953). This will be demonstrated further in the next section.

Additionally, the flow is assumed inviscid over the vertical.

Although one could impose another vertical profile for horizontal velocities (e.g., linear, quadratic, logarithmic, power, etc), the development of the subsequent equations would be complex and would lead to a different model than Serre's (which is the subject of this study). In addition, for some non-hydrostatic flow simulations, Ghamry and Steffler (2002) have tested the effect of applying different distribution shapes for velocities, and the predictions of overall flow characteristics suggest that the results are not very sensitive to different approximations of the presumed velocity shapes.

Contrary to the SV hypothesis, vertical acceleration is no longer negligible in the Serre model context and consequently, the distribution of pressure is no longer hydrostatic. Therefore, pressure gradient terms in the first two dynamic NS (3b) and (3c) cannot be simply reduced. Rather, they generate additional Serre terms that account for the impact of dynamic pressure on the flow.

Because of that Serre assumption, the third NS (3d) is simplified and it becomes:

$$-\frac{1}{\rho}\frac{\partial p}{\partial z} = g + \frac{\partial w}{\partial t} + U\frac{\partial w}{\partial x} + V\frac{\partial w}{\partial y} + w\frac{\partial w}{\partial z} \tag{8}$$

Once this simplification is made, the procedure to develop the Serre equations is identical to that used to establish the SV model. It consists of calculating the vertically-averaged expression of the continuity equation (3a) and of the three resulting NS (3b, 3c and 8). This leads to a system consisting exactly of the standard SV equations (6) but with some

additional terms due to the vertical integration of the dynamic pressure gradients. The overall procedure to develop the SV model is fully described by Tossou (2004), Hervouet (2003), Viollet et al. (1998) and Van Rijn (1994). However, this study will simply focus on the vertical integration of the gradient pressure terms and the resulting expressions must be added to the SV equations in order to form the Serre model.

2.4.- General expression of the vertical velocity

Given the following scheme (Figure 2.1),

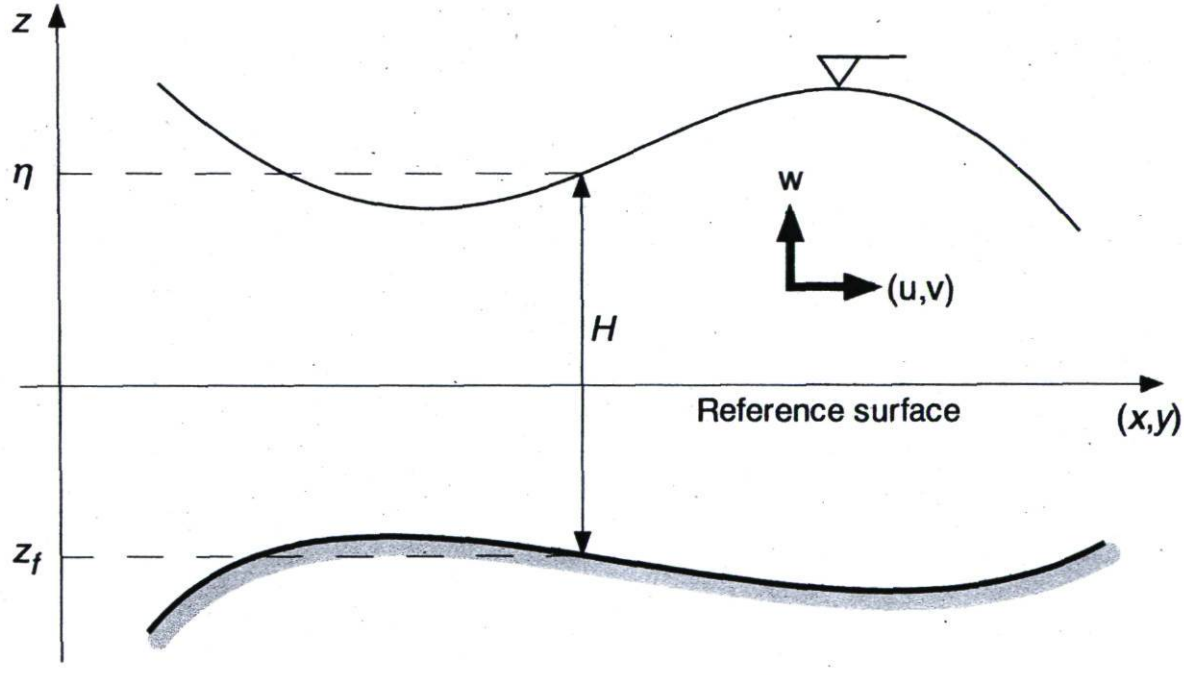

Figure 2.1: Conceptual scheme of the flow

the first step to obtain the general expression of the vertical velocity is to vertically integrate the continuity equation (3a), from the bed elevation (z_f) to an arbitrary level

(z) within the flow taking into account the Serre approximation of horizontal velocities constant over the vertical:

$$\int_{z_f}^{z}\left(\frac{\partial U}{\partial x}+\frac{\partial V}{\partial y}+\frac{\partial w}{\partial z}\right)dz=\left(\frac{\partial U}{\partial x}+\frac{\partial V}{\partial y}\right)\left(z-z_f\right)+w-w_f=0 \tag{9a}$$

where w_f represents the vertical velocity at the bottom of the flow.

For the sake of conciseness, the term $(\partial U/\partial x+\partial V/\partial y)$ which is independent of z, will be renamed $L(U,\ V)$ to give:

$$L(U,\ V)=\frac{\partial U}{\partial x}+\frac{\partial V}{\partial y} \tag{9b}$$

However, the variable $L(U,\ V)$ will be simply denoted L for the sake of simplicity.

Then, equation (9a) is reformulated and it leads to the general expression of the vertical velocity:

$$w=w_f-\left(z-z_f\right)L \tag{10}$$

According to (10), the vertical velocity varies linearly from the bottom of the flow through to the free surface.

In the following developments, w_η will be used to designate the vertical velocity calculated at the position η of the free surface of the flow.

2.5.- General expression of Serre pressure field

The first step here is to expand the simplified NS third dynamic equation (8) using the general expression of the vertical velocity, i.e., equation (10). Thereby considering the fact that w_f and z_f are constant over the vertical and whereas z is independent of x, y and t, gives

$$\frac{\partial w}{\partial t}=\frac{\partial w_f}{\partial t}-\left(z-z_f\right)\frac{\partial L}{\partial t}+\frac{\partial z_f}{\partial t}L \tag{11a}$$

$$U\frac{\partial w}{\partial x}=U\frac{\partial w_f}{\partial x}-U\left(z-z_f\right)\frac{\partial L}{\partial x}+U\frac{\partial z_f}{\partial x}L \tag{11b}$$

$$V\frac{\partial w}{\partial y}=V\frac{\partial w_f}{\partial y}-V\left(z-z_f\right)\frac{\partial L}{\partial y}+V\frac{\partial z_f}{\partial y}L \tag{11c}$$

$$w\frac{\partial w}{\partial z}=-w_f L+\left(z-z_f\right)L^2 \tag{11d}$$

Adding (11a), (11b), (11c) and (11d) gives,

$$\begin{aligned}\frac{\partial w}{\partial t}+U\frac{\partial w}{\partial x}+V\frac{\partial w}{\partial y}+w\frac{\partial w}{\partial z}=&\left(\frac{\partial w_f}{\partial t}+U\frac{\partial w_f}{\partial x}+V\frac{\partial w_f}{\partial y}\right)-\left(z-z_f\right)\left(\frac{\partial L}{\partial t}+U\frac{\partial L}{\partial x}+V\frac{\partial L}{\partial y}\right)\\&+L\left(\frac{\partial z_f}{\partial t}+U\frac{\partial z_f}{\partial x}+V\frac{\partial z_f}{\partial y}\right)-w_f L+\left(z-z_f\right)L^2\end{aligned} \tag{12}$$

Next, taking into account the fact that,

$$\frac{Dw_f}{Dt}=\frac{\partial w_f}{\partial t}+U\frac{\partial w_f}{\partial x}+V\frac{\partial w_f}{\partial y} \tag{13a}$$

$$\frac{DL}{Dt}=\frac{\partial L}{\partial t}+U\frac{\partial L}{\partial x}+V\frac{\partial L}{\partial y} \tag{13b}$$

$$w_f = \frac{Dz_f}{Dt} = \frac{\partial z_f}{\partial t} + U\frac{\partial z_f}{\partial x} + V\frac{\partial z_f}{\partial y} \tag{13c}$$

the expression (12) gives,

$$\frac{\partial w}{\partial t} + U\frac{\partial w}{\partial x} + V\frac{\partial w}{\partial y} + w\frac{\partial w}{\partial z} = \frac{Dw_f}{Dt} + \left(z - z_f\right)\left(L^2 - \frac{DL}{Dt}\right) \tag{14}$$

and equation (8) becomes,

$$-\frac{1}{\rho}\frac{\partial p}{\partial z} = g + \beta + \left(z - z_f\right)\left(L^2 - \frac{DL}{Dt}\right) \tag{15}$$

where the variable β is defined as follows,

$$\beta = \frac{Dw_f}{Dt} = \frac{D^2 z_f}{Dt^2} \tag{16}$$

The second step to establish the general expression for the pressure field is to vertically integrate (15) from an arbitrary surface (z) within the flow to the position of the free surface (η).

Therefore, the vertical integral of the left hand side (LHS) of (15) is calculated by taking into account the fact that the free surface pressure (p_η) is equal to atmospheric pressure, which is zero. This results in:

$$-\frac{1}{\rho}\int_z^\eta \frac{\partial p}{\partial z}dz = \frac{1}{\rho}\left(-p_\eta + p\right) = \frac{p}{\rho} \tag{17}$$

Next, the vertical integral of the right hand side (RHS) of (15) is calculated by taking into account the fact that β as well as L and its derivatives (temporal and spatial) are independent of the variable z. This results successively in:

$$\int_z^\eta g\,dz = g(\eta - z) \tag{18a}$$

$$\int_z^\eta \beta\,dz = \beta(\eta - z) \tag{18b}$$

$$\int_z^\eta (z - z_f)\left(L^2 - \frac{DL}{Dt}\right)dz = \left(L^2 - \frac{DL}{Dt}\right)\int_z^\eta (z - z_f)\,dz = \left(\frac{\eta^2 - z^2}{2} - z_f(\eta - z)\right)\left(L^2 - \frac{DL}{Dt}\right) \tag{18c}$$

The sum of equations (18a), (18b) and (18c) gives the vertical integral of the RHS of (15), which is put together with equation (17) to lead to the general expression of the Serre pressure field:

$$p(x,\ y,\ z,\ t) = \rho(g + \beta)(\eta - z) + \rho\left(\frac{\eta^2 - z^2}{2} - z_f(\eta - z)\right)\left(L^2 - \frac{DL}{Dt}\right) \tag{19}$$

This general expression of the Serre pressure field must be simplified by reformulating the expression of DL/Dt.

Consider the following equation of the total water depth:

$$H = \eta - z_f \tag{20}$$

The material derivative of (20) gives:

$$\frac{DH}{Dt} = \frac{D\eta}{Dt} - \frac{Dz_f}{Dt} = w_\eta - w_f \tag{21}$$

The evaluation of the vertical velocity at the free surface of the flow, using (10) gives:

$$w_\eta = w_f - LH \tag{22}$$

The substitution of equation (22) into (21) leads to

$$L = -\frac{1}{H}\frac{DH}{Dt} \tag{23}$$

By setting,

$$\alpha = \frac{D^2 H}{Dt^2} \tag{24}$$

The material derivative of equation (23) yields:

$$\frac{DL}{Dt} = L^2 - \frac{\alpha}{H} \tag{25}$$

Finally, the substitution of (25) into (19) gives the general equation for the Serre pressure field:

$$p(x,\ y,\ z,\ t) = \rho(g+\beta)(\eta - z) + \rho\frac{\alpha}{H}\left(\frac{\eta^2 - z^2}{2} - z_f(\eta - z)\right) \tag{26}$$

2.6.- General equations for pressure gradients

Having established the equation describing the Serre pressure field, it is now necessary to characterize the Serre pressure gradients. One obtains the pressure gradient along the x-axis by deriving each of the terms of equation (26) with respect to x. This derivation gives successively:

$$\frac{\partial}{\partial x}\left[(g+\beta)(\eta-z)\right]=(\eta-z)\frac{\partial \beta}{\partial x}+(g+\beta)\frac{\partial \eta}{\partial x} \tag{27a}$$

$$\frac{\partial}{\partial x}\left[\frac{\alpha}{H}\left(\frac{\eta^2-z^2}{2}-z_f(\eta-z)\right)\right]=\frac{\partial}{\partial x}\left(\frac{\alpha}{H}\right)\left(\frac{\eta^2-z^2}{2}-z_f(\eta-z)\right)+\frac{\alpha}{H}\left(H\frac{\partial \eta}{\partial x}-(\eta-z)\frac{\partial z_f}{\partial x}\right) \tag{27b}$$

and the sum of (27a) and (27b) gives the pressure gradient expression in the x direction

$$\frac{1}{\rho}\frac{\partial p}{\partial x}=(\eta-z)\frac{\partial \beta}{\partial x}+(g+\beta)\frac{\partial \eta}{\partial x}+\frac{\partial}{\partial x}\left(\frac{\alpha}{H}\right)\left(\frac{\eta^2-z^2}{2}-z_f(\eta-z)\right)+\frac{\alpha}{H}\left(H\frac{\partial \eta}{\partial x}-(\eta-z)\frac{\partial z_f}{\partial x}\right) \tag{28a}$$

The same procedure establishes equation (28b) that represents the pressure gradient expression in the y direction:

$$\frac{1}{\rho}\frac{\partial p}{\partial y}=(\eta-z)\frac{\partial \beta}{\partial y}+(g+\beta)\frac{\partial \eta}{\partial y}+\frac{\partial}{\partial y}\left(\frac{\alpha}{H}\right)\left(\frac{\eta^2-z^2}{2}-z_f(\eta-z)\right)+\frac{\alpha}{H}\left(H\frac{\partial \eta}{\partial y}-(\eta-z)\frac{\partial z_f}{\partial y}\right) \tag{28b}$$

2.7.- Vertically-averaged pressure gradients

Having characterized the pressure field and the pressure gradients, it is now required to integrate them over the vertical to establish mean expressions for a 2DH application. Therefore, each pressure gradient term will be considered individually and its integration over the vertical will be presented:

$$\frac{1}{H}\int_{z_f}^{\eta}(\eta-z)\frac{\partial\beta}{\partial x}dz=\frac{1}{H}\frac{\partial\beta}{\partial x}\int_{z_f}^{\eta}(\eta-z)dz=\frac{1}{2H}\frac{\partial\beta}{\partial x}(\eta-z_f)^2=\frac{\partial\beta}{\partial x}\frac{H}{2} \tag{29a}$$

$$\frac{1}{H}\int_{z_f}^{\eta}(g+\beta)\frac{\partial\eta}{\partial x}dz=\frac{1}{H}(g+\beta)\frac{\partial\eta}{\partial x}\int_{z_f}^{\eta}dz=\frac{1}{H}(g+\beta)\frac{\partial\eta}{\partial x}(\eta-z_f)=(g+\beta)\frac{\partial\eta}{\partial x} \tag{29b}$$

$$\frac{1}{H}\int_{z_f}^{\eta}\frac{\partial}{\partial x}\left(\frac{\alpha}{H}\right)\left(\frac{\eta^2-z^2}{2}-z_f(\eta-z)\right)dz=\frac{1}{3}\frac{\partial}{\partial x}\left(\frac{\alpha}{H}\right)H^2=\frac{H}{3}\frac{\partial\alpha}{\partial x}-\frac{\alpha}{3}\frac{\partial H}{\partial x} \tag{29c}$$

$$\frac{1}{H}\int_{z_f}^{\eta}\frac{\alpha}{H}\left(H\frac{\partial\eta}{\partial x}-(\eta-z)\frac{\partial z_f}{\partial x}\right)dz=\frac{1}{H}\frac{\alpha}{H}\int_{z_f}^{\eta}\left(H\frac{\partial\eta}{\partial x}-\eta\frac{\partial z_f}{\partial x}+z\frac{\partial z_f}{\partial x}\right)dz=\alpha\left(\frac{\partial\eta}{\partial x}-\frac{1}{2}\frac{\partial z_f}{\partial x}\right) \tag{29d}$$

The sum of (29a), (29b), (29c) and (29d) by taking into account, $z_f=\eta-H$, yields:

$$-\frac{1}{H}\int_{z_f}^{\eta}\frac{1}{\rho}\frac{\partial p}{\partial x}dz=-\frac{\partial \beta}{\partial x}\frac{H}{2}-(g+\beta)\frac{\partial \eta}{\partial x}-\left(\frac{H}{3}\frac{\partial \alpha}{\partial x}-\frac{\alpha}{3}\frac{\partial H}{\partial x}\right)-\alpha\left(\frac{\partial \eta}{\partial x}-\frac{1}{2}\frac{\partial(\eta-H)}{\partial x}\right) \tag{30}$$

After expansion, simplification and rearrangement, equation (30) results in (31a) which is the final mathematical formulation of the vertically-averaged pressure gradient in the x direction:

$$-\frac{1}{H}\int_{z_f}^{\eta}\frac{1}{\rho}\frac{\partial p}{\partial x}dz=-g\frac{\partial \eta}{\partial x}-H\frac{\partial}{\partial x}\left(\frac{\alpha}{3}+\frac{\beta}{2}\right)-\frac{\partial \eta}{\partial x}\left(\frac{\alpha}{2}+\beta\right)-\frac{\partial H}{\partial x}\left(\frac{\alpha}{6}\right) \tag{31a}$$

Similarly, equation (31b) is the mathematical formulation of the vertically-averaged pressure gradient in the y direction:

$$-\frac{1}{H}\int_{z_f}^{\eta}\frac{1}{\rho}\frac{\partial p}{\partial y}dz=-g\frac{\partial \eta}{\partial y}-H\frac{\partial}{\partial y}\left(\frac{\alpha}{3}+\frac{\beta}{2}\right)-\frac{\partial \eta}{\partial y}\left(\frac{\alpha}{2}+\beta\right)-\frac{\partial H}{\partial y}\left(\frac{\alpha}{6}\right) \tag{31b}$$

On the RHS of (31a) or (31b), the first term represents that of the hydrostatic pressure gradient while the other terms account for dynamic pressure forces on the flow (due to either rapid vertical flow variations and/or vertical curves in the flow paths).

2.8.- Mathematical formulation of the Serre equations

The 2DH Serre model is obtained by adding the dynamic pressure terms to the standard SV equations. Therefore, the hydrostatic pressure gradients terms (i.e., $-g\,\partial\eta/\partial x$ and $-g\,\partial\eta/\partial y$) on the RHS of the two SV dynamic equations (6b and 6c) are simply replaced with the RHS of (31a) and (31b) respectively. Adding the 2DH continuity equation to close the resulting system and rearranging yield:

$$\frac{\partial H}{\partial t}+\frac{\partial\left(HU\right)}{\partial x}+\frac{\partial\left(HV\right)}{\partial y}=0 \tag{32a}$$

$$\begin{aligned}&\frac{\partial U}{\partial t}+U\frac{\partial U}{\partial x}+V\frac{\partial U}{\partial y}+\frac{1}{\rho H}\left(\tau_x^f-\tau_x^s\right)-\frac{\partial}{\partial x}\left(\nu_{xx}\frac{\partial U}{\partial x}\right)-\frac{\partial}{\partial x}\left(\nu_{xy}\frac{\partial U}{\partial y}\right)\\&-\frac{\partial}{\partial y}\left(\nu_{yx}\frac{\partial U}{\partial x}\right)-\frac{\partial}{\partial y}\left(\nu_{yy}\frac{\partial U}{\partial y}\right)+g\frac{\partial\eta}{\partial x}=-H\frac{\partial}{\partial x}\left(\frac{\alpha}{3}+\frac{\beta}{2}\right)-\frac{\partial\eta}{\partial x}\left(\frac{\alpha}{2}+\beta\right)-\frac{\partial H}{\partial x}\left(\frac{\alpha}{6}\right)\end{aligned} \tag{32b}$$

$$\begin{aligned}&\frac{\partial V}{\partial t}+U\frac{\partial V}{\partial x}+V\frac{\partial V}{\partial y}+\frac{1}{\rho H}\left(\tau_y^f-\tau_y^s\right)-\frac{\partial}{\partial x}\left(\nu_{xx}\frac{\partial V}{\partial x}\right)-\frac{\partial}{\partial x}\left(\nu_{xy}\frac{\partial V}{\partial y}\right)\\&-\frac{\partial}{\partial y}\left(\nu_{yx}\frac{\partial V}{\partial x}\right)-\frac{\partial}{\partial y}\left(\nu_{yy}\frac{\partial V}{\partial y}\right)+g\frac{\partial\eta}{\partial y}=-H\frac{\partial}{\partial y}\left(\frac{\alpha}{3}+\frac{\beta}{2}\right)-\frac{\partial\eta}{\partial y}\left(\frac{\alpha}{2}+\beta\right)-\frac{\partial H}{\partial y}\left(\frac{\alpha}{6}\right)\end{aligned} \tag{32c}$$

In this system, all the variables have been previously defined.

The first equation in (32) represents the 2DH continuity equation (i.e., conservation of mass) while the two following equations represent the 2DH Serre dynamic equations (i.e., conservation of momentum). The principal unknown variables are the mean velocities (U and V), the position of the free surface of the flow (η) and/or the water depth (H).

These Serre equations can model the flows with dynamic pressure at a solid bottom, as well for the case where the bottom is also a free surface as in a free overfall (e.g., weirs). In the latter case, the bottom level z_f also becomes an unknown variable, which would require a fourth supplementary equation to close the system. For solid bed applications,

the Serre equations could be useful to simulate high-amplitude waves propagating in shallow water. They could also be used for many applications related to highly unsteady flows (e.g., dambreak simulations) or to highly non-uniform flows (e.g., spillway, transition flows).

The RHS of the two dynamics equations (32b) and (32c) are the supplementary terms that are added to the traditional SV equations to form the Serre equations and they translate the effects of dynamic pressure on flow. They are characterized by the presence of Serre's formulation of the vertical accelerations expressed as α (total water depth increase acceleration) and β (vertical acceleration of the bottom flow). If the effects of vertical accelerations are neglected or are negligible (i.e., if $\alpha = \beta = 0$), the RHS of the two dynamic equations (32b and 32c) become zero and they are reduced to the classic SV dynamic equations.

It should be noted that, at the mathematical level, the inclusion of the vertical acceleration terms on the RHS of equations (32b) and (32c) does increase the complexity of their resolution particularly since there is the presence of higher order derivatives. At the application level, this may result in additional computational effort. In the following section, a method to simplify their resolution is presented leading to a new formulation for the Serre PDE.

2.9.- Reformulating the Serre equations

The dynamic pressure terms in the RHS of equations (32b) and (32c) are very difficult to discretize because (1) they are mixed spatial-temporal terms (because α and β contain both temporal and spatial derivatives) and (2) they are higher order (since α and β are second order derivatives, the combined effect is third order). The objective of this section of this study is to separate variables and reduce the order of the derivatives. The resulting

new formulation of the Serre equations will then be amenable to be used in any given number of numerical schemes.

Although the separation of the variables is possible for free overfall types of flow (i.e., when the bottom of the flow is also a free surface), it is quite complex. Furthermore, because most applications entail flow with a known channel bottom (e.g., spillways and dambreak applications), only the solid bottom boundary condition will be treated in this section; even if the moving bottom boundary case is also possible, it is omitted.

For the solid bed case, after developing, simplifying and rearranging equations (32b) and (32c), the system of Serre equations can be put into the following form:

$$\frac{\partial H}{\partial t}+\frac{\partial(HU)}{\partial x}+\frac{\partial(HV)}{\partial y}=0 \tag{33a}$$

$$\begin{aligned}&\frac{\partial U}{\partial t}+U\frac{\partial U}{\partial x}+V\frac{\partial U}{\partial y}+\frac{1}{\rho H}\left(\tau_x^f-\tau_x^s\right)-\frac{\partial}{\partial x}\left(\nu_{xx}\frac{\partial U}{\partial x}\right)-\frac{\partial}{\partial x}\left(\nu_{xy}\frac{\partial U}{\partial y}\right)\\&-\frac{\partial}{\partial y}\left(\nu_{yx}\frac{\partial U}{\partial x}\right)-\frac{\partial}{\partial y}\left(\nu_{yy}\frac{\partial U}{\partial y}\right)+g\frac{\partial \eta}{\partial x}=-\frac{H}{3}\frac{\partial \alpha}{\partial x}-\frac{H}{2}\frac{\partial \beta}{\partial x}-\frac{\alpha}{2}\frac{\partial \eta}{\partial x}-\beta\frac{\partial \eta}{\partial x}-\frac{\alpha}{6}\frac{\partial H}{\partial x}\end{aligned} \tag{33b}$$

$$\begin{aligned}&\frac{\partial V}{\partial t}+U\frac{\partial V}{\partial x}+V\frac{\partial V}{\partial y}+\frac{1}{\rho H}\left(\tau_y^f-\tau_y^s\right)-\frac{\partial}{\partial x}\left(\nu_{xx}\frac{\partial V}{\partial x}\right)-\frac{\partial}{\partial x}\left(\nu_{xy}\frac{\partial V}{\partial y}\right)\\&-\frac{\partial}{\partial y}\left(\nu_{yx}\frac{\partial V}{\partial x}\right)-\frac{\partial}{\partial y}\left(\nu_{yy}\frac{\partial V}{\partial y}\right)+g\frac{\partial \eta}{\partial y}=-\frac{H}{3}\frac{\partial \alpha}{\partial y}-\frac{H}{2}\frac{\partial \beta}{\partial y}-\frac{\alpha}{2}\frac{\partial \eta}{\partial y}-\beta\frac{\partial \eta}{\partial y}-\frac{\alpha}{6}\frac{\partial H}{\partial y}\end{aligned} \tag{33c}$$

The first step in reformulating the Serre equations consists of creating two vertical velocity variables defined as:

$$w_H=\frac{DH}{Dt}=\frac{\partial H}{\partial t}+U\frac{\partial H}{\partial x}+V\frac{\partial H}{\partial y} \tag{34a}$$

$$w_{HL}=-\frac{\partial H}{\partial t}=\frac{\partial(HU)}{\partial x}+\frac{\partial(HV)}{\partial y} \tag{34b}$$

For the general conditions, the vertical velocity at the bed was w_f. To avoid confusion, for the solid bed applications, it is renamed w_{fs}.

Taking into account the continuity equation and the fact of the immobility of the bottom, from (13c), the vertical velocity at the bed becomes:

$$w_{fs} = U\frac{\partial z_f}{\partial x} + V\frac{\partial z_f}{\partial y} \tag{35a}$$

and, from equation (34), the vertical velocity of the water column becomes

$$w_H = -H\frac{\partial U}{\partial x} - H\frac{\partial V}{\partial y} \tag{35b}$$

In addition, the Serre accelerations α and β must be reformulated using w_{fs} and w_H, which leads to the following equations:

$$\alpha = \frac{\partial w_H}{\partial t} + U\frac{\partial w_H}{\partial x} + V\frac{\partial w_H}{\partial y} \tag{36a}$$

$$\beta = \frac{\partial w_{fs}}{\partial t} + U\frac{\partial w_{fs}}{\partial x} + V\frac{\partial w_{fs}}{\partial y} \tag{36b}$$

With the operation of the partial derivative being commutative, by taking into account equations (36a) and (36b), the five additional Serre terms of (33b) become respectively:

$$-\frac{H}{3}\frac{\partial \alpha}{\partial x} = -\frac{H}{3}\frac{\partial}{\partial t}\left(\frac{\partial w_H}{\partial x}\right) - \frac{H}{3}\frac{\partial}{\partial x}\left(U\frac{\partial w_H}{\partial x}\right) - \frac{H}{3}\frac{\partial}{\partial x}\left(V\frac{\partial w_H}{\partial y}\right) \tag{37}$$

$$-\frac{H}{2}\frac{\partial \beta}{\partial x} = -\frac{H}{2}\frac{\partial}{\partial t}\left(\frac{\partial w_{fs}}{\partial x}\right) - \frac{H}{2}\frac{\partial}{\partial x}\left(U\frac{\partial w_{fs}}{\partial x}\right) - \frac{H}{2}\frac{\partial}{\partial x}\left(V\frac{\partial w_{fs}}{\partial y}\right) \tag{38}$$

$$-\frac{\alpha}{2}\frac{\partial \eta}{\partial x} = -\frac{1}{2}\frac{\partial \eta}{\partial x}\frac{\partial w_H}{\partial t} - \frac{1}{2}\frac{\partial \eta}{\partial x}\left(U\frac{\partial w_H}{\partial x} + V\frac{\partial w_H}{\partial y}\right) \tag{39}$$

$$-\beta\frac{\partial \eta}{\partial x} = -\frac{\partial \eta}{\partial x}\frac{\partial w_{fs}}{\partial t} - \frac{\partial \eta}{\partial x}\left(U\frac{\partial w_{fs}}{\partial x} + V\frac{\partial w_{fs}}{\partial y}\right) \tag{40}$$

$$-\frac{\alpha}{6}\frac{\partial H}{\partial x} = -\frac{1}{6}\frac{\partial H}{\partial x}\frac{\partial w_H}{\partial t} - \frac{1}{6}\frac{\partial H}{\partial x}\left(U\frac{\partial w_H}{\partial x} + V\frac{\partial w_H}{\partial y}\right) \tag{41}$$

The first term of the RHS of equations (37) and (38) consists of a mixed spatial-temporal derivative and therefore a second step is required to separate them into distinct parts.

By using the general principle to calculate the derivative of a product, the first term of the RHS of (37) gives:

$$\frac{H}{3}\frac{\partial}{\partial t}\left(\frac{\partial w_H}{\partial x}\right) = \frac{\partial}{\partial t}\left(\frac{H}{3}\frac{\partial w_H}{\partial x}\right) - \frac{1}{3}\frac{\partial H}{\partial t}\frac{\partial w_H}{\partial x} \tag{42}$$

The substitution of equation (34b) into (42) yields:

$$\frac{H}{3}\frac{\partial}{\partial t}\left(\frac{\partial w_H}{\partial x}\right) = \frac{\partial}{\partial t}\left(\frac{H}{3}\frac{\partial w_H}{\partial x}\right) + \frac{w_{HL}}{3}\frac{\partial w_H}{\partial x} \tag{43}$$

Similarly, the first term of the RHS of equation (38) can be rewritten into the following:

$$\frac{H}{2}\frac{\partial}{\partial t}\left(\frac{\partial w_{fs}}{\partial x}\right) = \frac{\partial}{\partial t}\left(\frac{H}{2}\frac{\partial w_{fs}}{\partial x}\right) + \frac{w_{HL}}{2}\frac{\partial w_{fs}}{\partial x} \tag{44}$$

It is now necessary to reformulate the first term of the RHS of equations (39), (40) and (41) respectively. They consist of a product of a spatial derivative and of a temporal derivative. By using the general principle to calculate the derivative of a product, the first term of the RHS of equation (39) gives:

$$\frac{1}{2}\frac{\partial\eta}{\partial x}\frac{\partial w_H}{\partial t}=\frac{\partial}{\partial t}\left(\frac{w_H}{2}\frac{\partial\eta}{\partial x}\right)-\frac{w_H}{2}\frac{\partial}{\partial t}\left(\frac{\partial\eta}{\partial x}\right) \tag{45}$$

With the operation of the partial derivative being commutative, equation (45) becomes:

$$\frac{1}{2}\frac{\partial\eta}{\partial x}\frac{\partial w_H}{\partial t}=\frac{\partial}{\partial t}\left(\frac{w_H}{2}\frac{\partial\eta}{\partial x}\right)-\frac{w_H}{2}\frac{\partial}{\partial x}\left(\frac{\partial\eta}{\partial t}\right) \tag{46}$$

Also, because of the immobility of the bottom, relation (47) is true:

$$\frac{\partial H}{\partial t}=\frac{\partial\eta}{\partial t} \tag{47}$$

and equation (46) becomes:

$$\frac{1}{2}\frac{\partial\eta}{\partial x}\frac{\partial w_H}{\partial t}=\frac{\partial}{\partial t}\left(\frac{w_H}{2}\frac{\partial\eta}{\partial x}\right)-\frac{w_H}{2}\frac{\partial}{\partial x}\left(\frac{\partial H}{\partial t}\right) \tag{48}$$

The continuity equation is then introduced and the resulting equation (49) constitutes the reformulated version of the first term of the RHS of equation (39):

$$\frac{1}{2}\frac{\partial\eta}{\partial x}\frac{\partial w_H}{\partial t}=\frac{\partial}{\partial t}\left(\frac{w_H}{2}\frac{\partial\eta}{\partial x}\right)+\frac{w_H}{2}\frac{\partial w_{HL}}{\partial x} \tag{49}$$

The same procedure applies also to the first term of the RHS of (40), which becomes:

$$\frac{\partial\eta}{\partial x}\frac{\partial w_{fs}}{\partial t}=\frac{\partial}{\partial t}\left(w_{fs}\frac{\partial\eta}{\partial x}\right)+w_{fs}\frac{\partial w_{HL}}{\partial x} \tag{50}$$

As for the first term of equation (41), it becomes:

$$\frac{1}{6}\frac{\partial H}{\partial x}\frac{\partial w_H}{\partial t}=\frac{\partial}{\partial t}\left(\frac{w_H}{6}\frac{\partial H}{\partial x}\right)-\frac{w_H}{6}\frac{\partial}{\partial t}\left(\frac{\partial H}{\partial x}\right)=\frac{\partial}{\partial t}\left(\frac{w_H}{6}\frac{\partial H}{\partial x}\right)-\frac{w_H}{6}\frac{\partial}{\partial x}\left(\frac{\partial H}{\partial t}\right) \tag{51}$$

Thereafter, the substitution of the 2DH continuity equation into (51) leads to the reformulated version of the first term in the RHS of equation (41):

$$\frac{1}{6}\frac{\partial H}{\partial x}\frac{\partial w_H}{\partial t}=\frac{\partial}{\partial t}\left(\frac{w_H}{6}\frac{\partial H}{\partial x}\right)+\frac{w_H}{6}\frac{\partial w_{HL}}{\partial x} \tag{52}$$

Finally, the equations (43), (44), (49), (50) and (52) are substituted respectively into equations (37), (38), (39), (40) and (41), giving:

$$\begin{aligned}&-\frac{H}{3}\frac{\partial \alpha}{\partial x}-\frac{H}{2}\frac{\partial \beta}{\partial x}-\frac{\alpha}{2}\frac{\partial \eta}{\partial x}-\beta\frac{\partial \eta}{\partial x}-\frac{\alpha}{6}\frac{\partial H}{\partial x}=-w_{HL}\left(\frac{1}{3}\frac{\partial w_H}{\partial x}+\frac{1}{2}\frac{\partial w_{fs}}{\partial x}\right)-\frac{\partial w_{HL}}{\partial x}\left(\frac{2w_H}{3}+w_{fs}\right)\\&-\left(U\frac{\partial w_H}{\partial x}+V\frac{\partial w_H}{\partial y}\right)\left(\frac{1}{2}\frac{\partial \eta}{\partial x}+\frac{1}{6}\frac{\partial H}{\partial x}\right)-\frac{H}{2}\frac{\partial}{\partial x}\left(U\frac{\partial w_{fs}}{\partial x}+V\frac{\partial w_{fs}}{\partial y}\right)-\frac{\partial \eta}{\partial x}\left(U\frac{\partial w_{fs}}{\partial x}+V\frac{\partial w_{fs}}{\partial y}\right)\\&-\frac{H}{3}\frac{\partial}{\partial x}\left(U\frac{\partial w_H}{\partial x}+V\frac{\partial w_H}{\partial y}\right)-\frac{\partial}{\partial t}\left(\frac{H}{3}\frac{\partial w_H}{\partial x}+\frac{H}{2}\frac{\partial w_{fs}}{\partial x}+\frac{w_H}{2}\frac{\partial \eta}{\partial x}+w_{fs}\frac{\partial \eta}{\partial x}+\frac{w_H}{6}\frac{\partial H}{\partial x}\right)\end{aligned} \tag{53}$$

After creating the following intermediate variables defined below,

$$U_z=\frac{H}{3}\frac{\partial w_H}{\partial x}+\frac{H}{2}\frac{\partial w_{fs}}{\partial x}+\frac{w_H}{2}\frac{\partial \eta}{\partial x}+w_{fs}\frac{\partial \eta}{\partial x}+\frac{w_H}{6}\frac{\partial H}{\partial x} \tag{54a}$$

$$\begin{aligned}a_{zx}=&\,w_{HL}\left(\frac{1}{3}\frac{\partial w_H}{\partial x}+\frac{1}{2}\frac{\partial w_{fs}}{\partial x}\right)+\frac{\partial w_{HL}}{\partial x}\left(\frac{2w_H}{3}+w_{fs}\right)+\left(U\frac{\partial w_H}{\partial x}+V\frac{\partial w_H}{\partial y}\right)\left(\frac{1}{2}\frac{\partial \eta}{\partial x}+\frac{1}{6}\frac{\partial H}{\partial x}\right)\\&+\frac{H}{2}\frac{\partial}{\partial x}\left(U\frac{\partial w_{fs}}{\partial x}+V\frac{\partial w_{fs}}{\partial y}\right)+\frac{H}{3}\frac{\partial}{\partial x}\left(U\frac{\partial w_H}{\partial x}+V\frac{\partial w_H}{\partial y}\right)+\frac{\partial \eta}{\partial x}\left(U\frac{\partial w_{fs}}{\partial x}+V\frac{\partial w_{fs}}{\partial y}\right)\end{aligned} \tag{54b}$$

equation (53) becomes:

$$-\frac{H}{3}\frac{\partial\alpha}{\partial x}-\frac{H}{2}\frac{\partial\beta}{\partial x}-\frac{\alpha}{2}\frac{\partial\eta}{\partial x}-\beta\frac{\partial\eta}{\partial x}-\frac{\alpha}{6}\frac{\partial H}{\partial x}=-\frac{\partial U_z}{\partial t}-a_{zx} \tag{55}$$

Therefore, the first of the dynamic Serre equations (33b) becomes:

$$\begin{aligned}&\frac{\partial}{\partial t}\left(U+U_z\right)+U\frac{\partial U}{\partial x}+V\frac{\partial U}{\partial y}+\frac{1}{\rho H}\left(\tau_x^f-\tau_x^s\right)-\frac{\partial}{\partial x}\left(\nu_{xx}\frac{\partial U}{\partial x}\right)-\frac{\partial}{\partial x}\left(\nu_{xy}\frac{\partial U}{\partial y}\right)\\&-\frac{\partial}{\partial y}\left(\nu_{yx}\frac{\partial U}{\partial x}\right)-\frac{\partial}{\partial y}\left(\nu_{yy}\frac{\partial U}{\partial y}\right)+g\frac{\partial\eta}{\partial x}+a_{zx}=0\end{aligned} \tag{56}$$

Similarly, the second dynamic Serre equation (33c) becomes:

$$\begin{aligned}&\frac{\partial}{\partial t}\left(V+V_z\right)+U\frac{\partial V}{\partial x}+V\frac{\partial V}{\partial y}+\frac{1}{\rho H}\left(\tau_y^f-\tau_y^s\right)-\frac{\partial}{\partial x}\left(\nu_{xx}\frac{\partial V}{\partial x}\right)-\frac{\partial}{\partial x}\left(\nu_{xy}\frac{\partial V}{\partial y}\right)\\&-\frac{\partial}{\partial y}\left(\nu_{yx}\frac{\partial V}{\partial x}\right)-\frac{\partial}{\partial y}\left(\nu_{yy}\frac{\partial V}{\partial y}\right)+g\frac{\partial\eta}{\partial y}+a_{zy}=0\end{aligned} \tag{57}$$

where,

$$V_z=\frac{H}{3}\frac{\partial w_H}{\partial y}+\frac{H}{2}\frac{\partial w_f}{\partial y}+\frac{w_H}{2}\frac{\partial\eta}{\partial y}+w_{fs}\frac{\partial\eta}{\partial y}+\frac{w_H}{6}\frac{\partial H}{\partial y} \tag{58a}$$

$$\begin{aligned}a_{zy}=&\,w_{HL}\left(\frac{1}{3}\frac{\partial w_H}{\partial y}+\frac{1}{2}\frac{\partial w_{fs}}{\partial y}\right)+\frac{\partial w_{HL}}{\partial y}\left(\frac{2w_H}{3}+w_{fs}\right)+\left(\frac{1}{2}\frac{\partial\eta}{\partial y}+\frac{1}{6}\frac{\partial H}{\partial y}\right)\left(U\frac{\partial w_H}{\partial x}+V\frac{\partial w_H}{\partial y}\right)\\&+\frac{H}{2}\frac{\partial}{\partial y}\left(U\frac{\partial w_{fs}}{\partial x}+V\frac{\partial w_{fs}}{\partial y}\right)+\frac{H}{3}\frac{\partial}{\partial y}\left(U\frac{\partial w_H}{\partial x}+V\frac{\partial w_H}{\partial y}\right)+\frac{\partial\eta}{\partial y}\left(U\frac{\partial w_{fs}}{\partial x}+V\frac{\partial w_{fs}}{\partial y}\right)\end{aligned} \tag{58b}$$

The new condensed formulation of the Serre model for solid bed applications is therefore:

$$\frac{\partial \eta}{\partial t}+\frac{\partial (HU)}{\partial x}+\frac{\partial (HV)}{\partial y}=0 \tag{59a}$$

$$\frac{\partial}{\partial t}(U+U_z)+U\frac{\partial U}{\partial x}+V\frac{\partial U}{\partial y}+\frac{1}{\rho H}(\tau_x^f-\tau_x^s)-\frac{\partial}{\partial x}\left(\nu_{xx}\frac{\partial U}{\partial x}\right)-\frac{\partial}{\partial x}\left(\nu_{xy}\frac{\partial U}{\partial y}\right)$$
$$-\frac{\partial}{\partial y}\left(\nu_{yx}\frac{\partial U}{\partial x}\right)-\frac{\partial}{\partial y}\left(\nu_{yy}\frac{\partial U}{\partial y}\right)+g\frac{\partial \eta}{\partial x}+a_{zx}=0 \tag{59b}$$

$$\frac{\partial}{\partial t}(V+V_z)+U\frac{\partial V}{\partial x}+V\frac{\partial V}{\partial y}+\frac{1}{\rho H}(\tau_y^f-\tau_y^s)-\frac{\partial}{\partial x}\left(\nu_{xx}\frac{\partial V}{\partial x}\right)-\frac{\partial}{\partial x}\left(\nu_{xy}\frac{\partial V}{\partial y}\right)$$
$$-\frac{\partial}{\partial y}\left(\nu_{yx}\frac{\partial V}{\partial x}\right)-\frac{\partial}{\partial y}\left(\nu_{yy}\frac{\partial V}{\partial y}\right)+g\frac{\partial \eta}{\partial y}+a_{zy}=0 \tag{59c}$$

where all the intermediate variables have been previously defined.

This system of three equations inter-relates the three principal variables $(U,\ V,\ H)$ and thereby describes the 2DH hydrodynamic field subject to boundary and initial conditions. The effects of total vertical acceleration $\left(i.e., Dw/Dt=\partial w/\partial t+U\,\partial w/\partial x+V\,\partial w/\partial y+w\partial w/\partial z\right)$ and therefore the effects of non-hydrostatic pressure are accounted for by the supplementary Serre terms (i.e., U_z, V_z, a_{zx} and a_{zy}) appearing in the two dynamic equations.

Conclusion

In this chapter, the 2DH Serre model has been developed, step-by-step, from the 3D PDE of fluid motion in a gravity field. The basic hypothesis of the Serre equations is that the horizontal velocity components are constant over the vertical. Consequently, the vertical component of the velocity is linearly distributed over the depth (i.e., the vertical acceleration is constant over the vertical). The Serre equations are identical to the ones used in the SV model except for the addition of supplementary terms appearing on the RHS of equations (33b) and (33c) that account for the effects of dynamic pressure. Unlike the SV equations, which assume that there is no significant vertical acceleration in the flow, the Serre model can simulate flows that have significant vertical acceleration. Given that when the vertical flow acceleration exists, the fluid pressure is no longer hydrostatic; the Serre equations can be used to simulate those flows having a dynamic pressure component. The Serre model formulation shows the presence of higher derivatives that have mathematical implications and could require additional computational effort. Moreover, for applications wherein the bottom boundary is solid (i.e., no free overfalls), the additional highly non-linear Serre terms have been reduced from 3^{rd} to 2^{nd} order and have been separated into their spatial and temporal components (equations 59). This system of equations can be easily integrated into various numerical schemes (finite difference, finite volume, finite element, etc.). Applications include highly transient flows, such as a dambreak, or highly non-uniform flows, such as those over a spillway (be they transient or steady-state).

CHAPTER 3

Finite Element Solution of the 2DH Serre Model

Introduction

The new mathematical formulation of the Serre model is solved here by using the Finite Element Method (FEM), which is a numerical technique for finding approximate solution of a given PDE. Indeed, the FEM is a technique in which a given domain is represented as a collection of simple domains, called finite elements. Consequently, it is possible to systematically construct the weighted-residual approximation of the solution of a problem over each element (Reddy 1984). In other words, the FEM transforms the whole domain into a sum of several pieces and thus, allows calculating the solution of the given PDE on each of them. The most attractive feature of the FEM is its ability to handle complex geometries (and boundaries) with relative ease. Elements can change size and shape readily, allowing complex boundaries to be traced, as well as allowing refinement of the mesh in particularly important or rapidly varying areas. This method is fully described in (Reddy 1984, Dhatt and Touzot 1981) and it is widely used to solve the PDE of a large variety of physical phenomena.

The FEM equations are derived by using the Galerkin weighted method. In its most traditional implementation, commonly known as the Bubnov-Galerkin method, the weight functions are simply set equal to the basis functions. This results in a central approximation scheme. In open channel flow applications, the Bubnov-Galerkin method has been shown to be useful for modeling relatively flat waves, but it performs poorly in the vicinity of the steep gradients in the solution (Katopodes 1984). Instabilities appear

and the solution rapidly deteriorates (Hicks and Steffler 1994). For this reason, the Taylor–Galerkin (TG) scheme of second order is chosen in this study because it has some properties that make it possible to overcome the weakness of the most traditional Bubnov-Galerkin approach. For example, the TG solution approach is appropriate to correctly model some particular flow situations (e.g., dambreak flows) in which the advection is dominant and/or where the hydraulic parameters of the flow can vary suddenly (shock-capturing). It is also well known that the TG schemes provide a good compromise between the accuracy and speed of computations (Mabssout and Pastor 2003b).

In the rest of this chapter, the TG technique is presented as a special feature to add artificial diffusion terms in order to upwind the numerical scheme. Subsequently, the integral formulation of the weighted-residuals of the resulting Serre equations is calculated as well as its weak form. The triangular nonconforming element is described and is used for the spatial discretization of the weak form yielding the semi-discrete finite element model. Next, the temporal derivatives are approximated and the nonlinearity is solved leading to the finite element formulation of the Serre model in the form of an iterative scheme. Finally, the general initial and boundary conditions are investigated as well as the stability criterion, followed by the conclusion.

3.1.- The Taylor-Galerkin method

The basic TG approach, also known as the characteristic-Galerkin scheme, is an explicit formulation in which the unknown variables are written in terms of a Taylor series expansion in time (Donea 1984; Donea et al. 1984; Lohner et al. 1984; Selmin et al. 1985). That method was established for the study of transient stability problems but it can also be used to upwind the first order discretized spatial derivative (Robert 2008). Concretely, the main objective of the TG method is to define a scheme, which harmonizes the space and temporal precisions respectively (Robert 2008). The Taylor time series expansion is used to introduce numerical diffusion (Selmin et al. 1985).

Based on the Donea et al. (1984) approach, which consists of a Taylor series expansion of second order of the time derivatives, Robert (2008) made some simplifications and found the following artificial viscosity tensor that adds artificial diffusion terms to the SV equations:

$$k\begin{bmatrix} U^2 & UV \\ VU & V^2 \end{bmatrix} \tag{60}$$

The parameter k is given by:

$$k = C_{up}\frac{\Delta t}{2} \tag{61}$$

where Δt is the time step and C_{up} is an upwinding factor between 0 and 1.

The total diffusion coefficients in the SV dynamic equations become:

$$\begin{bmatrix} \nu_{xx} & \nu_{xy} \\ \nu_{yx} & \nu_{yy} \end{bmatrix} = \nu\begin{bmatrix} 1 & 1 \\ 1 & 1 \end{bmatrix} + k\begin{bmatrix} U^2 & UV \\ VU & V^2 \end{bmatrix} \tag{62}$$

In this study, the same tensor given by (60) is also used to add artificial diffusion terms to the Serre dynamic equations as well as to the continuity one. Additionally, the friction stresses at the free surface of the flow are neglected (i.e., $\tau_x^s = 0$ and $\tau_y^s = 0$) for the sake of simplicity and the Chézy formulation is chosen to model the friction resistance force at the bed (see, Molls and Chaudhry 1995):

$$\tau_x^f = \rho g U\frac{\sqrt{U^2+V^2}}{C_c^2} \tag{63a}$$

$$\tau_y^f = \rho g V\frac{\sqrt{U^2+V^2}}{C_c^2} \tag{63b}$$

where C_c is Chézy's coefficient.

However, when using the Strickler's roughness coefficient K_s, the following approximation should be used to estimate the Chézy's:

$$C_c = K_s R_H^{1/6} \tag{63c}$$

where R_H is the hydraulic radius.

Consequently, the implementation of the second-order TG for the Serre model is equivalent to the Bubnov-Galerkin formulation (i.e., by using the standard FEM rule) of the following modified equations:

$$\frac{\partial}{\partial t}\left(U+U_z\right)+U\frac{\partial U}{\partial x}+V\frac{\partial U}{\partial y}+gU\frac{\sqrt{U^2+V^2}}{C_c^2 H}-\frac{\partial}{\partial x}\left(\nu_{xx}\frac{\partial U}{\partial x}\right)$$
$$-\frac{\partial}{\partial x}\left(\nu_{xy}\frac{\partial U}{\partial y}\right)-\frac{\partial}{\partial y}\left(\nu_{yx}\frac{\partial U}{\partial x}\right)-\frac{\partial}{\partial y}\left(\nu_{yy}\frac{\partial U}{\partial y}\right)+g\frac{\partial \eta}{\partial x}+a_{zx}=0 \tag{64a}$$

$$\frac{\partial}{\partial t}\left(V+V_z\right)+U\frac{\partial V}{\partial x}+V\frac{\partial V}{\partial y}+gV\frac{\sqrt{U^2+V^2}}{C_c^2 H}-\frac{\partial}{\partial x}\left(\nu_{xx}\frac{\partial V}{\partial x}\right)$$
$$-\frac{\partial}{\partial x}\left(\nu_{xy}\frac{\partial V}{\partial y}\right)-\frac{\partial}{\partial y}\left(\nu_{yx}\frac{\partial V}{\partial x}\right)-\frac{\partial}{\partial y}\left(\nu_{yy}\frac{\partial V}{\partial y}\right)+g\frac{\partial \eta}{\partial y}+a_{zy}=0 \tag{64b}$$

$$\frac{\partial H}{\partial t}+\frac{\partial\left(HU\right)}{\partial x}+\frac{\partial\left(HV\right)}{\partial y}-\frac{\partial}{\partial x}\left(kU^2\frac{\partial H}{\partial x}\right)-\frac{\partial}{\partial x}\left(kUV\frac{\partial H}{\partial y}\right)$$
$$-\frac{\partial}{\partial y}\left(kVU\frac{\partial H}{\partial x}\right)-\frac{\partial}{\partial y}\left(kV^2\frac{\partial H}{\partial y}\right)=0 \tag{64c}$$

The TG algorithms have already been successfully applied to a wide variety of flow situations where the advection phenomenon is significant; such is the case for dambreak flow problems (Safjan and Oden 1995; Tamma and Namburu 1988; Zhang and Tabarrok 1999; Quecedo and Pastor 2003; Mabssout and Pastor 2003a). It was found that the TG

finite element schemes provide a good compromise between accuracy and speed of computations (Mabssout and Pastor 2003b). Finally, the TG algorithm described here is the basic one even if some other refined versions are available (Donea et al. 1987; Bottura and Zienkiewicz 1990; Donea et al. 1992).

3.2.- Integral formulation of the weighted-residuals

The next step is to calculate the integral formulation of the weighted-residuals of the resulting Serre equations (64), yielding:

$$R_1 = \int_D \varphi_U \left(\begin{array}{l} \dfrac{\partial}{\partial t}\left(U + U_z\right) + U\dfrac{\partial U}{\partial x} + V\dfrac{\partial U}{\partial y} + gU\dfrac{\sqrt{U^2+V^2}}{C_c^2 H} - \dfrac{\partial}{\partial x}\left(\nu_{xx}\dfrac{\partial U}{\partial x}\right) \\ -\dfrac{\partial}{\partial x}\left(\nu_{xy}\dfrac{\partial U}{\partial y}\right) - \dfrac{\partial}{\partial y}\left(\nu_{yx}\dfrac{\partial U}{\partial x}\right) - \dfrac{\partial}{\partial y}\left(\nu_{yy}\dfrac{\partial U}{\partial y}\right) + g\dfrac{\partial \eta}{\partial x} + a_{zx} \end{array} \right) dD = 0 \qquad (65a)$$

$$R_2 = \int_D \varphi_V \left(\begin{array}{l} \dfrac{\partial}{\partial t}\left(V + V_z\right) + U\dfrac{\partial V}{\partial x} + V\dfrac{\partial V}{\partial y} + gV\dfrac{\sqrt{U^2+V^2}}{C_c^2 H} - \dfrac{\partial}{\partial x}\left(\nu_{xx}\dfrac{\partial V}{\partial x}\right) \\ -\dfrac{\partial}{\partial x}\left(\nu_{xy}\dfrac{\partial V}{\partial y}\right) - \dfrac{\partial}{\partial y}\left(\nu_{yx}\dfrac{\partial V}{\partial x}\right) - \dfrac{\partial}{\partial y}\left(\nu_{yy}\dfrac{\partial V}{\partial y}\right) + g\dfrac{\partial \eta}{\partial y} + a_{zy} \end{array} \right) dD = 0 \qquad (65b)$$

$$R_3 = \int_D \varphi_H \left(\begin{array}{l} \dfrac{\partial H}{\partial t} + \dfrac{\partial\left(HU\right)}{\partial x} + \dfrac{\partial\left(HV\right)}{\partial y} - \dfrac{\partial}{\partial x}\left(kU^2\dfrac{\partial H}{\partial x}\right) - \dfrac{\partial}{\partial x}\left(kUV\dfrac{\partial H}{\partial y}\right) \\ -\dfrac{\partial}{\partial y}\left(kVU\dfrac{\partial H}{\partial x}\right) - \dfrac{\partial}{\partial y}\left(kV^2\dfrac{\partial H}{\partial y}\right) \end{array} \right) dD = 0 \qquad (65c)$$

In (65), D represents the global domain of study whereas R_1, R_2 and R_3 are the integral formulation of the weighted-residuals of the two dynamic equations and of the continuity one respectively. The weight functions φ_U and φ_V are those for the first and for the second dynamic equations respectively whereas φ_H is used for the continuity one.

To reduce the order of some derivatives in (65), the weak form of the integral formulation of the weighted residuals is then calculated and yields:

$$R_1 = \int_D \varphi_U \frac{\partial}{\partial t}\left(U + U_z\right) dD + \int_D \left(\varphi_U \left(\begin{array}{l} U\dfrac{\partial U}{\partial x} + V\dfrac{\partial U}{\partial y} + g\dfrac{\partial \eta}{\partial x} \\ +gU\dfrac{\sqrt{U^2+V^2}}{C_c^2 H} + a_{zx} \end{array} \right) + \nu_{xx}\frac{\partial \varphi_U}{\partial x}\frac{\partial U}{\partial x} \right. \\ \left. + \nu_{xy}\frac{\partial \varphi_U}{\partial x}\frac{\partial U}{\partial y} + \nu_{yx}\frac{\partial \varphi_U}{\partial y}\frac{\partial U}{\partial x} + \nu_{yy}\frac{\partial \varphi_U}{\partial y}\frac{\partial U}{\partial y} \right) dD \qquad (66a)$$

$$- \oint_\Gamma \varphi_U \left(\left(\nu_{xx}\frac{\partial U}{\partial x} + \nu_{xy}\frac{\partial U}{\partial y} \right) n_x + \left(\nu_{yx}\frac{\partial U}{\partial x} + \nu_{yy}\frac{\partial U}{\partial y} \right) n_y \right) d\Gamma$$

$$R_2 = \int_D \varphi_V \frac{\partial}{\partial t}\left(V + V_z\right) dD + \int_D \left(\varphi_V \left(\begin{array}{l} U\dfrac{\partial V}{\partial x} + V\dfrac{\partial V}{\partial y} + g\dfrac{\partial \eta}{\partial y} \\ +gV\dfrac{\sqrt{U^2+V^2}}{C_c^2 H} + a_{zy} \end{array} \right) + \nu_{xx}\frac{\partial \varphi_V}{\partial x}\frac{\partial V}{\partial x} \right. \\ \left. + \nu_{xy}\frac{\partial \varphi_V}{\partial x}\frac{\partial V}{\partial y} + \nu_{yx}\frac{\partial \varphi_V}{\partial y}\frac{\partial V}{\partial x} + \nu_{yy}\frac{\partial \varphi_V}{\partial y}\frac{\partial V}{\partial y} \right) dD \qquad (66b)$$

$$- \oint_\Gamma \varphi_V \left(\left(\nu_{xx}\frac{\partial V}{\partial x} + \nu_{xy}\frac{\partial V}{\partial y} \right) n_x + \left(\nu_{yx}\frac{\partial V}{\partial x} + \nu_{yy}\frac{\partial V}{\partial y} \right) n_y \right) d\Gamma = 0$$

$$R_3 = \int_D \varphi_H \frac{\partial H}{\partial t} dD + \int_D \begin{pmatrix} -HU\dfrac{\partial \varphi_H}{\partial x} - HV\dfrac{\partial \varphi_H}{\partial y} \\ +kU^2\dfrac{\partial \varphi_H}{\partial x}\dfrac{\partial H}{\partial x} + kUV\dfrac{\partial \varphi_H}{\partial x}\dfrac{\partial H}{\partial y} \\ +kVU\dfrac{\partial \varphi_H}{\partial y}\dfrac{\partial H}{\partial x} + kV^2\dfrac{\partial \varphi_H}{\partial y}\dfrac{\partial H}{\partial y} \end{pmatrix} dD + \oint_\Gamma \varphi_H q_n d\Gamma$$
$$- \oint_\Gamma \varphi_H \left(kU^2 \frac{\partial H}{\partial x} + kUV \frac{\partial H}{\partial y} \right) n_x d\Gamma - \oint_\Gamma \varphi_H \left(kVU \frac{\partial H}{\partial x} + kV^2 \frac{\partial H}{\partial y} \right) n_y d\Gamma = 0 \qquad (66c)$$

The notation $\vec{n}$ represents the unit normal vector, with n_x and n_y being its two components in the x and y directions respectively. The symbol Γ is the boundary of the domain and q_n is the unit discharge of the flow through the boundary.

3.3.- Spatial discretization

The mesh (Figure 3.1) to be used for the spatial discretization of the system (66) consists of the triangular nonconforming elements (see Figure 3.2).

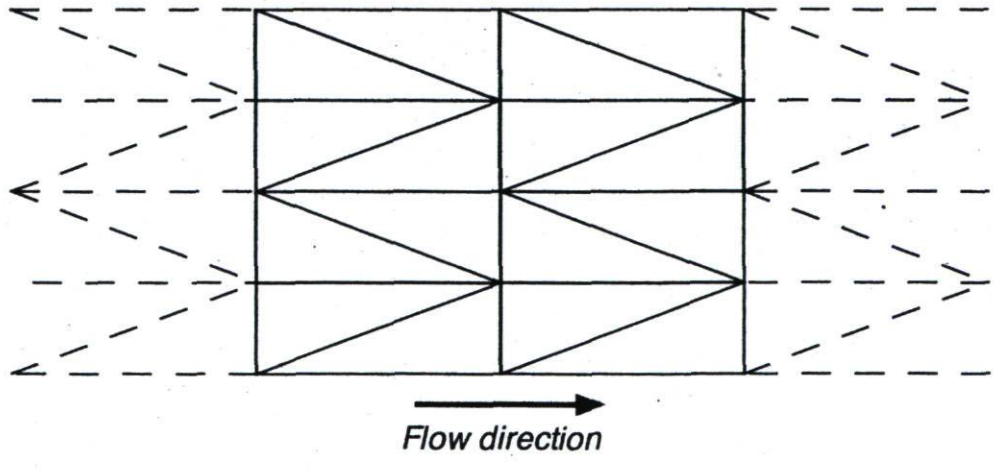

Figure 3.1: Typical mesh configuration

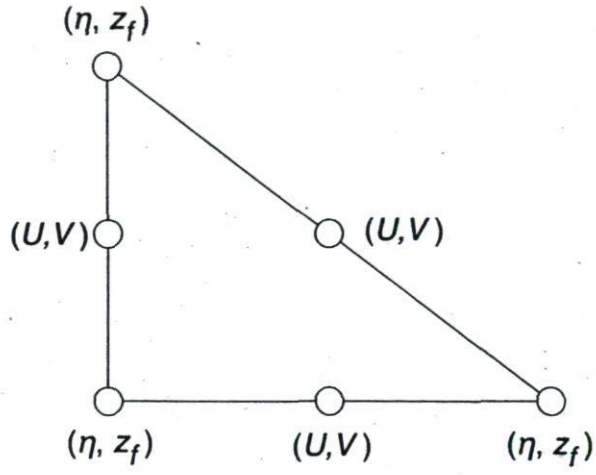

Figure 3.2: Triangular nonconforming element

For such elements, the total water depths are calculated at the vertex nodes whereas the velocity components are approximated at the mid-side nodes.

Indeed, it is a common feature of the finite element treatment of shallow water equations that small noise is produced by the spatial discretization, when both the water depth and the horizontal velocity components are approximated identically (Hua and Thomasset 1984). Shoenstadt (1980) and Williams (1981) have analyzed the solutions for one-dimensional meshes and they have recommended to staggering the variables for the shallow water equations variables. In other words, this means that the water depths (scalar quantities) are evaluated at the vertices of the triangle while the horizontal velocities (vector quantities) are evaluated at mid-sides of the triangle giving the nonconforming elements. This class of elements is preferred because they present several advantages. First, the mass matrix of the element is diagonal because of the orthogonality property of the basis functions. This means that exact calculation of some integrals is possible without lumping (which causes a loss of accuracy). Second, the continuity of diffusion fluxes between the element interfaces is automatically enforced without the need of any additional treatment, which is rather convenient for the discontinuous FEM (Hanert et al. 2004). Indeed, the grid points are also located at the mid-sides of each triangle, for boundary nodes, the direction of the normal to the boundary is defined

without ambiguity and therefore, circumvents the difficulty of satisfying exactly the no-normal flux condition at every boundary vertex (Pinder and Gray 1977). Consequently, the accuracy of the numerical solutions is improved and the time computation is reduced (Tossou 2004; Le Roux et al. 2008; Le Roux 2005).

Generally, the integrals are first calculated on a reference element after which, a Jacobian transformation is used to transpose the results obtained to the real domain. The reference element corresponding to the triangular nonconforming element is well described in (Dhatt and Touzot 1981) with the following basis functions:

$$N_H = \langle 1-\xi-\psi \quad \xi \quad \psi \rangle \tag{67a}$$

$$N = \langle 1-2\psi \quad -1+2\xi+2\psi \quad 1-2\xi \rangle \tag{67b}$$

Where N_H represent the basis functions associated respectively to each of the three vertex nodes while N are the basis functions associated to the mid-side nodes. The natural abscissa on reference element is ψ and the natural ordinate is ξ.

Consequently, equations (67a) and (67b) lead respectively to the following discrete expressions for the principal variables:

$$\tilde{\eta} = \sum_{j=1}^{3} N_{Hj} \eta_j^e \tag{68a}$$

$$\widetilde{H} = \sum_{j=1}^{3} N_{Hj} H_j^e \tag{68b}$$

$$\widetilde{z_f} = \sum_{j=1}^{3} N_{Hj} z_{fj}^e \tag{68c}$$

$$\widetilde{U} = \sum_{j=1}^{3} N_j U_j^e \tag{68d}$$

$$\widetilde{V} = \sum_{j=1}^{3} N_j V_j^e \tag{68e}$$

The symbols $\tilde{\eta}$, $\widetilde{H}$, $\widetilde{z_f}$, $\widetilde{U}$ and $\widetilde{V}$ represent the discrete expressions of η, H, z_f, U and V respectively while the notations η_j^e, H_j^e, z_{fj}^e, U_j^e and V_j^e are their respective element nodal values.

In addition, the weight functions are set equal to the basis ones, according to the Bubnov-Galerkin approach, which is used here to solve the modified Serre equations. This means that, $\varphi_U = \varphi_V = N$ for the two dynamic equations and $\varphi_H = N_H$ for the continuity one.

It is now possible to spatially discretize the weak form of the integral formulation of the weighted-residuals by substituting the discrete expressions (68) into the system (66) and by taking into account the appropriate weight functions.

For the sake of conciseness, the intermediate calculations are omitted and the operation leads to the following equation in matrix form, which corresponds to the element semi-discrete (spatially discrete) formulation of the Serre model:

$$\left\{R^e\right\} = \left[M^e\right]\left\{\frac{\partial \Omega^e}{\partial t}\right\} + \left\{\frac{\partial F_s^e}{\partial t}\right\} + \left[K^e\right]\left\{\Omega^e\right\} - \left\{F^e\right\} \tag{69}$$

In (69), $\left[M^e\right]$ is the element mass matrix; $\left[K^e\right]$ is the element stiffness matrix; $\left\{F^e\right\}$ is the element force vector while $\left\{F_s^e\right\}$ is the element force vector due to the Serre supplementary terms.

The vectors $\left\{R^e\right\}$ and $\left\{\Omega^e\right\}$ are defined respectively as follow:

$$\left\{R^e\right\} = \begin{Bmatrix} R_1^e \\ R_2^e \\ R_3^e \end{Bmatrix} \tag{70a}$$

$$\left\{\Omega^e\right\}=\begin{Bmatrix}\left\{U^e\right\}\\ \left\{V^e\right\}\\ \left\{H^e\right\}\end{Bmatrix} \tag{70b}$$

R_1^e, R_2^e and R_3^e are the respective discrete expressions of R_1, R_2 and R_3 defined previously while $\left\{U^e\right\}$, $\left\{V^e\right\}$ and $\left\{H^e\right\}$ are the vectors of the element nodal values of U, V and H respectively.

The terms of those different matrices and vectors are defined in the appendix.

3.4.- Time derivatives integration and solution to the nonlinearity

To obtain the final finite element scheme, it is now necessary to discretize the time derivative in equation (69) and to solve the nonlinearity. Indeed, the global (assembled) version of (69) must be considered. Therefore, a general temporal scheme is applied for the time derivative discretization while the substitution method is used to solve the nonlinearity (Tossou 2004; Robert 2008). This method is chosen instead of the Newton-Raphson's because the calculus of the first variation of the weighted-residuals is difficult enough and would lead to a complex expression.

The resulting numerical formulation (spatially and temporally discrete) of the Serre model gives the following iterative and incremental expression:

$$\begin{cases}\left\{\Omega_{t+\Delta t}\right\}=\left\{\Omega_t\right\}+\left\{\Delta\Omega\right\}\\ \left[K_{nl}\right]\left\{\Delta\Omega\right\}=\left\{F_{nl}\right\}\end{cases} \tag{71}$$

where,

$$\left[K_{nl}\right]=\left[\left[M\right]+\theta\Delta t\left[K\left(\Omega^{i}_{t+\Delta t}\right)\right]\right] \tag{72a}$$

$$\begin{aligned}\left\{F_{nl}\right\}=&-\left[\left[M\right]+\theta\Delta t\left[K\left(\Omega^{i}_{t+\Delta t}\right)\right]\right]\left\{\Omega^{i}_{t+\Delta t}\right\}-\left\{F_{s}\left(\Omega^{i}_{t+\Delta t}\right)\right\}+\left\{F_{s}\left(\Omega_{t}\right)\right\}\\&+\theta\Delta t\left\{F\left(\Omega^{i}_{t+\Delta t}\right)\right\}+\left(1-\theta\right)\Delta t\left\{F\left(\Omega_{t}\right)\right\}+\left[\left[M\right]-\left(1-\theta\right)\Delta t\left[K\left(\Omega_{t}\right)\right]\right]\left\{\Omega_{t}\right\}\end{aligned} \tag{72b}$$

In (72), $\left[M\right]$, $\left[K\right]$, $\left\{F_{s}\right\}$ and $\left\{F\right\}$ are the global (assembled) versions of the element matrices and vectors defined previously. The superscripts refer to the level of iteration whereas the subscripts refer to the time step. The symbol θ represents the coefficient that defines the temporal scheme to be considered. The most usual values are: $\theta=1$ for the backward difference scheme; $\theta=0$ for the forward difference scheme; $\theta=1/2$ for the Cranck-Nicolson scheme and $\theta=2/3$ for the Galerkin scheme.

Finally, it should be noted that the choice of the time step value (i.e., Δt), must be made in reference with the size of each element of the domain mesh (i.e., Δx and Δy). Therefore, this is subjected to the following stability condition characterized by the Number of Courant-Friedrichs-Lewy (N_{CFL}) (see, Liska and Wendroff 1999):

$$N_{CFL}=MAX\left[\frac{\Delta t}{\Delta x}\left|U\pm\sqrt{gH}\right|,\ \frac{\Delta t}{\Delta y}\left|V\pm\sqrt{gH}\right|\right]\leq 1 \tag{73}$$

3.5.- Initial conditions

The initial conditions describe the state of the flow at the beginning of the simulation. Therefore, the characteristics of the flow must be known and imposed. Generally, the primary output variables of the model (i.e., the initial flow depth and the velocity components) in the whole domain must be specified for each flow situation. However,

those initial conditions depend on the flow situation at hand so that they will be presented individually for each test of validation investigated in the next chapter.

3.6.- Boundary conditions

For the overall flow simulations in this study, a rectangular channel is used. Thus, the upstream, the downstream and the two sidewalls are the boundaries of the domain. As boundary conditions, the water level or the total water depth is known and imposed at the upstream whereas the sidewalls are assumed impermeable in each test. For the impermeability condition, the velocity component that is normal to the walls, is set equal to zero and the tangential component is let free. For the downstream, the condition to be imposed must be chosen delicately. Indeed, the definition of the boundary conditions at the open boundaries remains an old problem in Regional Ocean modeling so that in the past decade, there has been much interest in the development of such conditions for use in numerical models.

The purpose of the open boundary conditions is to permit the passage of outward propagating disturbances with a minimum of reflection. Many different schemes have been proposed in the literature and the principals are listed as follows:

- ✓ The Sommerfeld approach, which is the basis of the radiation methods (Sommerfeld 1949);
- ✓ The Orlanski method, which is an adaptative version of the previous one mentioned (Orlanski 1976);
- ✓ The Flather technique, which is a temporal integration of the Sommerfeld conditions (Flather 1976);
- ✓ The periodic boundary conditions for which, the flow hydrodynamics (velocity and water depth) are assumed cyclic or periodic (Brechler 1992);

- ✓ The characteristic boundary conditions for which, the incoming characteristic variable is specified while leaving the outgoing one free (Nycander et al. 2008);

- ✓ The sponge (relaxation) conditions, which have been found to have a robust performance in a variety of situations (Palma and Matano 1998; Nycander and Döös 2003).

Despite the numerous methods being available, none have been found to perform entirely satisfactorily (Nycander et al. 2008). Indeed, to avoid reflection, it is necessary to separate the gravity waves from the underlying geostrophic flow (Nycander and Döös 2003). This is a problem, since the geostrophic flow at the boundary depends on the distribution of the potential vorticity outside the boundary, which is unknown.

The objective of this study is not to find a consensus for the different methods available. Consequently, a very simple approach is adopted here. It consists to extend the channels to be long enough so that the flow does never reach the downstream region. Therefore, a zero flux is imposed as boundary conditions at the downstream and no Dirichlet conditions are needed (i.e., the total water depth and the velocity components are not specified). The weakness of this approach is that the simulations take too much time and computer space memory to run. However, it has the advantage of avoiding the numerical error due to bad imposition of such boundary conditions.

Conclusion

The FEM based on the second-order TG scheme is used to solve the Serre hydrodynamic model in this chapter. The initial system of PDE is then transformed into an algebraic equation in matrix form. Those matrices are functions of the unknown variables. Consequently, the substitution method is applied to solve the nonlinearity. The Serre finite element scheme obtained is coded into algorithms (the terms of the different matrices generated are calculated by numerical integration). The resulting Matlab® computer program is used in the next chapter to simulate some chosen hydrodynamic flow types in order to validate this new model.

CHAPTER 4

Preliminary Validation of the Serre Numerical Model

Introduction

The validation of the numerical scheme, described in the previous chapter, is presented in this chapter. The performance of the Serre model is tested for some test cases with a known analytical solution before applying it to complex situations. Three different flow situations are then considered for validation: a calm water basin, a permanent uniform flow (a.k.a., Chézy flow) and a solitary wave propagation with permanent form. For the overall simulations, the relative value 1E-6 of the Root Mean Square Error (RRMSE) was used as a stop criterium.

The first and the second tests (the calm water basin and the Chézy flow) are some basic tests for which the physical expected results are known without ambiguity. Thus, if there are any errors within the computer program, these tests can help to detect them. Finally, for the third test, a permanent wave form is expected since the nonlinear and dispersive effects counterbalance each other (Gobbi et al. 2000). Additionally, this test is interesting as the streamlines are highly curved for the solitary wave.

In the rest of this chapter, each test is described and the numerical results are presented. Then, they are compared with the corresponding analytical solution and commented upon.

4.1.- Calm water basin

This situation resembles a lake without both the wind effects and the free surface gradient. Such a validation test is used to check for possible programming errors. For this purpose, a rectangular closed basin with calm water serves as the control in this experiment. The expected physical solution is such that, without wind and a free surface gradient, the water will always stay calm (i.e., having no velocity) in the basin even after a long period of simulation. The basin is 40 m wide and 100 m long and the domain is meshed with 400 nonconforming triangular elements (see Figures 3.1 and 3.2) for a total of 900 nodes. The initial water level is $\eta = 4\ m$ throughout the domain. The velocity components are set to zero initially everywhere and the four boundaries are assumed impermeable (zero normal velocities). An upwinding factor of $C_{up} = 0.5$ is used. The algorithm is run at a time step increment of $\Delta t = 30\ s$ and the results are presented after $T = 600\ s$.

Figures 4.1 and 4.2 present the computed Serre solution (water level and flow velocity field) throughout the domain for a flat bottom condition (i.e., $S_x = 0$) and for the case where a bed slope $S_x = 0.001$ is imposed.

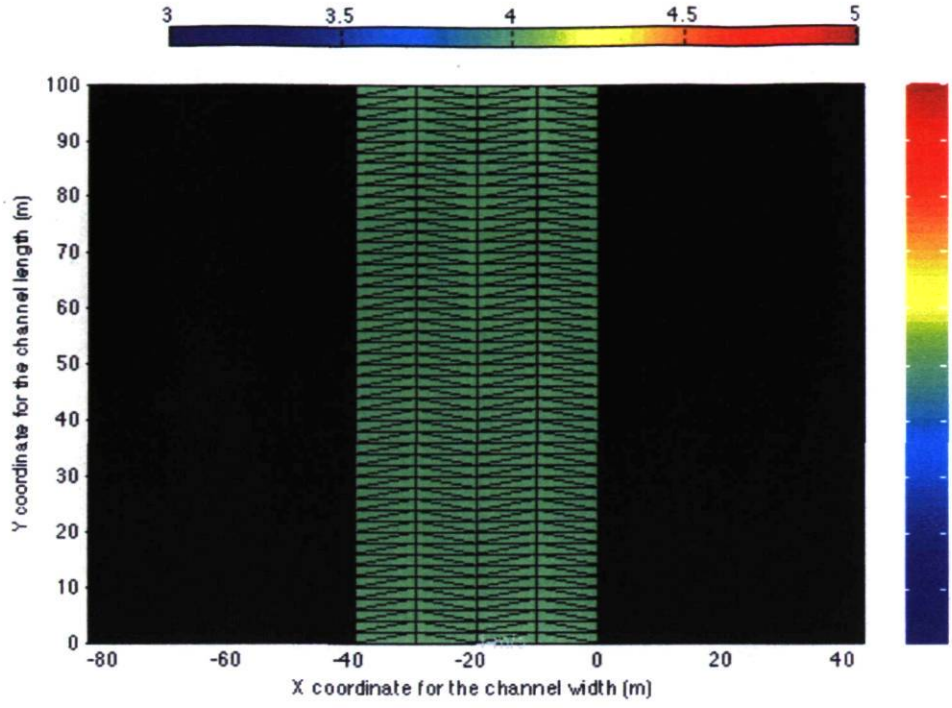

Figure 4.1: Water level and velocity field for calm water basin simulation (S_x=0)

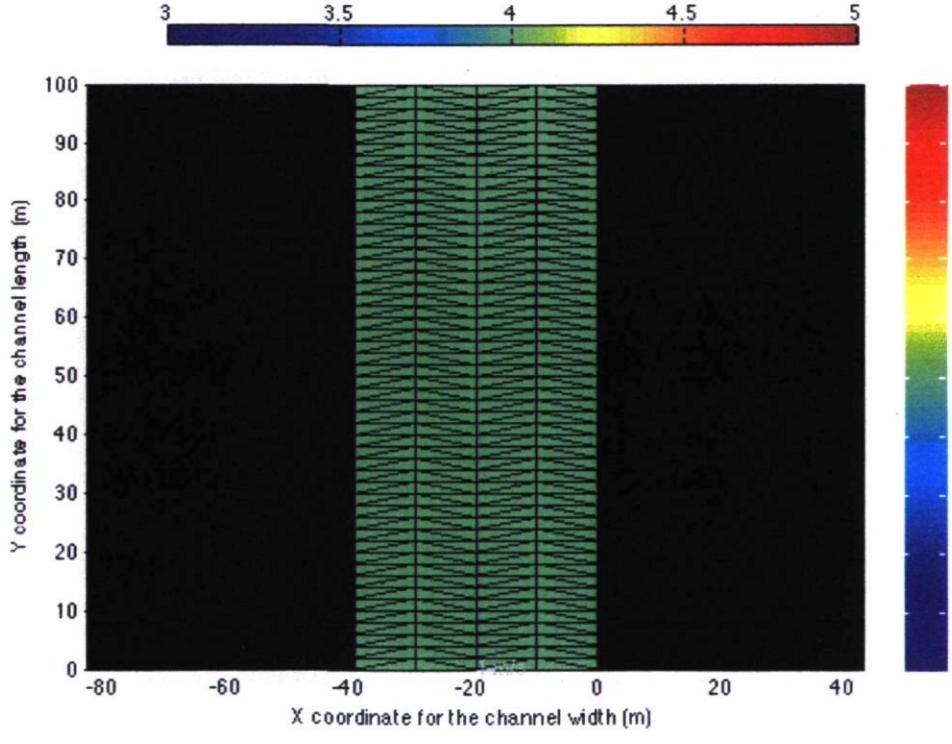

Figure 4.2: Water level and velocity field for calm water basin simulation (S_x=0.001)

It should be noted, as expected, that there is no flow (calm water) in the two cases, meaning that the horizontal velocity components are zero everywhere. Additionally, the water level does not change and it maintains its initial position until the end of the simulation. These numerical results lead to the conclusion that the numerical algorithm is well implemented and that there is no error within the corresponding computer program.

4.2.- Permanent uniform flow (the Chézy flow)

The permanent uniform flow test is also devoted to the validation of the quality of the computer program. It simulates an open channel flow for which the analytical solution is known. The principal characteristic is that there is a uniform bed roughness (i.e., a constant value of Chezy's coefficient) throughout the domain. A channel 2 m wide and 10 m long is used and it is meshed with 80 nonconforming triangular elements (see Figures 3.1 and 3.2) for a total of 189 nodes. The Chézy's coefficient is set to C_c = 50 $m^{1/2}/s$ and a negative bed slope of S_x = -0.001 is applied. The initial total water depth is set to H = 0.10 m throughout the domain and the horizontal velocity component is set to zero everywhere initially. The flow depth is kept at H = 0.10 m for the upstream boundary as well as for the downstream whereas the two sidewalls of the channel are assumed impermeable (zero normal velocity everywhere). An upwinding factor of C_{up} = 0.5 is used. The algorithm is run at a time step increment of Δt =30 s and the results are presented after T =600 s.

Figure 4.3 gives the computed Serre solution (water level and flow velocity field) throughout the domain.

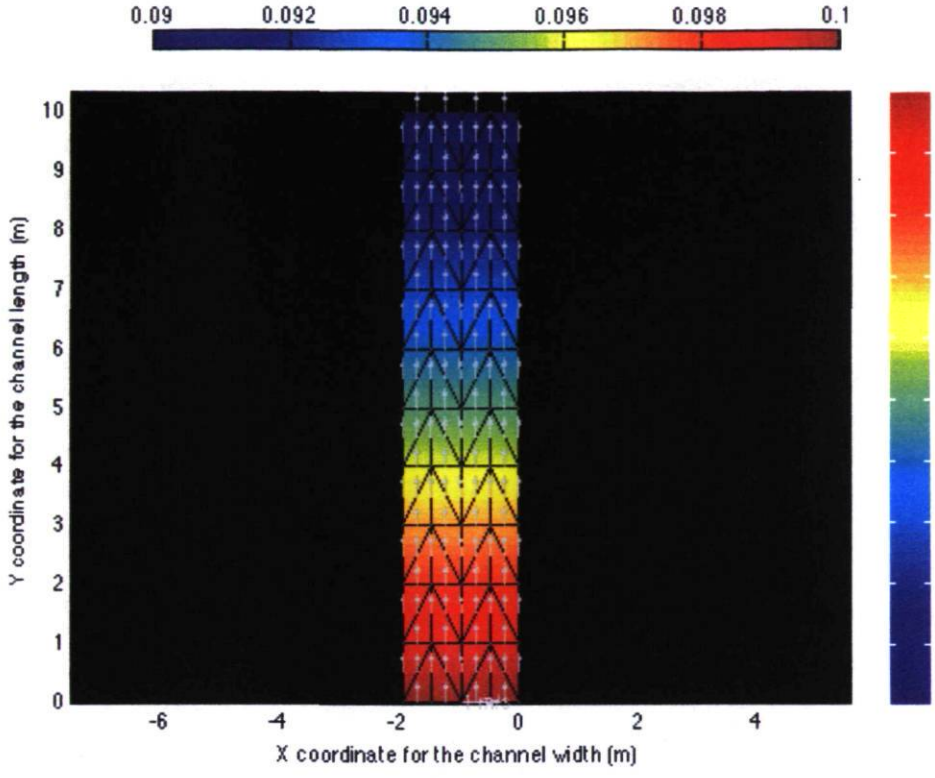

Figure 4.3: Water level and velocity field for Chézy flow simulation

Additionally, Figures 4.4 and 4.5 present the profile of the water level and that of the longitudinal component of the velocity through the centerline of the channel in comparison to the analytical solutions.

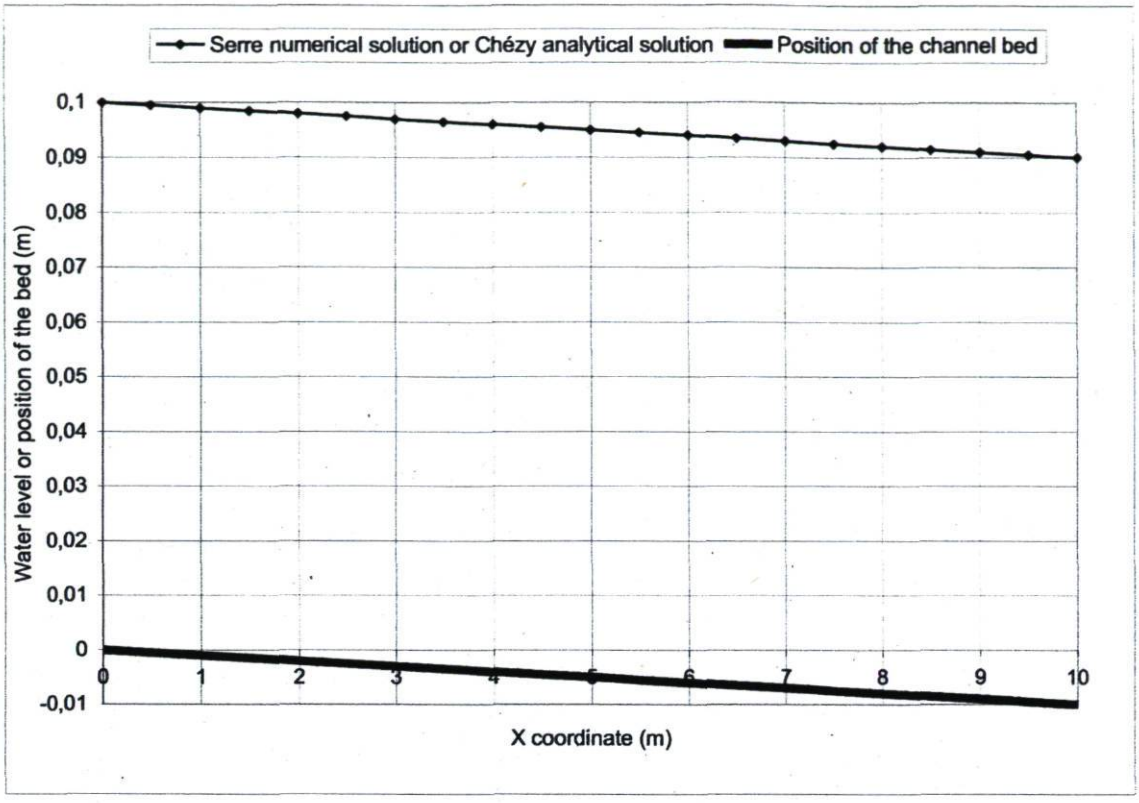

Figure 4.4: Water level profile from Chézy flow simulation

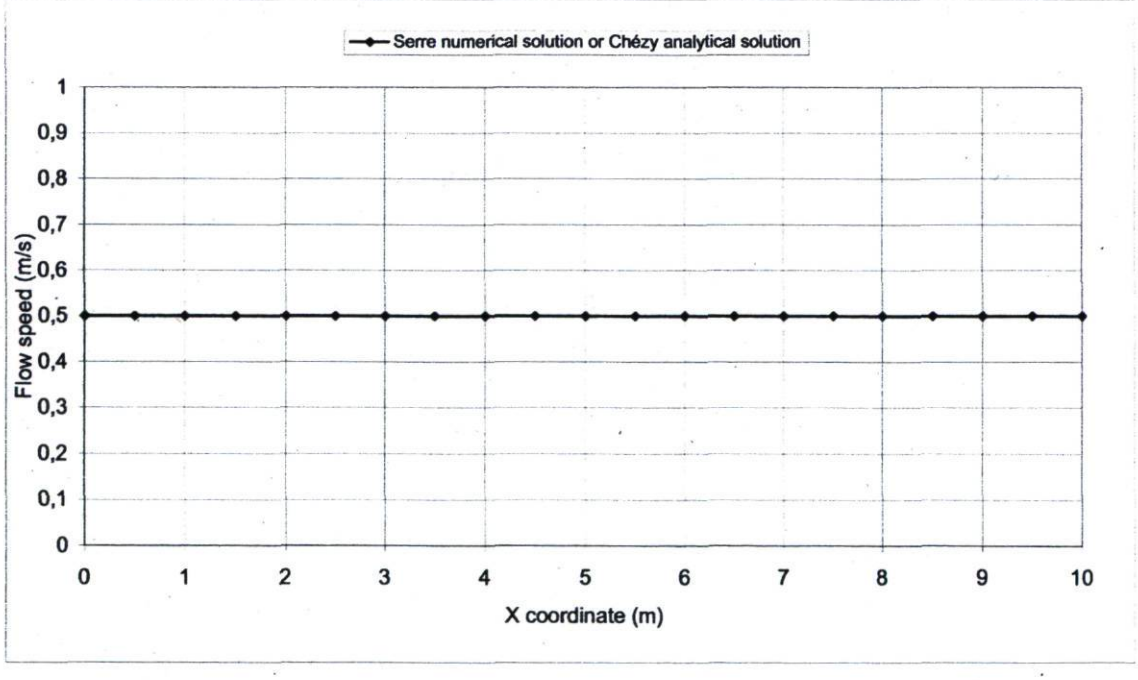

Figure 4.5: Profile of the longitudinal velocity from Chézy flow simulation

In the situation described above, the flow is one-dimensional in the direction of the slope of the channel bed. Consequently, the Serre model reduces itself to its first dynamic equation. Furthermore, the regime becomes permanent and uniform after the flow reaches its stability (after a short period of simulation).

Therefore, all the temporal and spatial derivatives of velocity become zero in the first Serre dynamic equation that remained. The flow is forever described by the following reduced and simplified version of the Serre model:

$$g\frac{\partial \eta}{\partial x} + gU\frac{\sqrt{U^2}}{C_c^2 H} = 0 \tag{74}$$

Also, the bottom of the flow becomes parallel to the free surface (the bed slope is equal to the gradient of the free surface of the flow) so that the following equation is true:

$$\frac{\partial \eta}{\partial x} = S_x \tag{75}$$

Therefore, equation (74) becomes:

$$U|U| = -S_x C_c^2 H \tag{76}$$

where the notation $|U|$ equals the absolute value of the longitudinal velocity component.

It is now possible to deduce the analytical *positive* solution for the velocity U giving the following mathematical formulation of the Chézy equation:

$$|U| = C_c\sqrt{-S_x H} \tag{77}$$

The application of the previous equation to the present flow situation gives:

$$|U| = C_c\sqrt{-S_x H} = 50\sqrt{-(-0.001)*0.1} = 0.5\ m/s \tag{78}$$

The expected analytical solutions are therefore, U = 0.5 *m/s* for the velocity and H = 0.10 *m* for the total water depth, throughout the domain.

According to the previous numerical results, a total water depth of H = 0.10 *m* and a longitudinal velocity of U = 0.5 *m/s* are truly obtained throughout the domain. It should be concluded that the Serre model perfectly simulates the Chézy flow giving exactly the expected analytical solutions.

4.3.- Solitary wave with permanent form

The purpose of this section is to verify how accurately the Serre numerical model, solved by the TG FEM, can compute the solitary wave propagation traveling without distortion.

Indeed, the phenomenon known as the solitary wave consists of a wave form with a single crest, which propagates in fairly shallow water of constant depth, and where *the nonlinear and dispersive effects counterbalance each other* yielding a permanent form solution (Gobbi et al. 2000).

Many authors have found approximate solutions for the solitary wave, including the early works of Boussinesq (1871), Korteweg and deVries (1895) and Laitone (1960). Fenton (1972) developed a model based on a perturbation expansion around the basic shallow water wave theory. However, his expansion led to a Boussinesq-type model of higher order. Later, Longuet-Higgins and Fenton (1974) used the conservation of integral quantities, such as mass and energy, to arrive at extremely accurate relationships between several solitary wave properties, such as the wave height, energy, mass, and the wave Froude number. They also proved that the solitary wave with maximum wave height does

not correspond to the one with maximum fluid velocity at the crest, or maximum mass. Additionally, in a study on the stability of solitary waves, Tanaka (1986) developed an accurate solution scheme for the full boundary value problem of solitary waves.

Throughout this section, the following known analytical solution is used to compare with the Serre numerical results (Antunes et al. 1993):

$$H = H_0 + Sech^2\left\{\left[\frac{3\delta}{4H_0^3\left(1+\delta/H_0\right)}\right]^{1/2}\left[x-\left[gH_0\left(1+\frac{\delta}{H_0}\right)\right]^{1/2}t\right]-x_0\right\} \tag{79a}$$

$$U = \left[gH_0\left(1+\frac{\delta}{H_0}\right)\right]^{1/2}\left(1-\frac{H_0}{H}\right) \tag{79b}$$

where δ is the wave amplitude, H_0 is the undisturbed water depth for $T = 0$, and x_0 is the initial position of the crest. All the other variables in (79a) and (79b) have previously been defined.

The theoretical celerity c of the solitary wave is calculated by using the formula below:

$$c = \sqrt{g\left(H_0+\delta\right)} \tag{80}$$

It should be kept in mind that when the computed celerity is superior to the theoretical value, the solitary wave is said to be *supersonic*.

For this validation test, a solitary wave traveling in a horizontal rectangular channel 1500 m x 2 m is used. Such a channel is meshed with 600 nonconforming triangular elements (see Figures 3.1 and 3.2) for a total of 1505 nodes. The Chézy's coefficient is set equal to a very large number (C_c = 1E17 $m^{1/2}/s$) corresponding to a flow with virtually no frictional resistance. The wave amplitude is δ = 0.40 m and the undisturbed water

depth is $H_0 = 10\ m$. The initial water depth profile throughout this simulation is given by the analytical equation (79a) and the initial position of the crest coincides with the origin of the channel centerline (i.e., $x_0 = 0$ for $T = 0$). This profile has already been used by a number of authors as an approximate initial condition for the numerical approximation of the dispersive shallow water equations (Peregrine 1967; Antunes et al. 1993; Kato et al. 1994). Additionally, the associated equation (79b) is also used to derive the initial profile of the longitudinal velocity. The flow never reaches the downstream since the channel is long enough. Therefore, a zero flux is imposed as boundary conditions at the downstream. However, the analytical equation (79a) is used to generate flow depth boundary conditions for the upstream whereas the two sidewalls of the channel are assumed impermeable (zero normal velocities). A zero upwinding factor (i.e., $C_{up} = 0$) is used so that the artificial diffusion terms cancel themselves. The algorithm is run at a time step increment of Δt =0.1 s and the results are presented successively for the time periods T =10 s, T =20 s, T =30 s and T =40 s.

Figures 4.6 and 4.7 show the computed results (the free surface elevation and the velocity along the centerline of the channel respectively) of the solitary wave simulated in comparison to the corresponding analytical solution profiles.

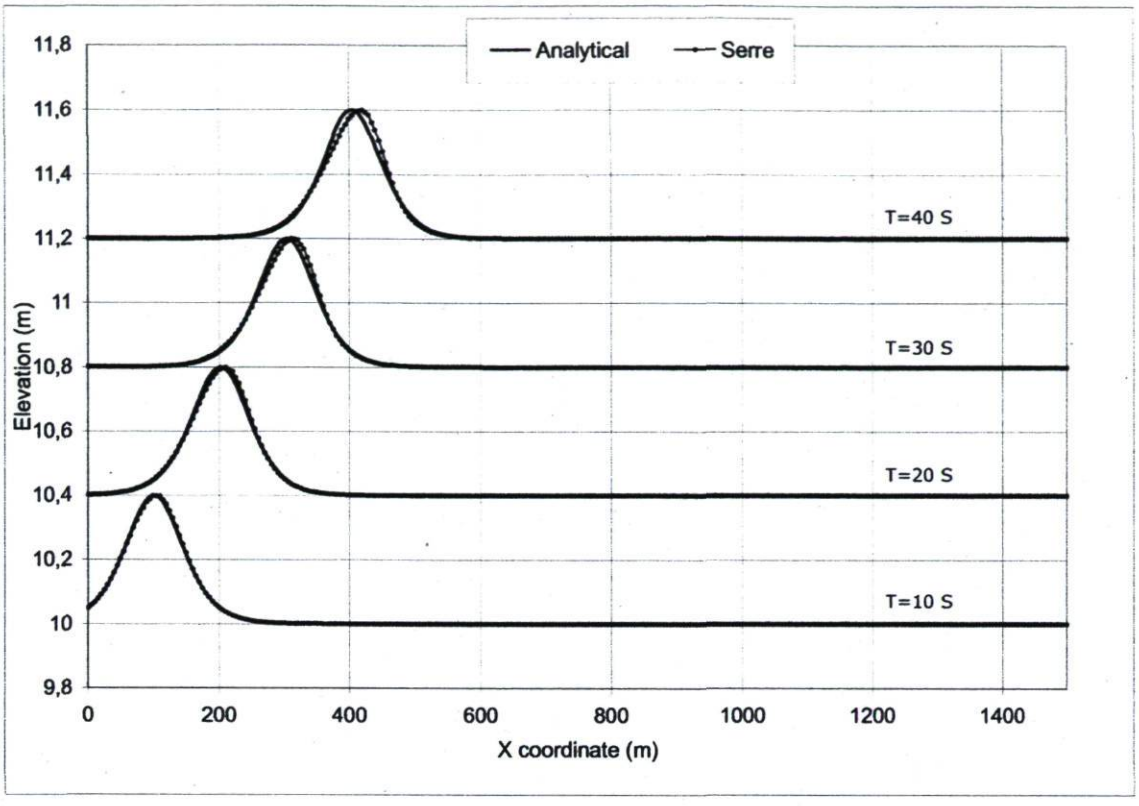

Figure 4.6: Water level profiles from the simulation of solitary wave propagation

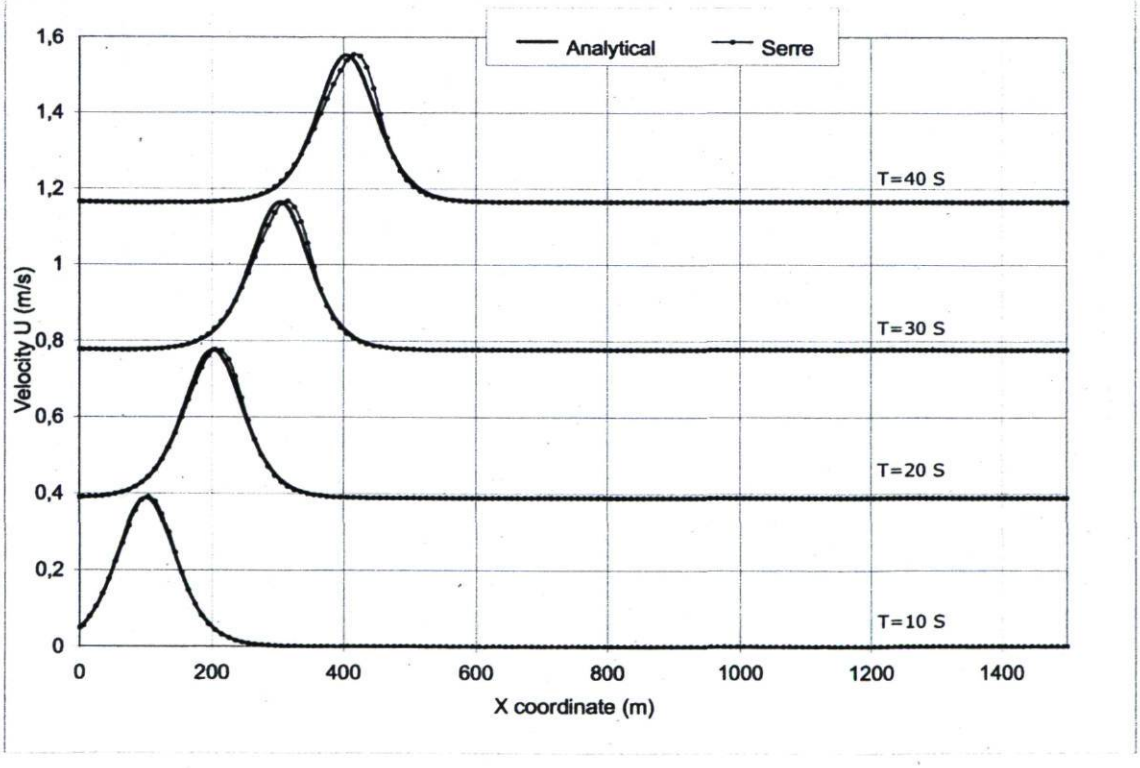

Figure 4.7: Profiles of the longitudinal velocity from the simulation of solitary wave propagation

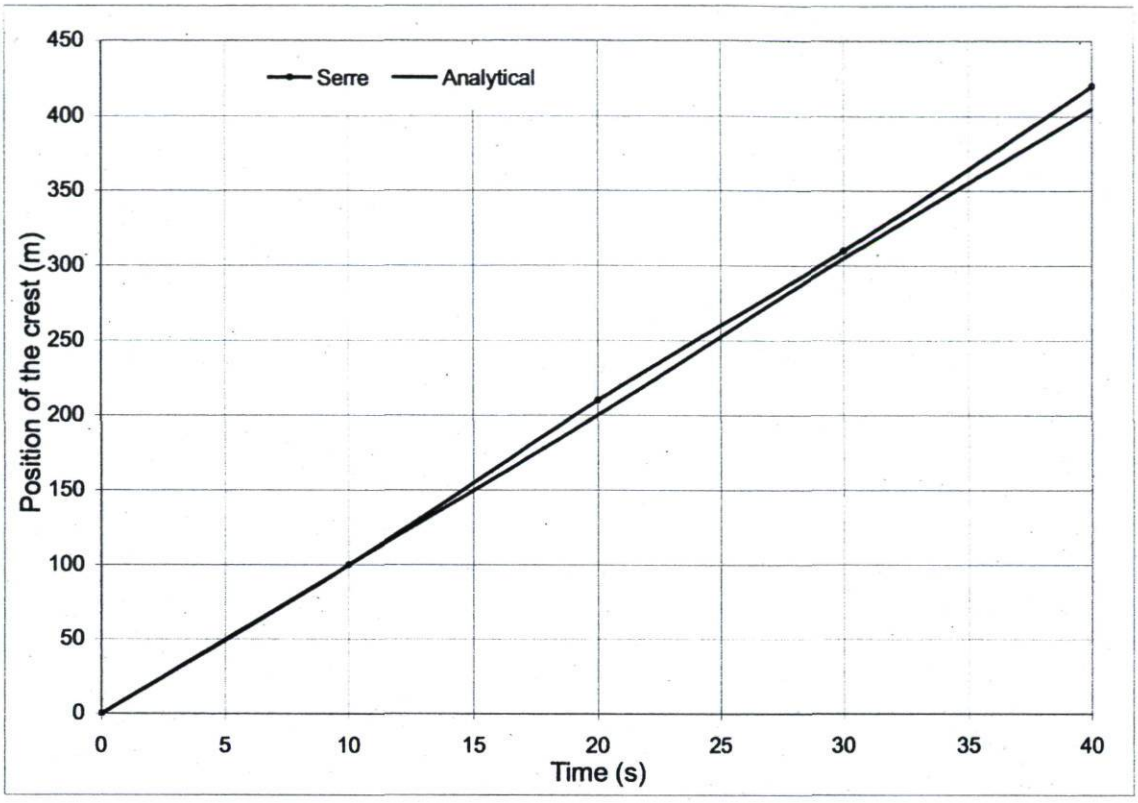

Figure 4.8: Position of the crest of the solitary wave versus the time

For such a solitary wave, the results from the Serre numerical model are very close to the expected solution since the profiles of the water depth and of the velocity coincide well with those analytical. The amplitude and phase accuracy is very good for the water depth as well as for the velocity. In all cases, the calculated wave celerity is $c = 10.1$ *m/s* which corresponds exactly to the theoretical value. However, it should be noted that for the time period of $T = 40$ *s*, the Serre numerical model overpredicts the position of the crest with approximatively 4 % of relative error in comparison to the theoretical expected position. Therefore, the wave crest tends to deviate forward slightly. We can conclude that the Serre model is appropriate when simulating the solitary wave propagation. This conclusion confirms the results obtained earlier by Antunes et al. (1993) for solitary wave by using the Serre equations solved by a completely different numerical approach (a MacCormack finite difference scheme). In their case, there was good phase accuracy.

However, the amplitude of the wave decays about 6-8% and the resulting loss of energy was supposed to be responsible of the generation of a small numerical dispersive wave.

Conclusion

In this chapter, the Serre model solved by the second-order TG FEM is used to simulate three chosen hydrodynamic flow types for the purpose of validation. The numerical results match exactly the known analytical solutions as well for the simulation of a calm water basin as for a permanent uniform flow analysis (the Chézy flow). For the overall simulations, the minimum value 1E-6 of the RRMSE was achieved with a variable total number of iterations.

The Serre model is also found to be suitable for the simulation of the solitary wave propagation. The water depth and velocity profiles that are obtained numerically show a good accuracy when they are compared to those analytical. Only the position of the wave crest after 40 s slightly deviated forward from the theoretical one. Given that for a solitary wave, the nonlinear and dispersive effects counterbalance each other, the artificial diffusion terms were not used in this last simulation. The analysis of dambreak flows is presented in the next chapter to complete the Serre model application.

CHAPTER 5

Dambreak Flows Analysis with the Serre Numerical Model

Introduction

Dambreak events are not frequent, but when they occur the consequences are usually disastrous. In order to prevent such situations or to understand how the process will develop when it actually happens, knowledge of the physical phenomena involved is of fundamental importance for many practical situations in hydraulics, for environmental engineering and for the safety of many people who may be at risk. Inundation maps are generally produced to make risk analyses for civil protection. Of importance on these maps, are the elevation of the peak water level and the time required for the peak to reach the locations of interest. They are currently based on the numerical simulation of the wave propagation process and, therefore, the appropriate governing equations must be used to adequately simulate the flow conditions.

Research to understand the dambreak flow processes have been of interest for quite some time. Indeed, Ritter (1892) established the analytical solution for the particular situation of a flow flooding from a basin to a rectangular, horizontal, frictionless and dry (empty) channel after the sudden failure of the wall between them. In his application, the basin and the channel have infinite lengths. Later, Dressler (1952) and Whithman (1955) included the effects of the bed roughness in the Ritter solution. Hunt (1982 and 1987) also reformulated the Ritter solution for the specific case where the basin and the channel have finite lengths. Stoker (1957) extended the solution to the initially wet channel bed. Wu et al. (1999) broadened Stoker's approach to the rivers with trapezoid sections.

Exceptionally, to simulate the dambreak flow situations, some authors have resorted to solving the NS PDE (Pohle 1952; Strelkoff 1986; Mohapatra et al. 1999). More usually, the assumption of hydrostatic pressure is made, and the NS equations are transformed into the well-known SV or SW equations, which are then applied (Katopodes and Strelkoff 1978; Savic and Holly 1991; Soulis 1992; Betamio de Almeida and Franco 1993; Lauber and Hager 1998a; Lauber and Hager 1998b; Garcia-Navarro 1999; Hervouet and Petitjean 1999; Brufau and Garcia-Navarro 2000; Aureli et al. 2000; Wang et al. 2000). Even if this approach has been relatively successful in certain applications, it remains that the assumption of a hydrostatic pressure distribution does not seem realistic nor very satisfactory.

Indeed, Basco (1989) demonstrated the weakness of the SV for dambreak modeling since, for this case, vertical acceleration could be quite significant. For this type of flow, the discharge varies rapidly in time and the vertical curvature of the streamlines (indicative of vertical acceleration) is non-negligible. Moreover, based on a Lagrangian resolution of the 2DV NS equations, Pohle (1952) and Strelkoff (1986) established that the pressure distribution is significantly non-hydrostatic immediately after the rupture of the dam. Dressler (1954) also experimentally observed that the flow depth and the breach discharge do not instantaneously reach constant values at the dam location. Because the pressure is initially non-hydrostatic, they gradually establish themselves over time. In addition, Kosorin (1983) demonstrated that non-hydrostatic pressure reduces the celerity of the dambreak wave by as much as 30 % when compared to Ritter's analytical solution (based on the hydrostatic pressure hypothesis). Fraccarollo and Toro (1995) experimentally investigated the pressure behavior at the position close to the dam location immediately after its sudden rupture for a horizontal bed case. They found that the pressure at the bottom was up to 60 % higher than hydrostatic during the first two seconds.

Therefore, and in this analysis of the dambreak flow, the Serre model is selected to overcome this SV weakness, since the dynamic pressure is taken into account in Serre's mathematical formulation.

However, for a correct representation of the dambreak phenomenon, the numerical schemes used must be able to model the sudden variations of the hydraulic parameters without introducing spurious oscillations. For this purpose, different methods have been proposed in the literature (see for e.g., Katopodes and Strelkoff 1978; Katopodes and Strelkoff 1979; Donea 1984; Katopodes 1984; Akanbi and Katopodes 1988; Shu and Osher 1988; Alcrudo and Garcia-Navarro 1993; Fraccarollo and Toro 1993; Hirsch 1995; Zhao et al. 1996; Louaked and Hanich 1998; Brufau and Garcia- Navarro 2000; Jha et al. 2000; Kurganov and Tadmor 2000; Wang and Liu 2000; Wang et al. 2000; Tseng and Chu 2000; Toro 2001). In this study, the TG approach, which was described previously, is used, since this scheme has already been applied successfully to dambreak problems (Quecedo and Pastor 2003) and to a wide variety of other situations where advection phenomenon is significant (Safjan and Oden 1995; Tamma and Namburu 1988; Zhang and Tabarrok 1999; Mabssout and Pastor 2003a).

For the overall dambreak flows simulated in this chapter, the relative value 1E-6 of the Root Mean Square Error (RRMSE) was used as a stop criterium.

The rest of this chapter is structured as follows: first, the basic test case and the Stoker (1957) analytical solution are described. Then, the numerical results are presented and discussed in light of the tradional SV solutions. Finally, the influence of the variation of the principal variables (bed slope, bed roughness and ratio of the water depths upstream and downstream respectively) is investigated before the conclusion.

5.1.- Description of the basic test case

The first test case simulates the flow in a horizontal frictionless 100 m x 1000 m channel, after the instantaneous failure of a dam situated at x_0 = 500 m. The domain is meshed with 800 nonconforming triangular elements (see Figures 3.1 and 3.2) for a total of 2005

nodes. The initial bed slope is set equal to zero and the Chézy's coefficient is set equal to a very large number (C_c = 1E17 $m^{1/2}/s$) corresponding to a flow with virtually no frictional resistance. The initial flow depth is H_u = 6 m for the upstream half and H_d = 2 m for the downstream half. The velocity components are equal to zero initially everywhere. The total water depth H_u = 6 m is imposed as boundary conditions at the upstream and the two sidewalls of the domain are assumed impermeable (zero normal velocities). In addition, the flow never reaches the downstream since the channel is too long. Therefore, a zero flux is imposed as boundary conditions at the downstream. Figure 5.1 presents a plot of the initial state of the system. An upwinding factor C_{up} = 0.5 is used for the artificial diffusion. The algorithm is run at a time step increment of Δt = 1 s and the results are presented after T = 30 s.

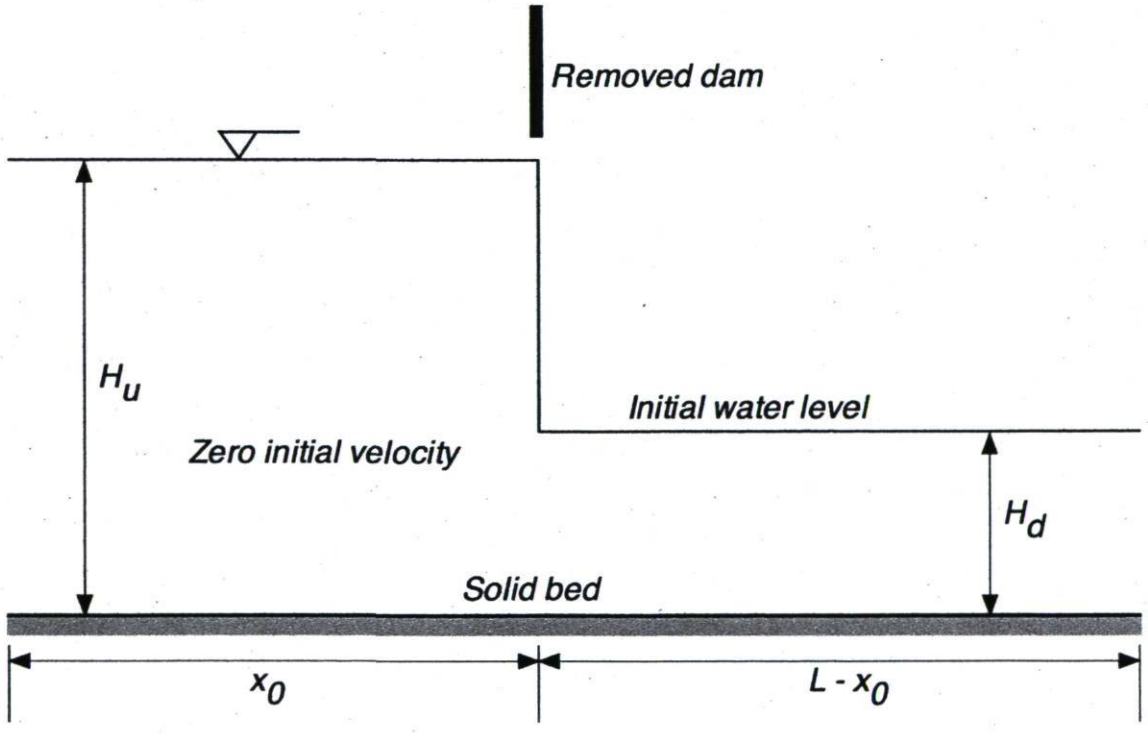

Figure 5.1: The initial state of the dambreak flow situation

5.2.- Analytical solution

For this basic test case, the Stoker (1957) analytical solution can be applied with the following mathematical formulation:

$$H(\tilde{x},\ t)=\begin{cases} H_u & if \quad \tilde{x}/t \le -\sqrt{gH_u} \\ \dfrac{1}{9g}\left(2\sqrt{gH_u}-\dfrac{\tilde{x}}{t}\right)^2 & if \quad -\sqrt{gH_u} < \tilde{x}/t \le \left(U_m-\sqrt{gH_m}\right) \\ H_m & if \quad \left(U_m-\sqrt{gH_m}\right) < \tilde{x}/t \le s_b \\ H_d & if \quad \tilde{x}/t > s_b \end{cases} \tag{81a}$$

$$U(\tilde{x},\ t)=\begin{cases} 0 & if \quad \tilde{x}/t \le -\sqrt{gH_u} \\ \dfrac{2}{3}\left(\dfrac{\tilde{x}}{t}+\sqrt{gH_u}\right) & if \quad -\sqrt{gH_u} < \tilde{x}/t \le \left(U_m-\sqrt{gH_m}\right) \\ U_m & if \quad \left(U_m-\sqrt{gH_m}\right) < \tilde{x}/t \le s_b \\ 0 & if \quad \tilde{x}/t > s_b \end{cases} \tag{81b}$$

where, $\tilde{x}=x-x_0$, with x_0 being the location of the discontinuity. The water depth H_m and the velocity U_m at the middle of the domain are two constant values, given below:

$$H_m=\frac{1}{2}\left(\sqrt{1+\frac{8s_b^2}{gH_d}}-1\right)H_d \tag{82a}$$

$$U_m=s_b-\frac{gH_d}{4s_b}\left(1+\sqrt{1+\frac{8s_b^2}{gH_d}}\right) \tag{82b}$$

The bore celerity s_b is determined by calculating the positive real root of the following equation after the substitution of (82a) and (82b) into (83):

$$U_m + 2\sqrt{gH_m} - 2\sqrt{gH_u} = 0 \tag{83}$$

5.3.- Numerical results

Figures 5.2 and 5.3 present respectively the computed Serre water level and flow velocity profiles along the centerline of the channel, and they are compared to the Stoker (1957) analytical solution and to the results from the classic SV model.

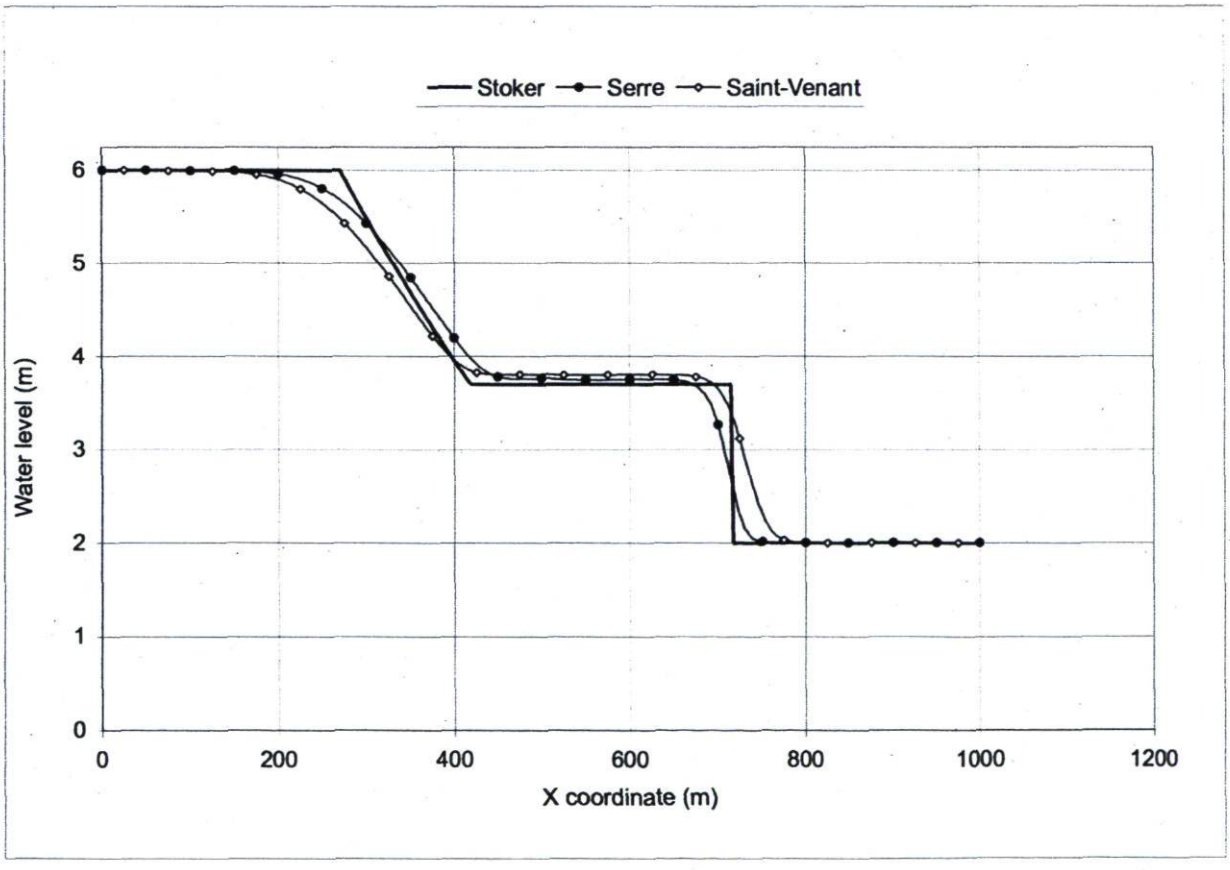

Figure 5.2: Dambreak water level profiles at T=30 s

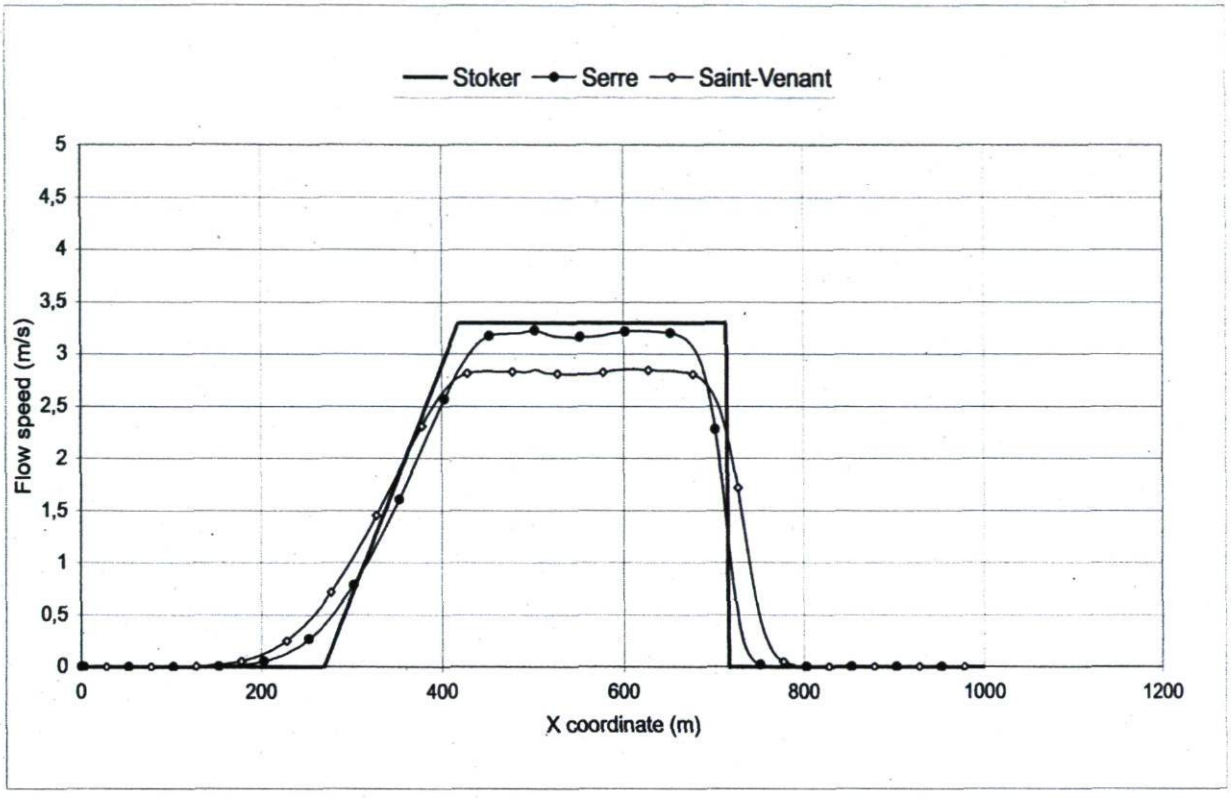

Figure 5.3: Dambreak flow speed profiles at T=30 s

Those results show that there are two waves: one traveling upstream, called a rarefaction wave (or depression) and one traveling downstream, called a bore. For this test, the shape of the profiles (water level and longitudinal velocity) simulated by the Serre model and those given by the SV are both in a good agreement with the Stoker analytical solution although there are some small differences in both wave amplitude and particularly wave celerity. As predicted by Stoker (1957), the flow is permanent and uniform in the bore region for the SV model. On one hand, the total water depth predicted by Serre is superior to that predicted by SV in the rarefaction region and inferior in the bore region. On the other hand, the celerity of both the positive and negative waves predicted by the Serre model is smaller than that predicted by the SV model. For example, at $T = 30\ s$, an approximate value of $s_b = 8.5\ m/s$ was obtained for the SV bore celerity whereas $s_b = 7.5\ m/s$ for the Serre's. Thus, the hydrostatic SV model has overpredicted the bore celerity by as much as 13.33 % when compared to Serre's non-hydrostatic solution. This

observation is consistent with what was found earlier by Kosorin (1983) who demonstrated that the non-hydrostatic pressure reduces the celerity of the dambreak bore predicted by the hydrostatic SV model.

Figure 5.4 shows the temporal overprediction (i.e., outdistancing) of the SV bore on Serre's.

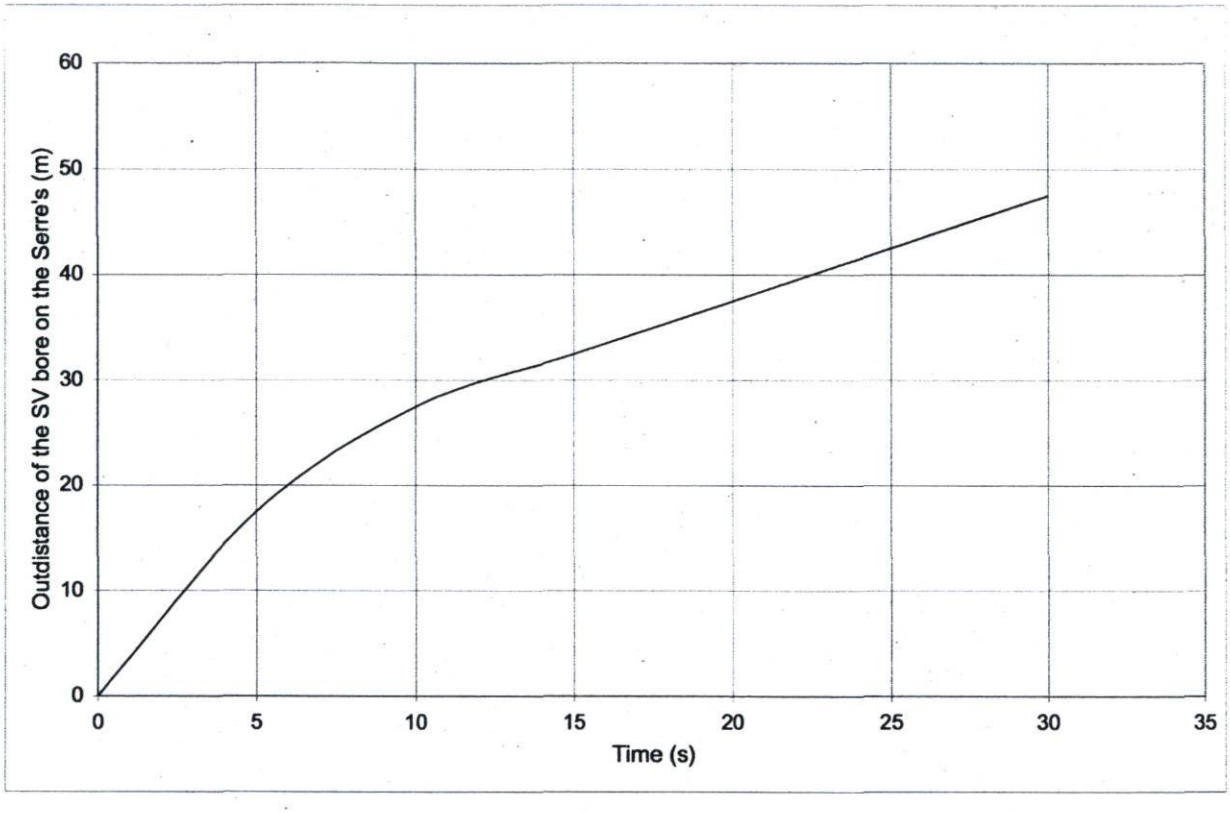

Figure 5.4: Outdistancing of the SV bore compared to Serre's

An approximate outdistancing of 47.5 *m* was observed after 30 *s* of simulation. The value of that outdistancing increases in time although its rate decreases. Thus, the dynamic pressure is truly present in a dambreak flow and it is caused by the vertical acceleration (due to the rapid variation of the flow over the vertical and to the significant vertical curvature of the flow path).

Additionally, the water depth profile predicted by SV crosses the Serre's in the bore region and the value of the wetted section passing there is the same for both models (see Figure 5.2). Since the positive horizontal pressure gradient does exist for the Serre model because of the dynamic pressure taken into account in its formulation (such gradient is always zero for SV), the flow rate must be greater through such a wetted section. Consequently, the flow speed must be superior for Serre than for SV at that position, which is consistent with the numerical results (see velocity profiles at Figure 5.3).

This simulation revealed also that the shock wave (the bore) is well resolved without post-shock oscillations evident in the solution. The upwinding technique that consists of adding artificial diffusion terms by using the second-order Taylor series expansion is efficient for shock-capturing in dambreak situation without decreasing the quality of the numerical results.

5.4.- Influence of the bed slope

The simulations presented here are devoted to the study of the channel bed slope influence. For this purpose, two other bed slopes ($S_x = 0.001$ and $S_x = 0.005$) were considered successively in addition to the first test case where $S_x = 0$.

Figure 5.5 presents the plots of the water level profiles for the Serre model for the different values of the bed slope. For the sake of conciseness, the velocity profiles are omitted.

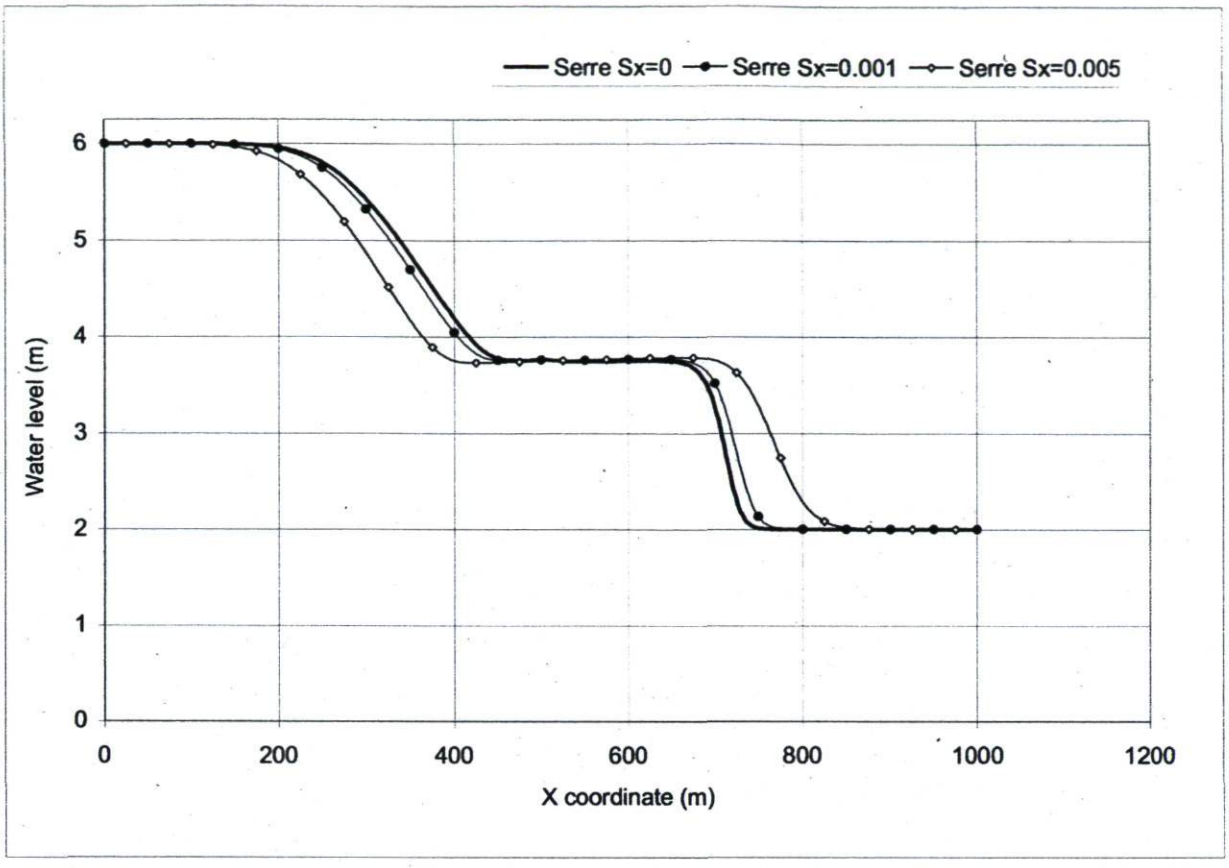

Figure 5.5: Influence of the bed slope (S_x) on the dambreak solution according to Serre

The numerical results show that the celerities of the dambreak waves (bore and rarefaction) increase when the bed slope is greater. This behavior is principally due to the fact that, when there is a bed slope, the total vertical forces within the flow, generate some additional horizontal components that contribute to accelerating the fluid downwards. For the Serre model, such total vertical forces are caused both by the hydrostatic and dynamic pressures. Therefore, the resulting horizontal forces are greater. Consequently, the celerity increases both for the bore and for the rarefaction. Such observations are true for the Serre model as well as for the SV.

Figure 5.6 presents a plot of the resulting outdistancing progression curves for the three bed slopes being investigated ($S_x = 0$, $S_x = 0.001$ and $S_x = 0.005$).

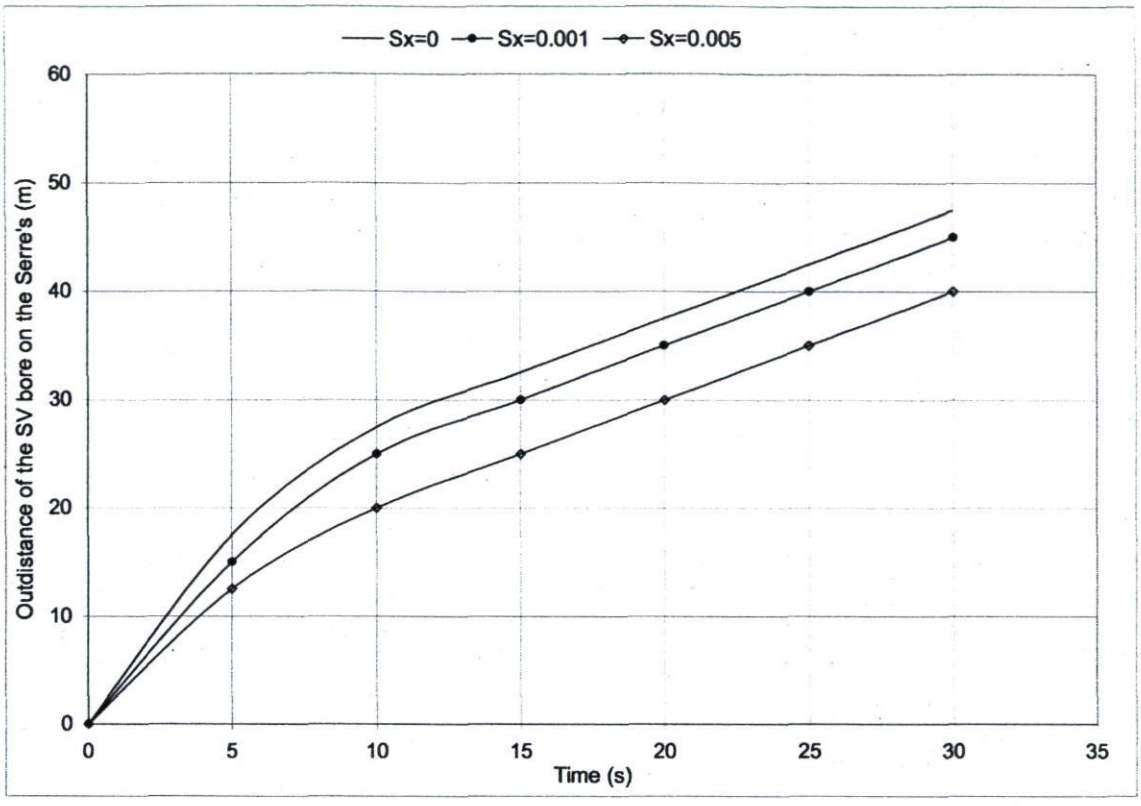

Figure 5.6: Influence of the bed slope on the outdistancing of the SV bore compared to Serre's

The outdistancing does decrease with the increase of the bed slope. As such, the celerity increases more for the Serre bore than for that of the SV. Indeed, the dynamic forces become greater due to the vertical accelerations that are taken into account in the Serre model. Consequently, the bore and the rarefaction move more quickly for the Serre model than for the SV such that the outdistancing is reduced.

5.5.- Influence of the bed roughness

The purpose of this section is to evaluate the influence of the domain bed roughness variation. Indeed, the Chézy's coefficient is successively set to $C_c = 60\ m^{0.5}/s$ and to $C_c = 30\ m^{0.5}/s$. The particularity of the Chézy's coefficient is that a smaller value of this parameter means that the bed is rough, whereas a great value would signify a smooth bed. For the sake of conciseness, the velocity profiles are omitted.

Figure 5.7 presents plots of the water level profiles respectively for the Serre model for the different values of the bed roughness.

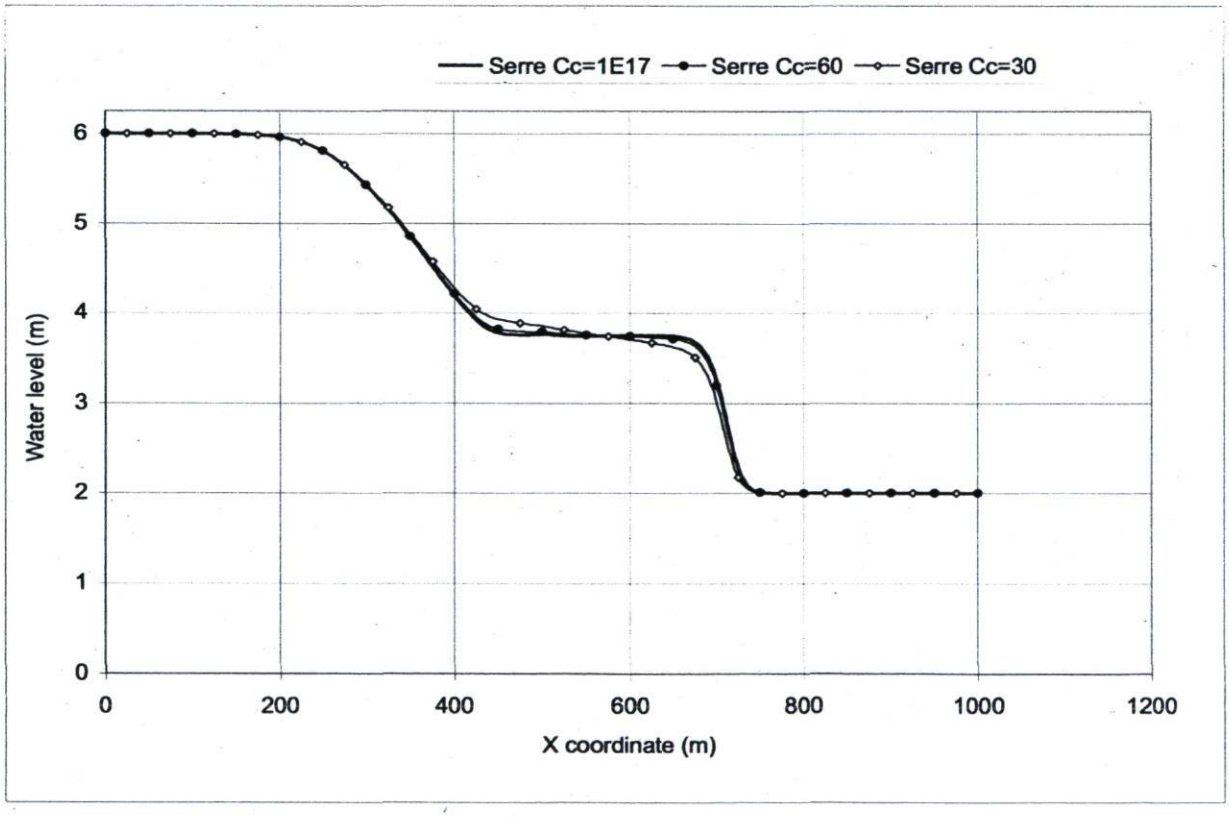

Figure 5.7: Influence of the bed roughness for T=30 s

The numerical results show that the increase of the bed roughness does not affect notably the celerity of the dambreak waves (bore and rarefaction) when the Chézy's coefficient changes from C_c = 1E17 $m^{0.5}/s$ to C_c = 60 $m^{0.5}/s$. However, for the case where C_c=30 $m^{0.5}/s$ is imposed, a significant decrease of wave celerities is observed. Therefore, it should be concluded that the increase of the bed roughness, delays the speed of the dambreak waves. Physically speaking, the frictional stresses become important and they reduce the velocity of the flow throughout the domain. Such behavior is observed for both the Serre model as for the SV.

Figure 5.8 presents a plot of the resulting outdistancing progression curves, for the three values of the bed roughness.

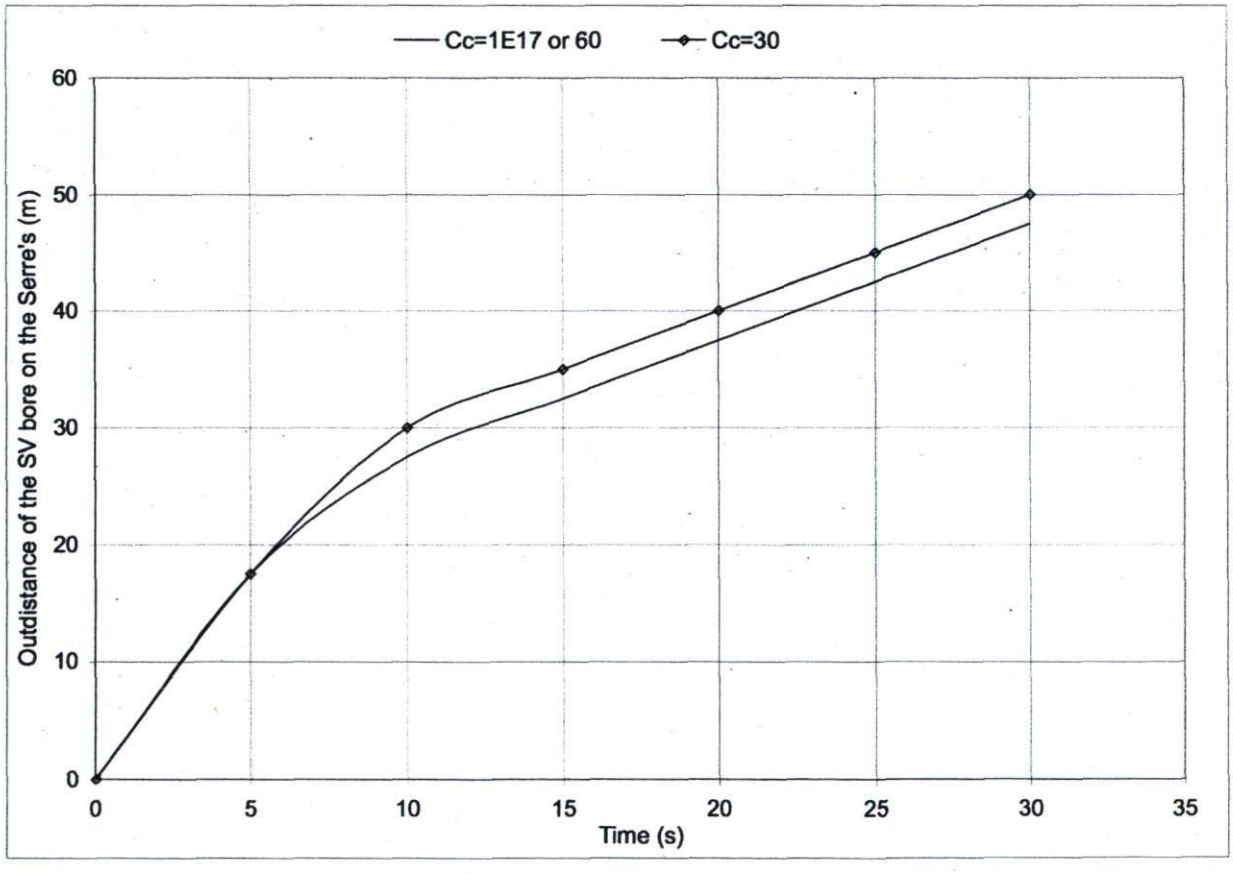

Figure 5.8: Influence of the bed roughness on the outdistancing of the SV bore compared to Serre's

The outdistancing increases with the significant increase of the bed roughness. As such, the bore is more delayed for the Serre model than for the SV. Indeed, it is well known that the forces of friction are proportional to those that are normal to the sheared surface. As such, the SV model considers only the hydrostatic pressure force as normal force; whereas in the Serre model, the normal force is generated both by the hydrostatic pressure and by the dynamic one. Consequently, in a dambreak flow, the forces of friction are greater for Serre than for SV and this situation results in a greater reduction of the celerity of the Serre bore.

5.6.- Influence of the water depths ratio

In this section, the impact of the variation of the ratio H_u/H_d of the two water depths upstream and downstream respectively is assessed for $S_x = 0$ and $C_c = 1E17\ m^{1/2}/s$. Therefore, the pair (H_u, H_d) is successively set to (6 m, 4 m) and (6 m, 3 m) for two additional simulations. It results in three different values for the water depths ratio left to be investigated: 6/4=1.5, 6/3=2 and 6/2=3.

Figure 5.9 presents the plots of the water level profiles for the Serre model for the different values of the water depths ratio. For the sake of conciseness, the velocity profiles are omitted.

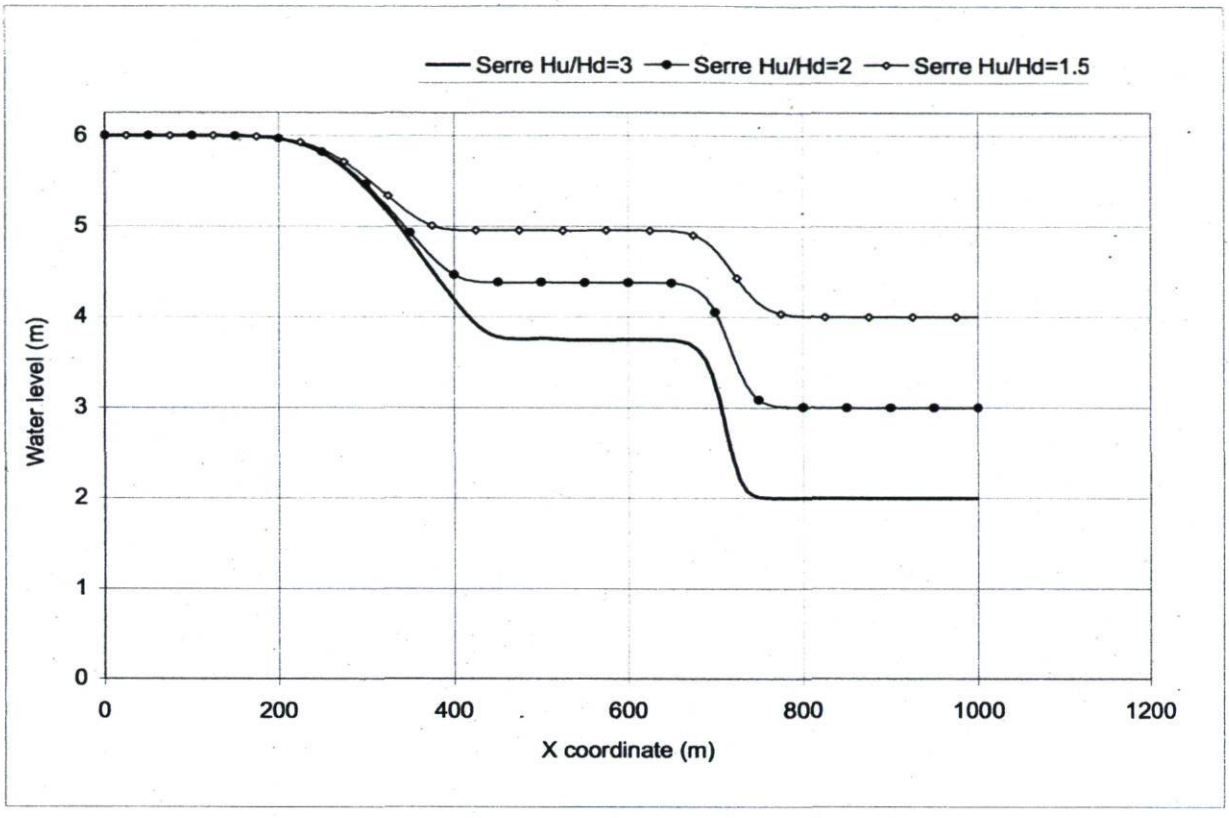

Figure 5.9: Influence of the water depths ratio for T=30s

The numerical results show that the increase of the water depths ratio H_u/H_d reduces the celerity of the dambreak waves especially for the bore because when that ratio becomes smaller, the intensity of the shock is weaker. The total force, normal to the bed, becomes more important when the ratio is greater and consequently, the flow speed is reduced.

Figure 5.10 presents a plot of the resulting outdistancing progression for the three values of the water depths ratio (H_u/H_d =1.5, 2 and 3).

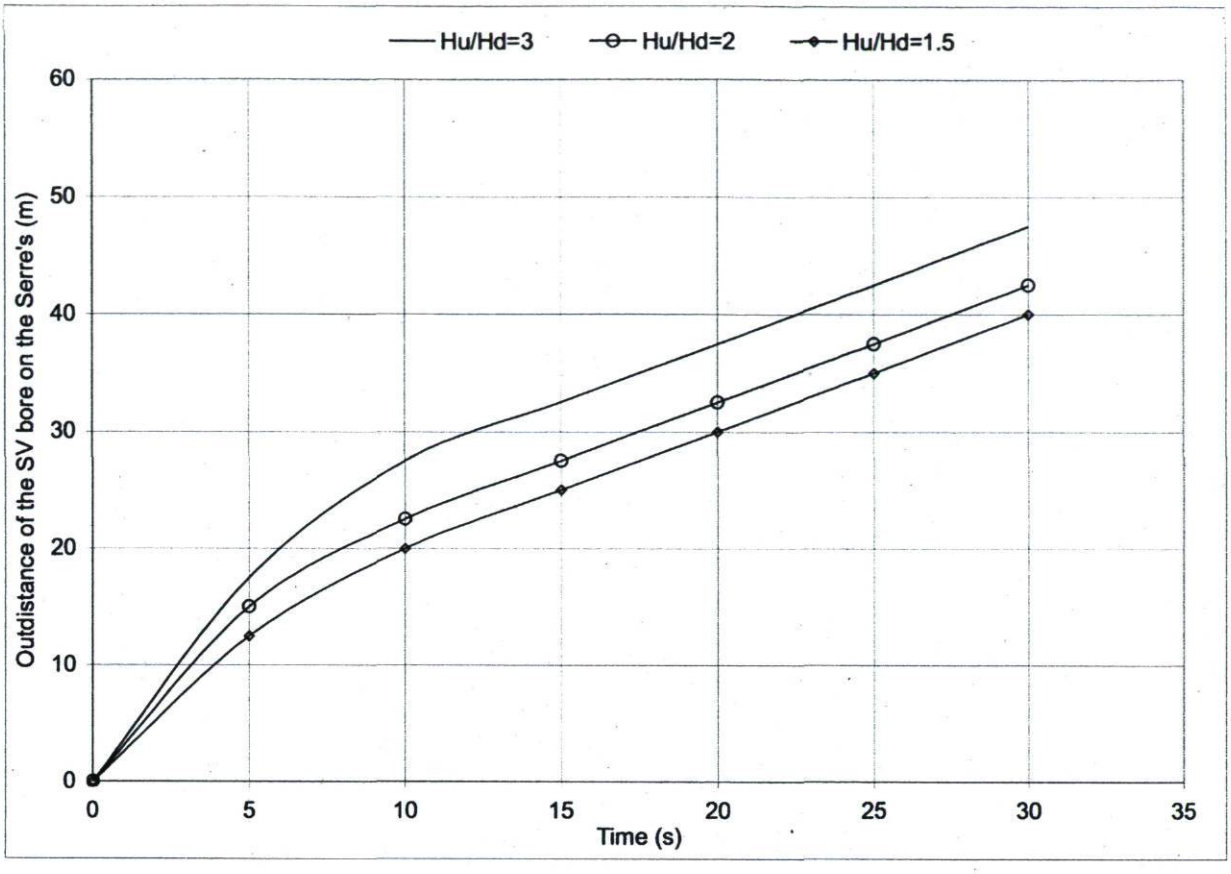

Figure 5.10: Influence of the ratio H_u/H_d on the outdistancing of the SV bore compared to Serre's

The outdistancing increases with the increase of the water depths ratio. The principal explanation could be that the supplementary dynamic pressure in the Serre model contributes to generate some additional forces, which delay the wave celerity.

Conclusion

In this chapter, the finite element solution of the 2DH Serre hydrodynamic model is applied to simulate some dambreak flow situations. In each case, the minimum value 1E-6 of the RRMSE was achieved with a variable total number of iterations.

The overall dambreak flow simulations considered here lead to the conclusion that the Serre additional terms delay the celerity of the bore (i.e., the dambreak wave traveling to the downstream). Consequently, the SV bore outruns that simulated by Serre. For the basic test case described firstly and after 30 *s* of simulation, the hydrostatic SV model has overpredicted the bore celerity by as much as 13.33 % when compared to Serre's non-hydrostatic solution yielding an approximate outdistancing of 47.5 *m*. Indeed, the Serre terms translate the presence of some vertical acceleration within the dambreak flow, which delays the flow speed. As a result, the celerity value is reduced as well for the bore as for the rarefaction (i.e., the dambreak wave traveling to the upstream). Physically speaking, the rapid variation of the dambreak flow and the significant curvature of the streamlines over the vertical cause some dynamic pressure whose impacts cannot be ignored.

Additionally, it was noted that as the bed slope increases, the celerity for the Serre bore increases more rapidly than the SV one. Consequently, the amount of the outdistancing of the SV bore decreases with increasing the bed slope. Furthermore, as bed roughness and water depths ratio increase, outdistancing increases due to the greater importance of pressure in the hydrodynamics and Serre's ability to correctly account for that effect.

From a technical point of view, the shock wave (the bore) was well resolved without any significant post-shock oscillations evident in the solution. It is concluded that the upwinding technique, which consists of adding some artificial diffusion terms using the second-order Taylor series expansion, is then efficient means for shock-capturing in dambreak situation without decreasing the quality of the numerical results.

CHAPTER 6

Extension of the Serre Model for Fully Non-Hydrostatic Flows

Introduction

The 2DH Serre hydrodynamic model has been used in the previous parts of this thesis to take into account the dynamic pressure, which could be significant in some types of free surface flow. In the Serre model, such dynamic pressure is caused only by the total vertical acceleration. Therefore, an assumption of inviscid flow over the vertical is also made, which leads to the cancellation of the viscous shear stresses terms in the third NS momentum equation, while they are retained in the two others. Consequently, the Serre model does not represent a generalized solution applicable to all types of non-hydrostatic flow situations.

This chapter presents the development of a new 2DH model called the "Saint-Venant Plus" (SVP). It describes the hydrodynamic characteristics of free surface flows while specifically accounting for the total dynamic pressure effects. In SVP, the dynamic pressures are induced both by the viscous shear stresses over the vertical and by the total vertical acceleration. The SVP is similar to the Serre, but the pressure is entirely non-hydrostatic. The dynamic component is established in a much more generalized manner by including the vertical viscous frictions. Even if the physical water viscosity is small, a number of factors make the Serre and SV assumption of inviscid flow over the vertical invalid in many cases. The effect of even a small amount of viscosity cannot be neglected near vertical fluid boundaries because of the presence of a boundary layer. For example, the viscous shear stresses on rough walls could become significant for many open-

channel flows particularly when the flow varies rapidly over the vertical. As such, the SVP aims to be an accurate representation of 2DH flows that truly account for both local and convective vertical accelerations as well as for the inner viscous frictions over the vertical.

In the rest of this chapter, the basic SVP hypothesis is presented as well as the general equation for pressure and its gradients within flow. Subsequently, the step-by-step development of the two dynamic SVP equations follows. Finally, a discussion of the equations derived is presented, with a mathematical comparison to the SV and Serre models.

6.1.- SVP model assumption

The SVP equations rest fundamentally upon the hypothesis that the horizontal velocities are constant over the vertical (i.e., $u = U$ and $v = V$). This means that the deviations, over the vertical, of the horizontal velocity components from their averaged value, are negligible as it was assumed previously for the development of the Serre equations. However, contrary to Serre and SV, the assumption of inviscid flow over the vertical is not made. As such, the vertical viscous shear stresses are not simplified and the overall terms in the third NS momentum equation are considered for the development of the SVP. However, only the physical water viscosity is used to calculate the friction shear stresses in the third NS momentum equation.

The procedure to develop the SVP equations is exactly identical to that used to establish the Serre model. It consists of calculating the vertically-averaged expression of the continuity equation (3a) and of the three resulting NS equations (3b, 3c and 3d). This leads to a system consisting exactly of the standard SV equations (6) but with some additional terms due to the vertical integration of the dynamic pressure gradients. The overall procedure to develop the SV model is fully described by Tossou (2004), Hervouet

(2003), Viollet et al. (1998) and Van Rijn (1994). However, this work will simply focus on the vertical integration of the gradient pressure terms, and the resulting expressions must be added to the SV equations in order to form the SVP. The first step of the procedure is to establish the general expression of the vertical velocity. This leads exactly to the same equation (10) obtained for the Serre model and it will be considered for the following development.

6.2.- General expression of the pressure field

Starting with the mathematical expression of the vertical velocity, i.e., equation (10), it is possible to establish the general equation of the pressure field. To proceed, it is necessary to calculate the material derivative of the vertical velocity and then replace the expression obtained into the third NS momentum equation, i.e., equation (3d).

From equation (10), the material derivative of w gives:

$$\frac{Dw}{Dt}=\frac{Dw_f}{Dt}-\frac{DL}{Dt}\left(z-z_f\right)-L\left(w-w_f\right) \tag{84}$$

For the sake of conciseness, the total acceleration of the bottom of the flow, i.e., the variable Dw_f/Dt that is independent of z will be renamed $\beta\left(x,\ \ y\right)$ defined as follows:

$$\beta\left(x,\ \ y\right)=\frac{Dw_f}{Dt} \tag{85}$$

However, the variable $\beta\left(x,\ \ y\right)$ will be simply denoted β for the sake of simplicity.

The substitution of the general expression (10) of the vertical velocity into (84) taking into account equation (85) yields:

$$\frac{Dw}{Dt} = \beta + \left(z - z_f\right)\left(L^2 - \frac{DL}{Dt}\right) \tag{86}$$

The vertical velocity w_η calculated at the position η of the free surface of the flow gives:

$$w_\eta = w_f - LH \tag{87}$$

The vertical velocity w_H of the water column gives:

$$\frac{DH}{Dt} = \frac{D\eta}{Dt} - \frac{Dz_f}{Dt} = w_\eta - w_f \tag{88}$$

The substitution of equation (87) into (88) gives:

$$\frac{DH}{Dt} = -LH \tag{89}$$

Moreover, the material derivative of equation (89) yields:

$$\frac{D^2H}{Dt^2} = -\frac{DL}{Dt}H - L\frac{DH}{Dt} \tag{90}$$

For the sake of conciseness, the acceleration of the total flow depth, i.e., the variable D^2H/Dt^2, which is independent of z will be renamed $\alpha\left(x,\ \ y\right)$ defined as follows:

$$\alpha\left(x,\ \ y\right) = \frac{D^2H}{Dt^2} \tag{91}$$

However, the variable $\alpha\left(x,\ \ y\right)$ will be simply denoted α for the sake of simplicity.

Substituting (89) and (91) into (90) and rearranging the resulting equation yield:

$$\frac{DL}{Dt} = L^2 - \frac{\alpha}{H} \tag{92}$$

The substitution of (92) into (86) yields the final expression of the derivative of the vertical velocity:

$$\frac{Dw}{Dt} = \beta + \left(z - z_f\right)\frac{\alpha}{H} \tag{93}$$

In addition, by using the physical water viscosity to calculate the friction shear stresses, the third term in the LHS of the third NS momentum equation (3d) becomes:

$$\frac{1}{\rho}\left(\frac{\partial \tau_{zx}}{\partial x} + \frac{\partial \tau_{zy}}{\partial y} + \frac{\partial \tau_{zz}}{\partial z}\right) = \nu\left(\frac{\partial^2 w}{\partial x^2} + \frac{\partial^2 w}{\partial y^2} + \frac{\partial^2 w}{\partial z^2}\right) \tag{94a}$$

Thereby substituting the general expression of the vertical velocity, i.e., equation (10), into the term $\nu\left(\partial^2 w/\partial x^2 + \partial^2 w/\partial y^2 + \partial^2 w/\partial z^2\right)$, it is reformulated and yields:

$$\nu\left(\frac{\partial^2 w}{\partial x^2} + \frac{\partial^2 w}{\partial y^2} + \frac{\partial^2 w}{\partial z^2}\right) = \nu\left(\begin{array}{l} L\left(\dfrac{\partial^2 z_f}{\partial x^2} + \dfrac{\partial^2 z_f}{\partial y^2}\right) + \dfrac{\partial^2 w_f}{\partial x^2} \\ + \dfrac{\partial^2 w_f}{\partial y^2} + 2\dfrac{\partial L}{\partial x}\dfrac{\partial z_f}{\partial x} + 2\dfrac{\partial L}{\partial y}\dfrac{\partial z_f}{\partial y} \end{array}\right) - \nu\left(\frac{\partial^2 L}{\partial x^2} + \frac{\partial^2 L}{\partial y^2}\right)\left(z - z_f\right) \tag{94b}$$

For the sake of conciseness, two intermediate variables $A\left(x,\ y\right)$ and $B\left(x,\ y\right)$ are created and defined as follow:

$$A\left(x,\ y\right) = \nu\left(\frac{\partial^2 L}{\partial x^2} + \frac{\partial^2 L}{\partial y^2}\right) \tag{95a}$$

$$B(x,\ y)=\nu\left(L\left(\frac{\partial^2 z_f}{\partial x^2}+\frac{\partial^2 z_f}{\partial y^2}\right)+\frac{\partial^2 w_f}{\partial x^2}+\frac{\partial^2 w_f}{\partial y^2}+2\frac{\partial L}{\partial x}\frac{\partial z_f}{\partial x}+2\frac{\partial L}{\partial y}\frac{\partial z_f}{\partial y}\right) \tag{95b}$$

However, the variables $A(x,\ y)$ and $B(x,\ y)$ will be simply denoted A and B respectively for the sake of simplicity.

The substitution of (95a) and (95b) into (94b) gives:

$$\nu\left(\frac{\partial^2 w}{\partial x^2}+\frac{\partial^2 w}{\partial y^2}+\frac{\partial^2 w}{\partial z^2}\right)=-A\left(z-z_f\right)+B \tag{96}$$

After those preliminary transformations, (93) and (96) are substituted into the third simplified NS momentum equation (3d) to give:

$$-\frac{1}{\rho}\frac{\partial p}{\partial z}=\left(g-B+\beta\right)+\left(\frac{\alpha}{H}+A\right)\left(z-z_f\right) \tag{97}$$

Finally, the last step to establish the general expression for the pressure field is to vertically integrate (97) from an arbitrary surface (z) within the flow to the position of the free surface (η).

Therefore, the vertical integral of the LHS of (97) is calculated by taking into account the fact that free surface pressure (p_η) is equal to atmospheric pressure, which is zero. This results in:

$$-\frac{1}{\rho}\int_z^\eta \frac{\partial p}{\partial z}dz=\frac{1}{\rho}\left(-p_\eta+p\right)=\frac{p}{\rho} \tag{98}$$

Next, the vertical integral of the RHS of (97) is calculated by taking into account the fact that, except z, the other variables (i.e., $\alpha, \beta, A, B, H, z_f$ and g) are independent of z. This results successively in:

$$\int_z^{\eta} \left(g - B + \beta\right) dz = \left(g - B + \beta\right)\left(\eta - z\right) \tag{99a}$$

$$\int_z^{\eta} \left(\frac{\alpha}{H} + A\right)\left(z - z_f\right) dz = \left(\frac{\alpha}{H} + A\right)\left(\frac{\eta^2 - z^2}{2} - z_f\left(\eta - z\right)\right) \tag{99b}$$

The sum of equations (99a) and (99b) gives the vertical integral of the RHS of (97):

$$\int_z^{\eta} \left(\left(g - B + \beta\right) + \left(\frac{\alpha}{H} + A\right)\left(z - z_f\right)\right) dz = \left(\eta - z\right)\left(g - B + \beta\right) + \left(\eta - z\right)\left(\frac{\alpha}{H} + A\right)\left(\frac{\eta + z}{2} - z_f\right) \tag{100}$$

Finally, the vertical integral of the third NS momentum equation (3d) is formed by using equations (98) and (100) and yields the general expression of the SVP pressure field:

$$p\left(x,\ y,\ z,\ t\right) = \rho g\left(\eta - z\right) + \rho\left[\left(-B + \beta\right)\left(\eta - z\right) + \left(\frac{\alpha}{H} + A\right)\left(\frac{\eta^2 - z^2}{2} - z_f\left(\eta - z\right)\right)\right] \tag{101}$$

The first term in the RHS of (101) represents the equation of the hydrostatic pressure distribution whereas the other terms represent the expression of the SVP dynamic pressure due to the total vertical acceleration as well as to the viscous frictions within the flow over the vertical. If the vertical viscous frictions are neglected (i.e., if $A = B = 0$), the RHS of (101) is reduced to the Serre pressure field equation.

6.3.- General equations for pressure gradients

Having established the equation describing the SVP pressure field, it is now necessary to characterize the SVP pressure gradients.

One obtains the pressure gradient along the x-axis by deriving each of the terms of equation (101) with respect to x. This derivation gives successively:

$$\frac{\partial}{\partial x}\left[\rho\left(g+\beta-B\right)\left(\eta-z\right)\right]=\rho\left(\frac{\partial\beta}{\partial x}-\frac{\partial B}{\partial x}\right)\left(\eta-z\right)+\rho\left(g+\beta-B\right)\frac{\partial\eta}{\partial x} \tag{102a}$$

$$\frac{\partial}{\partial x}\left[\rho\left(\frac{\alpha}{H}+A\right)\left(\frac{\eta^2-z^2}{2}-z_f\left(\eta-z\right)\right)\right]=\rho\frac{\partial}{\partial x}\left(\frac{\alpha}{H}+A\right)\left(\frac{\eta^2-z^2}{2}-z_f\left(\eta-z\right)\right)+\rho\left(\frac{\alpha}{H}+A\right)\left(H\frac{\partial\eta}{\partial x}-\left(\eta-z\right)\frac{\partial z_f}{\partial x}\right) \tag{102b}$$

and the sum of the equations (102a) and (102b) gives the pressure gradient expression in the x direction:

$$\begin{aligned}\frac{1}{\rho}\frac{\partial p}{\partial x}&=\left(\frac{\partial\beta}{\partial x}-\frac{\partial B}{\partial x}\right)\left(\eta-z\right)+\left(g+\beta-B\right)\frac{\partial\eta}{\partial x}\\&+\frac{\partial}{\partial x}\left(\frac{\alpha}{H}+A\right)\left(\frac{\eta^2-z^2}{2}-z_f\left(\eta-z\right)\right)+\left(\frac{\alpha}{H}+A\right)\left(H\frac{\partial\eta}{\partial x}-\left(\eta-z\right)\frac{\partial z_f}{\partial x}\right)\end{aligned} \tag{103a}$$

The same procedure establishes equation (103b) that represents the pressure gradient expression in the y direction:

$$\begin{aligned}\frac{1}{\rho}\frac{\partial p}{\partial y}&=\left(\frac{\partial\beta}{\partial y}-\frac{\partial B}{\partial y}\right)\left(\eta-z\right)+\left(g+\beta-B\right)\frac{\partial\eta}{\partial y}\\&+\frac{\partial}{\partial y}\left(\frac{\alpha}{H}+A\right)\left(\frac{\eta^2-z^2}{2}-z_f\left(\eta-z\right)\right)+\left(\frac{\alpha}{H}+A\right)\left(H\frac{\partial\eta}{\partial y}-\left(\eta-z\right)\frac{\partial z_f}{\partial y}\right)\end{aligned} \tag{103b}$$

6.4.- Vertically-averaged pressure gradients

Having characterized the SVP pressure gradients, it is now required to integrate them over the vertical to establish mean expressions for a 2DH application. Therefore, each pressure gradient term will be considered individually and its integration over the vertical will be presented:

$$\frac{1}{H}\int_{z_f}^{\eta}\left(\frac{\partial\beta}{\partial x}-\frac{\partial B}{\partial x}\right)(\eta-z)dz=\frac{1}{H}\left(\frac{\partial\beta}{\partial x}-\frac{\partial B}{\partial x}\right)\int_{z_f}^{\eta}(\eta-z)dz=\frac{H}{2}\left(\frac{\partial\beta}{\partial x}-\frac{\partial B}{\partial x}\right) \tag{104a}$$

$$\frac{1}{H}\int_{z_f}^{\eta}(g+\beta-B)\frac{\partial\eta}{\partial x}dz=\frac{1}{H}(g+\beta-B)\frac{\partial\eta}{\partial x}\int_{z_f}^{\eta}dz=(g+\beta-B)\frac{\partial\eta}{\partial x} \tag{104b}$$

$$\frac{1}{H}\int_{z_f}^{\eta}\frac{\partial}{\partial x}\left(\frac{\alpha}{H}+A\right)\left(\frac{\eta^2-z^2}{2}-z_f(\eta-z)\right)dz=\frac{1}{3}\frac{\partial}{\partial x}\left(\frac{\alpha}{H}+A\right)H^2=\frac{H}{3}\frac{\partial\alpha}{\partial x}-\frac{\alpha}{3}\frac{\partial H}{\partial x}+\frac{1}{3}\frac{\partial A}{\partial x}H^2 \tag{104c}$$

$$\frac{1}{H}\int_{z_f}^{\eta}\left(\frac{\alpha}{H}+A\right)\left(H\frac{\partial\eta}{\partial x}-(\eta-z)\frac{\partial z_f}{\partial x}\right)dz=(\alpha+AH)\left(\frac{\partial\eta}{\partial x}-\frac{1}{2}\frac{\partial z_f}{\partial x}\right) \tag{104d}$$

The sum of (104a), (104b), (104c) and (104d) by taking into account the fact that, $z_f=\eta-H$, yields:

$$-\frac{1}{H}\int_{z_f}^{\eta}\frac{1}{\rho}\frac{\partial p}{\partial x}dz=-\frac{H}{2}\left(\frac{\partial \beta}{\partial x}-\frac{\partial B}{\partial x}\right)-\left(g+\beta-B\right)\frac{\partial \eta}{\partial x}-\left(\frac{H}{3}\frac{\partial \alpha}{\partial x}-\frac{\alpha}{3}\frac{\partial H}{\partial x}+\frac{1}{3}\frac{\partial A}{\partial x}H^2\right)$$
$$-\left(\alpha+AH\right)\left(\frac{\partial \eta}{\partial x}-\frac{1}{2}\frac{\partial\left(\eta-H\right)}{\partial x}\right) \qquad (105)$$

After expansion, simplification and rearrangement, equation (105) results in (106a), which is the final mathematical formulation of the vertically-averaged pressure gradient in the x direction:

$$-\frac{1}{H}\int_{z_f}^{\eta}\frac{1}{\rho}\frac{\partial p}{\partial x}dz=-g\frac{\partial \eta}{\partial x}-H\frac{\partial}{\partial x}\left(\frac{\beta-B}{2}+\frac{\alpha}{3}\right)-\frac{\partial \eta}{\partial x}\left(\frac{\left(\alpha+AH\right)}{2}+\left(\beta-B\right)\right)-\frac{\partial H}{\partial x}\left(\frac{\alpha}{6}+\frac{AH}{2}\right)-\frac{H^2}{3}\frac{\partial A}{\partial x} \qquad (106a)$$

Similarly, equation (106b) is the mathematical formulation of the vertically-averaged pressure gradient in the y direction:

$$-\frac{1}{H}\int_{z_f}^{\eta}\frac{1}{\rho}\frac{\partial p}{\partial y}dz=-g\frac{\partial \eta}{\partial y}-H\frac{\partial}{\partial y}\left(\frac{\beta-B}{2}+\frac{\alpha}{3}\right)-\frac{\partial \eta}{\partial y}\left(\frac{\left(\alpha+AH\right)}{2}+\left(\beta-B\right)\right)-\frac{\partial H}{\partial y}\left(\frac{\alpha}{6}+\frac{AH}{2}\right)-\frac{H^2}{3}\frac{\partial A}{\partial y} \qquad (106b)$$

On the RHS of (106a) or (106b), the first term represents that of the hydrostatic pressure gradient while the other terms account for dynamic pressure forces on the flow (due to the sudden vertical flow variations, the vertical curves in the flow paths and the viscous friction over the vertical).

6.5.- Mathematical formulation of the SVP equations

The 2DH SVP model is obtained by adding the dynamic pressure terms to the standard SV equations. Therefore, the hydrostatic pressure gradients terms (i.e., $-g\,\partial\eta/\partial x$ and $-g\,\partial\eta/\partial y$) on the RHS of the two SV dynamic equations (6b and 6c) are simply replaced with the RHS of (106a) and (106b) respectively. Adding the 2DH continuity equation to close the resulting system and rearranging yield:

$$\frac{\partial H}{\partial t}+\frac{\partial(HU)}{\partial x}+\frac{\partial(HV)}{\partial y}=0 \tag{107a}$$

$$\frac{\partial U}{\partial t}+U\frac{\partial U}{\partial x}+V\frac{\partial U}{\partial y}+\frac{1}{\rho H}\left(\tau_x^f-\tau_x^s\right)-\frac{\partial}{\partial x}\left(\nu_{xx}\frac{\partial U}{\partial x}+\nu_{xy}\frac{\partial U}{\partial y}\right)-\frac{\partial}{\partial y}\left(\nu_{yx}\frac{\partial U}{\partial x}+\nu_{yy}\frac{\partial U}{\partial y}\right)$$
$$+g\frac{\partial\eta}{\partial x}=-H\frac{\partial}{\partial x}\left(\frac{\beta-B}{2}+\frac{\alpha}{3}\right)-\frac{\partial\eta}{\partial x}\left(\frac{(\alpha+AH)}{2}+(\beta-B)\right)-\frac{\partial H}{\partial x}\left(\frac{\alpha}{6}+\frac{AH}{2}\right)-\frac{H^2}{3}\frac{\partial A}{\partial x} \tag{107b}$$

$$\frac{\partial V}{\partial t}+U\frac{\partial V}{\partial x}+V\frac{\partial V}{\partial y}+\frac{1}{\rho H}\left(\tau_y^f-\tau_y^s\right)-\frac{\partial}{\partial x}\left(\nu_{xx}\frac{\partial V}{\partial x}+\nu_{xy}\frac{\partial V}{\partial y}\right)-\frac{\partial}{\partial y}\left(\nu_{yx}\frac{\partial V}{\partial x}+\nu_{yy}\frac{\partial V}{\partial y}\right)$$
$$+g\frac{\partial\eta}{\partial y}=-H\frac{\partial}{\partial y}\left(\frac{\beta-B}{2}+\frac{\alpha}{3}\right)-\frac{\partial\eta}{\partial y}\left(\frac{(\alpha+AH)}{2}+(\beta-B)\right)-\frac{\partial H}{\partial y}\left(\frac{\alpha}{6}+\frac{AH}{2}\right)-\frac{H^2}{3}\frac{\partial A}{\partial y} \tag{107c}$$

In this system, all the variables have been previously defined.

The first equation (107a) represents the 2DH continuity equation (i.e., conservation of mass) while the two following equations represent the 2DH SVP dynamic equations, i.e., conservation of momentum). The principal unknown variables are the mean velocities (U and V), the position of the free surface of the flow (η) and/or the water depth (H).

These SVP equations can model the flows with dynamic pressure at a solid bottom, as well for the case where the bottom is also a free surface as in a free overfall (e.g., weirs). In the latter case, the bottom level z_f also becomes an unknown variable, which would require a fourth supplementary equation to close the system.

For solid bed applications, the SVP equations could be useful to simulate high-amplitude waves propagating in shallow water. They could also be used for many applications related to highly unsteady flows (e.g., dambreak simulations) or to highly non-uniform flows (e.g., spillway, transition flows).

The RHS of the two dynamic equations (107b) and (107c) are the supplementary terms that are added to the traditional SV equations to form the SVP ones and they translate the effects of dynamic pressure on flow. They are characterized by the presence of Serre's formulation of the vertical accelerations expressed as α (total water depth increase acceleration) and β (vertical acceleration of the bottom flow). Moreover, the SVP dynamic pressure consists of the Serre's with some additional terms caused by the vertical viscous frictions. Then, SVP model puts into evidence the variable A (the increase of the acceleration α per unit of flow depth due to the vertical viscous frictions) and the variable B (the increase of the acceleration β due to the vertical viscous frictions). If the flow is assumed inviscid over the vertical (i.e., if $A = B = 0$), the effects of the vertical viscous frictions on dynamic pressure become zero and the SVP equations reduce themselves to the classic Serre model. Moreover, if the effects of vertical accelerations are neglected or are negligible (i.e., if $\alpha = \beta = 0$) and the flow assumed inviscid over the vertical (i.e., if $A = B = 0$), the RHS of the two dynamic equations (107b and 107c) become zero and they reduce themselves to the classic dynamic 2DH SV equations.

Conclusion

The 2DH SVP model is established to describe the hydrodynamic characteristics of free surface flows under dynamic pressure effects due both to the total vertical acceleration and to the vertical viscous frictions. The only assumption about the horizontal velocity components constant over the vertical is used to simplify the 3D NS and the resulting equations are then integrated vertically to generate the SVP. The system obtained consists of a 2DH continuity equation and two dynamic 2DH equations. This model is an extended version of the SV equations in which, the effects of both the total vertical acceleration and the vertical viscous frictions are included. It can also be considered as a more general formulation of the Serre model. Indeed, if the flow is assumed inviscid over the vertical, the viscous shear stresses in the third NS are cancelled and the SVP is reduced to the Serre model. Moreover, the SVP equations contain the same terms as those found in the SV and Serre formulations but they also contain supplementary terms that correctly account for dynamic pressure, which allows for the simulation of a number of very diverse natural flows. Thus, the SV, Serre and SVP all exploit the same types of entry variables, boundary conditions and exit variables but the SVP also outputs a more general formulation of the total pressure profile than that provided by Serre. In the SVP supplementary terms, there is the presence of higher order derivatives, which particularly increases the complexity of their resolution. Consequently, at the application level, this may result in additional computational effort. However, its numerical solution is not presented here because it is not the focus.

CHAPTER 7

Conclusion and perspectives

The Serre equations (Serre 1953) that describe the horizontal two-dimensional (2DH) hydrodynamics (water velocity and water level) of free surface flows are presented in this study. They are proposed as an alternative to the 2DH shallow water (SW) equations, i.e., the Saint-Venant (SV) model, for non-hydrostatic free surface flows modeling.

The mathematical formulation of the Serre model is very similar to the more traditional 2DH SV equations except, in the latter, a hydrostatic pressure distribution is assumed whereas Serre includes some additional terms in the momentum equations to account for some types of non-linear pressure dynamics due to the water having some important vertical acceleration. Thus, the effects of the sudden variations in flow over the vertical and the significant vertical curvature of the streamlines are taken into account in the resulting equations. To develop such formulation, the main assumptions were that the vertical velocity component of the flow varies linearly from the bottom of the flow to the free surface and that the flow is inviscid over the vertical. However, the presence of higher order and mixed (spatial-temporal) derivative terms in the Partial Differential Equations (PDE) makes the model very difficult to resolve numerically making it so poorly documented and/or so poorly understood. Therefore, this work allows the model to be more widely used by clearly explaining its assumptions and by deriving its equations step-by-step. Subsequently, the mixed spatio-temporal derivatives in the PDE are separated for solid bed applications (i.e., no free overfall) so that the principal difficulty is eliminated.

For the numerical resolution of the new formulation of the Serre PDE, the second-order Taylor-Galerkin (TG) scheme is used. Thus, under some simplifications and based on a Taylor series expansion of the time derivatives, some artificial numerical diffusion terms

are introduced both in the continuity and two dynamic equations. Subsequently, the more traditional finite element procedure is applied to the resulting modified model, which is suitable for the simulation of the flow situations with dominant advection phenomenon. The triangular nonconforming elements are used for the spatial discretization since they have some interesting orthogonality properties that improve the accuracy of the numerical results and also reduce the duration of the computations. Therefore, the water depth is calculated only at the vertex nodes while the velocity components are estimated at the middle nodes. Thus, the Serre system, which initially consists of some PDE, is transformed into an algebraic equation in matrix form. The resulting computer program is implemented with Matlab® to simulate some chosen flow situations. However, the imposition of the unknown open downstream boundary conditions was the principal difficulty encountered since there is no consensus in the literature about the methods being used. Consequently, in our applications, the channels are chosen to be long enough so that the flow never reaches the downstream region. Thus, only a zero flux is imposed as boundary conditions. The weakness of this approach is that the simulations take too much time and computer space memory to run. However, it has the advantage of avoiding the numerical error due to bad imposition of such boundary conditions.

For the preliminary validation, a calm water basin, a permanent uniform flow (the Chézy flow) and a solitary wave propagation are simulated before applying the model to a complex situation (i.e., dambreak flow). In each case, the analytical solution is known and is compared to the numerical results. For the two first tests, the boundary conditions are adequately imposed at the overall limits of the domain since they are known. As numerical results, the calm water basin, still without flow (zero velocity and no change to the flow depth throughout the domain) for the case where the bottom of the channel is flat as well as for the case where a constant bed slope is imposed. This means that there is no error within the computer program. Also, the simulation of the Chézy flow showed that the water depth is constant throughout the channel; the flow is one-dimensional and the velocity is uniform in the direction of the flow. The corresponding constant value of the velocity is equal to the amount estimated by means of the Chézy theoretical equation. It was deduced that even with some additional artificial diffusion, the Serre numerical model can adequately simulate the permanent uniform flow. The third test is the solitary

wave propagation with the particularity that the artificial diffusion terms are neglected since for this flow situation, the nonlinear and dispersive effects counterbalance each other. The analytical solution is also available. The downstream boundary conditions are unknown, thus the zero flux approach is imposed at that open downstream limit of the domain. The water depth and the velocity profiles that are obtained numerically with the Serre model are consistent with the analytical ones.

After successfully completing the three preliminary tests, dambreak flows are simulated, given that they are characterized by the presence of non-hydrostatic pressure distribution and the fact that the advection phenomenon is dominant. On one hand, a horizontal and frictionless channel is used for the basic test case so that the Stoker (1957) analytical solution can be applied. On the other hand, the additional tests are devoted to the study of the influence of some important parameters (i.e., bed slope, bed roughness and ratio of the water depths upstream and downstream). Once again, a zero flux is also imposed at the downstream as open boundary conditions in overall cases. The simulations underline two dambreak waves: one traveling upstream, called a rarefaction wave (or depression) and one traveling downstream, called a bore. For this basic test, the shape of the profiles (water level and longitudinal velocity) simulated by the Serre model and those given by the SV are both in a good agreement with the Stoker analytical solution although there are some small differences in both wave amplitude and particularly wave celerity. The celerity of both the positive and negative waves predicted by the Serre model is smaller than that predicted by the SV model. Consequently, the SV bore outruns that simulated by Serre. This observation is consistent with what was found earlier by Kosorin (1983). For example, the SV bore celerity was up to 13.33 % higher than what was predicted by the Serre non-hydrostatic model after 30 s yielding an approximate outdistancing of 47.5 m. Thus, dynamic pressure is truly present in a dambreak flow and it is caused by the vertical acceleration (due to the rapid variation of the flow over the vertical and to the significant vertical curvature of the flow path). Additionally, it was noted that as the bed slope increases, the celerity for the Serre bore increases more rapidly than the SV one. Therefore, the amount of the outdistancing of the SV bore decreases with increasing the bed slope. Furthermore, as bed roughness and water depths ratio increase, outdistancing

increases due to the greater importance of pressure in the hydrodynamics and Serre's ability to correctly account for that effect.

It was also remarked that when the Serre dynamic equations and the continuity one are upwinded by using the second-order Taylor series expansion, the resulting system becomes efficient for shock-capturing in a dambreak situation (any oscillations) without decreasing the quality of the numerical results.

From a technical point of view, the Serre model is suggested to replace the SV one when a great accurateness is needed for a dambreak project. Even if many other models that take into account the dynamic pressure effects are available, the Serre formulation is still directly the SV one to which, some supplementary terms are added. Both models use the same types of entry variables and boundary conditions and they produce the same types of exit variables so that it will be easy to modify the more usual computer programs based on the SV equations.

This study is completed by the development of the 'Saint-Venant Plus' (SVP) equations that are proposed to extend the Serre model. The particularity of the SVP is that the flow is not assumed inviscid over the vertical. However, the horizontal velocity components are supposed constant over the vertical similarly to the Serre model. Even if the physical water viscosity is small, a number of factors make the Serre and SV assumption of inviscid flow over the vertical invalid in many cases. The effects of even a small amount of viscosity cannot be neglected near vertical fluid boundaries because of the presence of a boundary layer. For example, the viscous shear stresses on rough walls could become significant for many open-channel flows particularly when the flow varies rapidly over the vertical. The resulting mathematical formulation contains the same terms as those found in the SV and Serre models but it also contains some supplementary terms that more adequately account for dynamic pressure. In the SVP, the dynamic component is established in a much more generalized manner by including the vertical viscous, which allows for the simulation of a number of very diverse natural flows.

The main contributions of this thesis are listed below:

- ✓ The Serre model is now well documented and understood; its assumptions, the procedure for its development and its real mathematical formulation are presented and the link to the more traditional SV equations.

- ✓ The spatial derivatives are separated from the temporal ones and a new formulation of the Serre equations is available, which is amenable to be used in any given number of numerical schemes. The spatial derivatives can be discretized separately from the temporal ones. Therefore, the principal difficulty when using this type of model is eliminated.

- ✓ The Serre model is solved with the finite element method (FEM) and the resulting numerical formulation is validated by simulating a number of chosen flow situations. This contribution can also be considered as a reply to the need to have a FEM solution of the Serre model so as that it could be compared not only to the SV but also to the non-hydrostatic Navier-Stokes (NS) model, which have already been investigated by using the FEM (Hervouet 2003).

- ✓ The importance of the dynamic pressure effects is demonstrated for flow situations where the vertical acceleration is significant such as a dambreak flow. Thus, the Serre model is recommended for a more accurate design process when the flow is non-hydrostatic.

- ✓ The upwind technique based on the second-order Taylor series expansion of the time derivatives to add some artificial diffusion terms is shown to be efficient for shock-capturing and the quality of the numerical results is not decreased.

- ✓ Finally, an extended version of the Serre model (i.e., the SVP) was established for the fully non-hydrostatic flows without making the assumption of inviscid flow over the vertical. The resulting equations constitute a generalized solution applicable to a number of very diverse natural flows.

Despite these numerous contributions, this Serre model developed here should be improved. Thus, in a further work, the drying-wetting phenomenon should be considered and a more efficient technique for open boundary conditions imposing should be implemented. Subsequently, the resulting scheme could be applied to simulate a real dambreak case study especially with progressive breach. Thereafter, the Serre numerical results will be compared to those from the same simulations by using both the non-hydrostatic Navier-Stokes (NS) model and a higher-order Boussinesq equation. Also, it should be mentioned that the Serre numerical model does not succeed in simulating the propagation of a wave over-passing an asymmetric trapezoid underwater bar (the Dingemans test) because the FEM scheme was not suitable for such a flow situation. Therefore, it is suggested to solve the new formulation of the Serre model by means of some other numerical schemes like the 'Total Diminish Volume' (TVD) method and to simulate the Dingemans test for validation purpose. Additionally, the time-space derivatives separation formulation of the Serre model could also be established for the cases where the bottom of the flow is also a free surface (i.e., free overfalls). Finally, the resolution of the SVP model with the FEM will be useful in comparing it with the Serre model, principally for the flow situations where the vertical viscous frictions are important.

REFERENCES

Akanbi, A. and Katopodes, N. (1988). Model for flood propagation on initially dry land. J. Hydraul. Eng., 114(7): 689-706.

Alcrudo, F. and Garcia-Navarro, P. (1993). A high-resolution Godunov-type scheme in finite volumes for the 2D shallow-water equations. Int. J. Numer. Methods Fluids, 16:489-505.

Antunes Do Carmo, J.S., Seabra Santos, F.J., and Almeida, A. B. (1993). Numerical solution of the generalized Serre equations with the MacCormack finite-difference scheme. Int. J. Numer. Methods Fluids, 16: 725-738.

Aureli, F., Mignos, P. and Tomirotti, M. (2000). Numerical Simulation and Experimental Verification of Dam-Break Flows with Shocks. J. Hydraul. Res., 38:197-206.

Barré de Saint-Venant, A.J.C. (1871). Théorie et Équations Générales du Mouvement Non Permanent des Eaux Courantes. Comptes Rendus des séances de l'Académie des Sciences, Paris, France, Séance 17 July 1871, Vol. 73, pp. 147-154.

Basco, D.R. (1989). Limitation of the Saint-Venant equations in dam-break analysis. J. Hydraul. Eng., 115(7): 950-965.

Betamio de Almeida, A. and Franco, B. (1993). Modelling of Dam Break Flows. In Computer Modelling of Free Surface and Presurised Flows. Chaudhry and Mays (Editors). NATO ASI Serie E : Applied Sciences, Vol. 274.

Bottura, L. and Zienkiewicz, O.C. (1990). Experiments on iterative solution for the semi-implicit characteristic-Galerkin algorithm. Communications in Applied Numerical Methods, 6:387-393.

Boussinesq, J. (1871). Theorie de l'intumescence liquide appelée onde solitaire ou de translation se propageant dans un canal retangulaire. Comptes Rendus. Acad Sci. 72, 755-759.

Boussinesq, J. (1877). Essai sur la théorie des eaux courantes. Mémoires présentés par divers savants à l'Académie des Sciences, Paris 23 (1), 1-680.

Brechler, J. (1992). A radiation boundary condition for finite-element models: 1-d linear advection test. J. Studia geoph., et geod. 36: 188-197.

Brufau, P. and Garcia-Navarro, P. (2000). Two-dimensional dam break flow simulation. Int. J. Numer. Methods Fluids, 33:35-57.

Casulli, V. and Zanolli, P. (2002). Semi-Implicit Numerical Modelling of Non-Hydrostatic Free-Surface Flows for Environmental Problems. Mathematical and Computer Modelling, 36: 1131-1149.

Cienfuegos, R., Barthélemy, E. and Bonneton, P. (2005). Résolution numérique en volumes finis d'un système d'équations de Serre étendu. Revue européenne de génie civil, 9(7-8): 889-902.

Dhatt, G. and Touzot, G. (1981). Une présentation de la méthode des éléments finis. Presse de l'Université Laval. ISBN 2763769128 (Canada).

Donea, J. (1984). A Taylor–Galerkin method for convective transport problems. Int. J. Numer. Methods Fluids, 20:101-119.

Donea, J., Giuliani, S., Laval, H. and Quartapelle, L. (1984). Time-accurate solution of advection–diffusion problems by finite elements. Computer Methods in Applied Mechanics and Engineering, 45:123-145.

Donea, J., Quartapelle, L. and Selmin, V. (1987). An analysis of time discretization in the finite element solution of hyperbolic problems. J. Comp. Phys., 70:463-499.

Donea, J., Quartapelle, L. and Selmin, V. (1992). An introduction to finite element methods for transient advection problems. Computer Methods in Applied Mechanics and Engineering, 95:169-203.

Dressler, R.F. (1952). Hydraulic Resistance Effect upon the Dam-Break Functions. Journal of Research, NBS, 49(3) :217-225.

Dressler, R.F. (1954). Comparison of theories and experiments for hydraulic Dam-Break wave. Int. Assoc. Sci. Pubs., 3(38): 319-328.

Dufresne, Z.M. (1997). Modélisation de la houle par éléments finis. Thèse de Doctorat. Université de Compiègne, Compiègne France.

Fenton, J.D. and Zerihum, Y. T. (2007). A Boussinesq approximation for open channel flow, in Proc. 32nd Congress, Int. Assoc. Hydraulic Engng and Res., Venice, Italy, 2-6 July, 2007, IAHR, published on CD.

Fenton, J.D. (1972). A ninth-order solution for the solitary wave. J. Fluid Mech. 53(2): 237-246.

Flather, R. (1976). A tidal model of the north-west european continental shelf. Mémoire Société Royale des Sciences de Liège, X: 141–164.

Fraccarollo, L. and Toro, E.F. (1993). A Shock-Capturing Method for Two Dimensional Dam-Break Problems. Proceedings of the Fifth International Symposium in Computational Fluid Dynamics, Sendai, Japan.

Fraccarollo, L. and Toro, E.F. (1995). Experimental and numerical assessment of the shallow water model for two-dimensional dam-break problems. J. Hydraul. Res., 33:843-864.

Garcia-Navarro, P. (1999). Dam-Break Flow Simulation. In Numerical Modelling of Hydrodynamical Systems. Garcia-Navarro, P. and Playan, E. (Editors), pages 27-56. University of Zaragoza, Spain.

Ghamry, H.K. and Steffler, P.M. (2002). Effect of applying different distribution shapes for velocities and pressure on simulation of curved open channels. J. Hydraul. Eng., 128(11): 969–982.

Gobbi, M.F., Kirby J.T. and Wei, G. (2000). A fully nonlinear Boussinesq model for surface waves. Part 2. Extension to O(kh)4. Int. J. Numer. Methods Fluids, 405: 181–210.

Griffith, A.R., Rutherford, J.H., Alavi, A., Moore, D.D. and Groeneveld, J. (2007). Stability review of the Wanapum spillway using CFD analysis. Canadian Dam Association Bulletin. Fall 2007. 16-27.

Hager, W.H. (1983). Hydraulics of the plane overfall. J. Hydraul. Eng., 109(2): 1683–1697.

Hanert, E., Le Roux, D.Y., Legat, V. and Deleersnijder, E. (2004). Advection schemes for unstructured grid ocean modeling. Ocean Modelling, 7: 39-58.

Hervouet, J.M. (2003). Hydrodynamique des écoulements à surface libre. Modélisation numérique par la méthode des éléments finis. Presses de l'École Nationale des Ponts et Chaussées (ENPC). ISBN 2-85978-379-2

Hervouet, J.M. and Petitjean, A. (1999). Malpaset Dam-Break Revisited with Two-Dimensional Computations. J. Hydraul. Res., 37(6): 777-788.

Hicks, F.E. and Steffler, P.M. (1994). Comparison of finite element methods for the St. Venant equations. Int. J. Numer. Methods Fluids, 20:99-113.

Hirsch, C. (1995). Numerical computation of internal and external flows. Chichester: John Wiley & Sons.

Hua, B. and Thomasset, F. (1984). A noise free finite element scheme for the two layer shallow equations. Tellus, 36A :157-165.

Hunt, B. (1982). Asymptotic solution for dam-break problem. J. Hydraul. Div., Am. Soc. Civ. Eng., 109(12): 1698-1706.

Hunt, B. (1987). A perturbation solution of the flood-routing problem. J. Hydraul. Res., 25(2): 215-234.

Jankowski, J.A. (1999). A non-hydrostatic model for free surface flows. Ph.D. thesis, Hannover University, Germany.

Jha, A.K., Akiyama, J. and Ura, M. (2000). Flux-difference splitting schemes for 2D flood flows. J. Hydraul. Eng., 126(1): 33-42.

Kato, S., Anju, A. and Kawahara, M. (1994). A finite element study of solitary wave by Boussinesq equation. In Computational Methods in Water Resources X (Kluwer, Dordrecht / Norwell, MA, 1994), p. 1067.

Katopodes, N. (1984). Two-dimensional surges and shocks in open channels. J. Hydraul. Eng., 110(6): 794-812.

Katopodes, N. and Strelkoff, T. (1978). Computing two-dimensional dam-break flood waves. J. Hydraul. Div., Am. Soc. Civ. Eng., 104(9): 1269-1288.

Katopodes, N. and Strelkoff, T. (1979). Two-dimensional shallow water-wave models. J. Hydraul. Eng., 105(2): 317-334.

Khan, A.A. and Steffler, P.M. (1996). Modelling overfalls using vertically and moment equations. J. Hydraul. Eng., 122(7): 397-402.

Korteweg, D.J. and deVries, G. (1895). On the change of form of long waves advancing in a rectangular canal and on a new type of long stationary wave. Phil. Mag. 5(39), 422-443.

Kosorin, K. (1983). Hydraulics characteristics of some dam-break waves singularities. 20th IAHR congress, Moscow, pp. 520-528.

Kurganov, A. and Tadmor, E. (2000). New high-resolution central schemes for nonlinear conservation laws and convection–diffusion equations. J. Comp. Phys., 160:241-282.

Laitone, E.V. (1960). The second approximation to cnoidal and solitary waves. J. Fluid Mech. 9, 430-444.

Lauber, G. and Hager, W.H. (1998a). Experiments to Dambreak Wave : Horizontal Channel. J. Hydraul. Res., 36(3): 291-307.

Lauber, G. and Hager, W.H. (1998b). Experiments to Dambreak Wave : Sloping Channel. J. Hydraul. Res., 36(5): 761-773.

Law, A.W.K. (1997). Steady flow over an obstacle with contraction and sill, in Proc. 27th Congress IAHR, San Francisco, Vol. A, ASCE, New York, pp. 787-792.

Le Roux, D.Y., Robert, J.L. and Gabbouhy, M. (2008). A non conforming finite-element method for solving non-hydrostatic free-surface flow problems. Int. J. Numer. Methods Fluids, 58: 91-109.

Le Roux, D.Y. (2005). Dispersion relation analysis of the P1NC-P1 finite-element pair in shallow-water models. SIAM J. Sci. Comput., 27, 394-414.

Levermore, C.D. and Sammartino, M. (2001). A shallow water model with eddy viscosity for basins with varying bottom topography. Nonlinearity 14 (6): 1493–1515.

Liska, R. and Wendroff, B. (1999). Two-dimensional shallow water equations by composite schemes. Int. J. Numer. Methods Fluids, 30: 461-479.

Lohner, R.L., Morgan, K. and Zienkiewicz, O.C. (1984). The solution of non-linear hyperbolic equation systems by the finite element method. Int. J. Numer. Methods Fluids, 4:1043-1063.

Longuet-Higgins, M.S. and Fenton, J.D. (1974). On the mass, momentum, energy and circulation of a solitary wave. Proc. Roy. Soc. London A 340, 471- 493.

Louaked, M. and Hanich, L. (1998). TVD scheme for the shallow water equations. J. Hydraul. Res., 36:363-378.

Mabssout, M. and Pastor, M. (2003a). A Taylor–Galerkin algorithm for shock wave propagation and strain localization failure of viscoplastic continua. Computer Methods in Applied Mechanics and Engineering, 192:955-971.

Mabssout, M. and Pastor, M. (2003b). A two-step Taylor–Galerkin algorithm applied to shock wave propagation in soils. Int. J. Numer. Anal. Meth. Geomech., 27 : 685 :704.

Madsen, P.A. and Sorensen, O.R. (1992). A new form of the Boussinesq equations with improved linear dispersion characteristic. Part II. A slowly-varying bathymetry. Coastal Engineering, 18, 183-204.

Marchi, E. (1993). On the free overfall. J. Hydraul. Res., 31(6): 777–790.

McCowan, A.D. (1987). The range of application of Boussinesq type numerical short waves models. 22nd Congress, International Association for Hydraulic Research, Lausanne, Switzerland, pp. 379-384.

Meftah, K, Sergent, P. and Gomi, P. (2004). Linear analysis of a new type of extended Boussinesq model. J. Coastal Eng., 51: 185–206.

Mohapatra, P.K., Eswaran, V. and Bhallamudi, S.M. (1999). Two-dimensional analysis of dam-break flow in vertical plane. J. Hydraul. Eng., 125 (2): 183-192.

Molls, T. and Chaudhry, H. (1995). Depth-averaged open-channel flow model. J. Hydraul. Eng., 121 (6): 453-465.

Montes, J.S. (1992). A potential flow solution for the free overfall, Water. Maritime and Energy Proceedings of Institution of Civil Engineers. London 96 (December) (1992) 259–266.

Namin, M.M., Lin, B. and Falconer, R.A. (2001). An implicit numerical algorithm for solving non-hydrostatic free-surface flow problems. Int. J. Numer. Methods Fluids, 35(3): 341–356.

Nwogu, O. (1993). Alternative form of Boussinesq equations for nearshore wave propagation. Journal of Waterways, Port, Coastal and Ocean Engineering, vol. 119, numéro 6.

Nycander, J. and Döös, K. (2003). Open boundary conditions for barotropic waves. J. Geophys. Res. 108 (C5), 3168, doi:10.1029/2002JC001529.

Nycander, J., Hogg A.M. and Frankcombe L.M. (2008). Open boundary conditions for nonlinear channel flow. Ocean Modelling, 24: 108-121.

Orlanski, I. (1976). A simple boundary condition for unbounded hyperbolic flows. J. Comput. Phys., 21: 251–269.

Palma, E.D. and Matano, R.P. (1998). On the implementation of passive open boundary conditions for a general circulation model: the barotropic mode. J. Geophys. Res. 103 (C1) : 1319–1341.

Peregrine, D.H. (1967). Long waves on a beach. J. Fluid Mech. 27, 815.

Pinder, G.F. and Gray, W.G. (1977). Finite elements simulation in surface and subsurface hydrology. New York : Academic Press.

Pohle, F.V. (1952). Motion of water due to breaking of a dam and related problems. USNBS, Circ. 521(8): 47-53.

Quecedo, M. and Pastor, M. (2003). A reappraisal of Taylor–Galerkin algorithm for drying-wetting areas in shallow water computations. Int. J. Numer. Methods Fluids, 38:515-531.

Reddy, J.N. (1984). An introduction to finite element method. McGraw-Hill Company.

Ritter, A. (1892). The propagation of water waves. Ver Deutsch Ingenieur Zeitschr, Berlin, Vol. 36, Part 3, No. 33, pp.947-954.

Robert, J.L. (2008). Éléments finis en Hydraulique. Cours GCI-64313 de deuxième et de troisième cycle. Département de génie civil, Université Laval, Québec.

Rubin, M.B. (1997). Relationship of critical flow in waterfall to minimum energy head. J. Hydraul. Eng., 123(1): 82–84.

Safjan, A. and Oden, J.T. (1995). High-order Taylor–Galerkin methods for linear hyperbolic systems. J. Comp. Phys., 120:206-230.

Savic, L. and Holly, F.M. (1991). Modified Godunov Method for Dam-Break Flows. Proceedings of the XXIV IAHR Congress, Madrid, pp. A203-210.

Selmin, V., Donea J. and Quartapelle, L. (1985). Finite Element Methods for Nonlinear Advection. J. Comput. Meth. Appl. Mech. Eng., 52: 817-845.

Serre, F. (1953). Contribution à l'étude des écoulements permanents et variables dans les canaux. Houille Blanche, 8: 374-388.

Shames, L.H. (1962). Mechanics of fluids. McGraw-Hill Book Company.

Shoenstadt, A.L. (1980). A transfer function analysis of numerical schemes used to simulate geostrophic adjustment. Mon. Wea. Rev. 108, 1248-1259.

Shu, C.W. and Osher, S. (1988). Efficient implementation of essentially non- oscillatory shock-capturing schemes. J. Comp. Phys. 77: 439-471.

Sommerfeld, A. (1949). Partial differential equations. Vol. 6, Academic Press.

Soulis, J. (1992). Computation of Two Dimensional Dam-Break Flood Flows. Int. J. Numer. Methods Fluids, 14:631-664.

Stansby, P.K. and Zhou, J.G. (1998). Shallow-water solver with non-hydrostatic pressure: 2D vertical plane problems. Int. J. Numer. Methods Fluids, 28(3): 541–563.

Steffler, P.M. and Jin, Y. (1993). Depth-averaged and moment equations for moderately shallow free surface flow. J. Hydraul. Res., 31(1): 5–18.

Stelling, G. and Zijlema, M. (2003). An accurate and efficient finite difference algorithm for non-hydrostatic free-surface flow with application to wave propagation. Int. J. Numer. Methods Fluids, 43(1): 1–23.

Stoker, J.J. (1957). Water waves. Interscience Publishers, pp. 331-341.

Strelkoff, T. (1986). Dam-Break Flood Waves. Megatrends in Hydraulic Engineering, eds. M.L. Albertson, and C.N. Papadakis, California State University, pp. 257-266

Tamma, K.K. and Namburu, R.R. (1988). A new finite element based Lax–Wendroff/Taylor–Galerkin methodology for computational dynamics. Computer Methods in Applied Mechanics and Engineering, 71:137-150.

Tanaka, M. (1986). The stability of solitary waves. Phys. Fluids 29, 650-655.

Toro, E.F. (2001). Shock-capturing methods for free-surface shallow flows. New York: Wiley.

Tossou, E. (2004). La modélisation du ruissellement par éléments finis et son application au drainage routier. Mémoire de Maîtrise. Département de génie civil, Université Laval, Québec.

Tossou E., Robert J.L., Morse B. and Le Roux D. (2009). Dambreak Flow Simulation using a Finite Element Solution of the 2DH Serre Model. J. Adv. Wat. Res. (submitted).

Tossou E., Robert J.L., Morse B. and Le Roux D. (2008). 2D Vertically-Averaged Serre Hydrodynamic Model. J. Adv. Wat. Res. (submitted).

Tossou E., Robert J.L., Morse B. and Le Roux D. (2008). Extented Saint-Venant Model for Fully Non-Hydrostatic Pressure Flows. J. Wat. Res. (submitted).

Tseng, M.H. and Chu, C.R. (2000). Two-dimensional shallow water flows simulation using TVD-MacCormak scheme. J. Hydraul. Res., 38:123-131.

Van Rijn, L.C. (1994). Principle of fluid flow and surface waves in rivers, estuaries, seas and oceans (2nd Ed.), Aqua Publications, Amsterdam, The Netherlands (1994).

Viollet, P.L., Chabard, J.P., Esposito, P. and Laurence, D. (1998). Mécanique des fluides appliquée. Écoulements incompressibles dans les circuits, canaux et rivières, autour de structures et dans l'environnement. Presses de l'École Nationale des Ponts et Chaussées. ISBN 2-85978-301-6.

Wang, J.S., Ni, H.G. and He, Y.S. (2000). Finite-difference TVD scheme for computation of dam-break problems. J. Hydraul. Eng., 126(4): 253-262.

Wang, J.W. and Liu, R.X. (2000). A comparative study of finite volume methods on unstructured meshes for simulation of 2D shallow water wave problems. Math. Comput. Simul., 53: 171-184.

Whithman, G.B. (1955). The Effect of Hydraulic Resistance in the Dam-Break Problem. Royal Society of London. Proceedings Series – A, pp.226-227.

Williams, R.T. (1981). On the formulation of the finite-element prediction models. Mon. Wea. Rev. 109, 463-466.

Wu, C., Huang, G. and Zheng, Y. (1999). Theoretical solution of Dam-Break shock wave. J. Hydraul. Eng., 125(11): 1210-1215.

Xia, C. and Jin, Y.C. (2006). Multilayer Averaged and Moment Equations for One-Dimensional Open-Channel Flows. J. Hydraul. Eng., 132(8): 839-849.

Zarrati, A. R., Jin, Y.C., Shanehsaz-zadeh, A. and Ahadi, F. (2004). Potential flow solution for a free surface flow past a sudden slope change. Can. J. Civ. Eng., 31(4): 553–560.

Zerihum, Y. T. (2004). A One-dimensional Boussinesq-type Momentum Model for Steady Rapidly Varied Open Channel Flows. Ph.D. thesis, Department of Civil and Environmental Engineering, Melbourne University, http://eprints.infodiv.unimelb.edu.au/archive/00000856/

Zerihum, Y.T. and Fenton, J.D. (2006). One-dimensional simulation model for steady transcritical free surface flows at short length transition. Advances in Water Resources 29(11): 1598-1607.

Zerihum, Y.T. and Fenton, J.D. (2007). A Boussinesq-type model for flow over trapezoidal profile weirs. J. Hydraul. Eng., 45(4): 519–528.

Zhang, Y. and Tabarrok, B. (1999). Modifications to the Lax–Wendroff scheme for hyperbolic systems with source terms. Int. J. Numer. Meth. Eng., 44:27-40.

Zhao, D.H., Shen, H.W., Lai, J.S. and Tabios, G.Q. (1996). Approximate Riemann solvers in FVM for 2D hydraulic shock wave modeling. J. Hydraul. Eng., 122(2): 692-702.

APPENDIX

Integral terms of the element matrices and vectors

Consider the equation (69) established previously, i.e.,

$$\{R^e\}=[M^e]\left\{\frac{\partial\Omega^e}{\partial t}\right\}+\left\{\frac{\partial F_s^e}{\partial t}\right\}+[K^e]\{\Omega^e\}-\{F^e\} \tag{69}$$

The expanded expressions of the two element matrices (i.e., $[M^e]$ and $[K^e]$) and of the two element vectors (i.e., $\{F_s^e\}$ and $\{F^e\}$) give respectively:

$$[M^e]=\begin{bmatrix}[M^{1e}] & [0] & [0]\\ [0] & [M^{2e}] & [0]\\ [0] & [0] & [M^{3e}]\end{bmatrix} \tag{a1}$$

$$[K^e]=\begin{bmatrix}[K^{11e}] & [K^{12e}] & [K^{13e}]\\ [K^{21e}] & [K^{22e}] & [K^{23e}]\\ [K^{31e}] & [K^{32e}] & [0]\end{bmatrix} \tag{a2}$$

$$\{F_s^e\}=\begin{Bmatrix}\{F_s^{1e}\}\\ \{F_s^{2e}\}\\ \{0\}\end{Bmatrix} \tag{a3}$$

$$\{F^e\}=\begin{Bmatrix}\{F^{1e}\}\\ \{F^{2e}\}\\ \{F^{3e}\}\end{Bmatrix} \tag{a4}$$

The integral terms of the different intermediate matrices and vectors are defined as follow.

$$M_{ij}^{1e} = M_{ij}^{2e} = \int_{D^e} N_i N_j \, dD^e \tag{a5}$$

$$M_{ij}^{3e} = \int_{D^e} N_{Hi} N_{Hj} \, dD^e \tag{a6}$$

$$K_{ij}^{11e} = \int_{D^e} \left(N_i \left(N_j \frac{\partial \tilde{U}}{\partial x} + g N_j \frac{\sqrt{\tilde{U}^2 + \tilde{V}^2}}{C_c^2 \tilde{H}} \right) + \left(\begin{array}{l} \tilde{\nu}_{xx} \dfrac{\partial N_i}{\partial x} \dfrac{\partial N_j}{\partial x} + \tilde{\nu}_{xy} \dfrac{\partial N_i}{\partial x} \dfrac{\partial N_j}{\partial y} \\ + \tilde{\nu}_{yx} \dfrac{\partial N_i}{\partial y} \dfrac{\partial N_j}{\partial x} + \tilde{\nu}_{yy} \dfrac{\partial N_i}{\partial y} \dfrac{\partial N_j}{\partial y} \end{array} \right) \right) dD^e \tag{a7}$$

$$K_{ij}^{12e} = \int_{D^e} N_i N_j \frac{\partial \tilde{U}}{\partial y} dD^e \tag{a8}$$

$$K_{ij}^{13e} = \int_{D^e} N_i g \frac{\partial N_{Hj}}{\partial x} dD^e \tag{a9}$$

$$K_{ij}^{21e} = \int_{D^e} N_i N_j \frac{\partial \tilde{V}}{\partial x} dD^e \tag{a10}$$

$$K_{ij}^{22e} = \int_{D^e} \left(N_i \left(N_j \frac{\partial \tilde{V}}{\partial y} + g N_j \frac{\sqrt{\tilde{U}^2 + \tilde{V}^2}}{C_c^2 \tilde{H}} \right) + \left(\begin{array}{l} \tilde{\nu}_{xx} \dfrac{\partial N_i}{\partial x} \dfrac{\partial N_j}{\partial x} + \tilde{\nu}_{xy} \dfrac{\partial N_i}{\partial x} \dfrac{\partial N_j}{\partial y} \\ + \tilde{\nu}_{yx} \dfrac{\partial N_i}{\partial y} \dfrac{\partial N_j}{\partial x} + \tilde{\nu}_{yy} \dfrac{\partial N_i}{\partial y} \dfrac{\partial N_j}{\partial y} \end{array} \right) \right) dD^e \tag{a11}$$

$$K_{ij}^{23e} = \int_{D^e} gN_i \frac{\partial N_{Hj}}{\partial y} dD^e \tag{a12}$$

$$K_{ij}^{31e} = \int_{D^e} \left(kN_j \tilde{U} \frac{\partial N_{Hi}}{\partial x} \frac{\partial \tilde{H}}{\partial x} + kN_j \tilde{V} \frac{\partial N_{Hi}}{\partial x} \frac{\partial \tilde{H}}{\partial y} - HN_j \frac{\partial N_{Hi}}{\partial x} \right) dD^e \tag{a13}$$

$$K_{ij}^{32e} = \int_{D^e} \left(kN_j \tilde{U} \frac{\partial N_{Hi}}{\partial y} \frac{\partial \tilde{H}}{\partial x} + kN_j \tilde{V} \frac{\partial N_{Hi}}{\partial y} \frac{\partial \tilde{H}}{\partial y} - HN_j \frac{\partial N_{Hi}}{\partial y} \right) dD^e \tag{a14}$$

$$F_{si}^{1e} = \int_{D^e} N_i \tilde{U}_z \, dD^e \tag{a15}$$

$$F_{si}^{2e} = \int_{D^e} N_i \tilde{V}_z \, dD^e \tag{a16}$$

$$F_i^{1e} = \oint_{\Gamma^e} N_i \left(\left(\tilde{\nu}_{xx} \frac{\partial \tilde{U}}{\partial x} + \tilde{\nu}_{xy} \frac{\partial \tilde{U}}{\partial y} \right) n_x + \left(\tilde{\nu}_{yx} \frac{\partial \tilde{U}}{\partial x} + \tilde{\nu}_{yy} \frac{\partial \tilde{U}}{\partial y} \right) n_y \right) d\Gamma^e - \int_{D^e} N_i \left(g \frac{\partial N_{Hj}}{\partial x} + \tilde{a}_{zx} \right) dD^e \tag{a17}$$

$$F_i^{2e} = \oint_{\Gamma^e} N_i \left(\left(\tilde{\nu}_{xx} \frac{\partial \tilde{V}}{\partial x} + \tilde{\nu}_{xy} \frac{\partial \tilde{V}}{\partial y} \right) n_x + \left(\tilde{\nu}_{yx} \frac{\partial \tilde{V}}{\partial x} + \tilde{\nu}_{yy} \frac{\partial \tilde{V}}{\partial y} \right) n_y \right) d\Gamma^e - \int_{D^e} N_i \left(g \frac{\partial N_{Hj}}{\partial y} + \tilde{a}_{zy} \right) dD^e \tag{a18}$$

$$F_i^{3e} = \oint_{\Gamma^e} N_{Hi} \left(\left(k\tilde{U}^2 \frac{\partial \tilde{H}}{\partial x} + k\tilde{U}\tilde{V} \frac{\partial \tilde{H}}{\partial y} \right) n_x + \left(k\tilde{V}\tilde{U} \frac{\partial \tilde{H}}{\partial x} + k\tilde{V}^2 \frac{\partial \tilde{H}}{\partial y} \right) n_y - q_n \right) d\Gamma^e \tag{a19}$$

The symbols $\tilde{a}_{zx}$, $\tilde{a}_{zy}$ $\tilde{U}_z$, $\tilde{V}_z$, $\tilde{v}_{xx}$, $\tilde{v}_{xy}$, $\tilde{v}_{yx}$ and $\tilde{v}_{yy}$ are the discrete expressions of a_{zx}, a_{zy} U_z, V_z, v_{xx}, v_{xy}, v_{yx} and v_{yy} respectively.

Those integral terms are calculated automatically by Matlab® computer programming using the numerical Gauss-Legendre method, which is fully described in (Dhatt and Touzot 1981).